**Ana Cristina Gaspar Silva**

BSc in Health and Biological Sciences

# Synthesis and biological evaluation of novel anti-cancer agents

Dissertation for the Master's Degree in Molecular Genetics and Biomedicine

Orientador: Maria Alexandra Núncio de Carvalho Ramos Fernandes, Professora Auxiliar, FCT/UNL

Co-orientadores: Maria Manuel Duque Vieira Marques dos Santos, Doutora, FF/ULisboa

Pedro Miguel Ribeiro Viana Baptista, Professor Associado com Agregação, FCT/UNL

Júri:

Presidente: Professora Doutora Paula Maria Theriaga Mendes Bernardo Gonçalves

Arguente: Professora Doutora Maria Luísa Teixeira de Azevedo Rodrigues Corvo

Vogal: Professora Doutora Maria Alexandra Núncio de Carvalho Ramos Fernandes

FACULDADE DE CIÊNCIAS E TECNOLOGIA
UNIVERSIDADE NOVA DE LISBOA

**Julho, 2017**

**UNIVERSIDADE NOVA DE LISBOA**

**FACULDADE DE CIÊNCIAS E TECNOLOGIA**

**DEPARTAMENTO DE CIÊNCIAS DA VIDA**

Ana Cristina Gaspar Silva

# Synthesis and biological evaluation of novel anti-cancer agents

*Dissertation for the Master's Degree in Molecular Genetics and Biomedicine, by Universidade Nova de Lisboa, Faculdade de Ciências e Tecnologia*

**Orientador:**

Professora Auxiliar Alexandra R. Fernandes (FCT/UNL)

**Co-orientadores:**

Doutora Maria M. M (FF/ULisboa)

Professor Associado com Agregação Pedro M. R. V. Baptista (FCT/UNL)

**Lisboa**

**2017**

# Synthesis and biological evaluation of novel anti-cancer agents

## ACKNOWLEDGMENTS

To everyone here mentioned I would like to express my immense gratitude for the opportunity and trust placed in me and, above all, thank you for walking alongside me during this journey.

Firstly, I would like to thank Professor Alexandra Fernandes which, besides being my supervisor during this project, was a mentor for the beginning of my career, triggering in me an insatiable will of discovery and ambition. To Professor Pedro Batista, my co-supervisor, which always calmed my anxiety with his good mood and cheer. Both have given me the opportunity to develop as a scientist and as a human being. To Professor Maria Santos, also my co-supervisor, for all her availability and support in the subject where I was less comfortable.

I believe that, without a team, it is impossible to achieve our goals brilliantly. For that, I am thankful to both teams of 319 and 315 laboratories, wherein, besides companions, where also my second home. To Catarina Rodrigues, for all her support and counseling, that appeased me so many times. To Elizabeth Lopes, for providing one of the chemical intermediated necessary for the final work. I would also like to thank Dário Valezim for all the care and companionship during the compound synthesis.

Well, the truth is that I would have not make it through this year if I had not had my friends by my side. To Vanessa Silva, for her amazing glee, your strident days will always be remembered. To Andreia Carvalho, my loyal companion during this journey, thank you for all the calmness that you were able to transmit when I needed the most.

To Joana Rodrigues, to you I am thankful for your friendship and unconditional support, you gave me the strength that I needed to achieve my goal. You were also the one responsible for the pounds I gained and all the laughs during this time. I learned a lot with you, I even learned how to be more chilled; how is it possible? I lived incredible moments with you. To our friendship. Cátia Raposo, my best friend, you are one of the persons that knows me better. Thank you for all the support, trust and friendship, for all the tears and laughs but most of all, thank you for being there! You were always there for me when I needed the most!

To my family, for all the faith in me and understanding for the missing moments. Without you and your support, I would not be prepared to take on this madness that is science. Even with an ocean between us, you have never failed me, you were always there, willing to listen to me at any given time.

To Fábio Costa, my person. There were so many times, where you were my motivation and strength. You always believed in me and in my capabilities, even when I did not believe. I am sorry for every hour that I have been away, and thank you for turning miles in such a short distance. You will always be the reason for me to overcome myself, to push forward, to not give up.

**“It is hard to fail, but it is worse never to have tried to succeed.”**

(Franklin Roosevelt)

## RESUMO

O cancro continua a ser uma das principais causas de morte a nível mundial, apesar da profunda compreensão não só acerca da sua etiologia e dos esforços para uma deteção precoce, como também do desenvolvimento de abordagens terapêuticas mais personalizadas. A preocupação major em quimioterapia tem sido sintetizar novas moléculas capazes de inibir seletivamente o crescimento de células neoplásicas, evitando, assim, os efeitos adversos e/ou resistência adquirida. Neste contexto, a molécula sintetizada AM130, composta por um motivo espiro [pirrolidina-3, 3´-oxindole], apresenta atividades antiproliferativa contra células neoplásicas e antimalária. No presente estudo, debruçámo-nos sobre a síntese e o potencial antiproliferativo deste composto, bem como ao seu mecanismo de ação em células tumorais.

Os ensaios de viabilidade foram realizados não só em linhagens celulares de carcinoma do ovário, colorretal e da mama, como também em fibroblastos humanos normais, permitindo a caracterização do potencial citotóxico da molécula AM130. Os resultados revelaram que esta possui um maior efeito antiproliferativo contra as células do carcinoma do ovário, demonstrando, igualmente, maior seletividade para células tumorais em comparação com as células normais.

A atividade antiproliferativa observada deveu-se à indução de morte celular pela via apoptótica mediada pela mitocôndria e pela autofagia. Os estudos de interação com o DNA demonstraram que a AM130 interage com o DNA através de uma ligação aos sulcos, sem causar genotoxicidade ou paragem do ciclo celular. Além disso, a AM130 apresentou uma forte afinidade para a albumina de soro bovino. A análise de protéomica revelou que a maioria das proteínas identificadas estão associadas com a regulação da apoptose e da resposta ao stress, corroborando os resultados anteriormente obtidos acerca do mecanismo de morte celular induzido nas células do carcinoma de ovário pelo composto AM130.



**Palavras-chave:** Carcinogénese, quimioterapia, espirooxindole, interação fármacos-DNA, citotoxicidade

## ABSTRACT

Cancer is still one of the deadliest diseases worldwide despite the deep understanding of its etiology and efforts toward an early detection and the development of personalized therapeutic approaches. Thus, the development of novel molecules that maybe selectively inhibit the growth of cancer cells, avoid side effects and/or acquired resistance has long been the focus in chemotherapy. One such compounds, AM130 with the spiro[pyrrolidine-3, 3´-oxindole] moiety has shown antiproliferative and antimalarial activity. Here, we report the synthesis and the biological anitproliferative potential of this compound, as well as its mechanism of action in cancer cells.

Viability assays were performed in ovarian, colorectal and breast carcinoma cell lines and normal human fibroblasts, allowing the characterization of the antiproliferative potential of AM130. Results showed that AM130 has a higher cytotoxic effect as well as higher selectivity for the ovarian carcinoma cell line.

The observed antiproliferative activity was due to the induction of cell death by mitochondria-mediated apoptotic pathway and autophagy. DNA interaction studies demonstrated that AM130 interacts with DNA by groove-binding, however without causing genotoxicity or cell cycle arrest. In addition, AM130 showed a strong affinity to bovine serum albumin. Proteomics analysis revealed that the majority of the identified proteins are involved in apoptosis and stress response regulation, corroborating the previous results about ovarian carcinoma cells death.

**Keywords:** Carcinogenesis, Chemotherapy, Spirooxindole, Drugs-DNA interaction, cytotoxicity

**GENERAL CONTENTS**

## FIGURE INDEX

## TABLE INDEX

## ABBREVIATION LIST

| | |
|---|---|
| **APAF-1** | Apoptosis protease activating factor-1 |
| **A2780** | Ovarian carcinoma cell line |
| **BAX** | Bcl-2-associated X protein |
| **BCL-2** | B-cell lymphoma protein 2 |
| **Bid** | BH3-interacting domain death agonist |
| **BSA** | Bovine serum albumin |
| **Caspase** | Cysteine-aspartic protease |
| **CCR** | Complete culture medium recipe |
| **CD** | Circular dichroism |
| **CDKs** | Cyclin-dependent protein kinases |
| **CKI** | Cyclin-dependent kinase inhibitor |
| **CT-DNA** | Calf Thymus-DNA |
| **DCF** | 2,7-dichloroflurescein |
| **DISC** | Death inducing signalling complex |
| **DMEM** | Dulbecco's Modified Eagle Medium |
| **DMSO** | Dimethyl Sulfoxide |
| **DNA** | Deoxyribonucleic acid |
| **DOX** | Doxorubicin |
| **DTT** | Dithiothreitol |
| **ECM** | Extracellular matrix |
| **EC** | Endothelial cell |
| **ER** | Endoplasmic reticulum |
| **FADD** | Fas-associated death domain |
| **FasL** | Fatty acid synthetase ligand |
| **FBS** | Fetal Bovine Serum |
| **FITC** | Fluorescein isothiocyanate |
| **GLOBOCAN** | International Agency for Research on Cancer |
| **HCT116** | Colorectal carcinoma cell line |
| **$H_2$DCF-DA** | 2,7-dichlorodihydrofluorescein diacetate |
| **HPR** | Horseradish peroxidase |
| **IEF** | Isoelectric focusing |
| **IPG** | Immobilized pH gradient |
| **JC-1** | 5,5',6,6'-tetrachloro-1,1',3,3'- tetraethylbenzimi-dazolyl-carbocyanine iodide |
| **LB** | Luria–Bertani liquid medium |
| **MDA-MB-453** | Breast adenocarcinoma cell line |
| **MDM2** | Murine double minute 2 |
| **MDR** | Multidrug resistance |
| **MTS** | [3-(4,5dimethylthiazol-2-yl)-5-(3-carboxymethoxyphenyl)-2-(4-sulfophenyl)-2H tetrazolium] |
| **OC** | Ovarian carcinoma |
| **PBS** | Phosphate Buffered Saline |
| **pDNA** | Plasmids DNA |
| **PFA** | Paraformaldehyde |
| **PI** | Propidium Iodide |
| **PMSF** | Phenylmethylsulfonyl fluoride |
| **pRB** | Retinoblastoma protein |
| **RNA** | Ribonucleic acid |
| **ROS** | Reactive oxygen species |
| **RT** | Room temperature |

| | |
|---|---|
| **SDS** | Sodium dodecyl sulfate |
| **TP53** | p53 protein encoding gene |
| **WHO** | World Health Organization |

**Symbol List**

| | |
|---|---|
| **[Compound]** | Compound concentration |
| **[DNA]** | DNA concentration |
| **ε** | Molar extinction coefficient of DNA |
| **εa** | Apparent molar extinction coefficient |
| **εb** | Bound complex molar extinction coefficient |
| **εf** | Free molar extinction coefficient |
| $\ell$ | Optical path |
| $\delta$ | Chemical shifts |
| $\Delta\Psi_M$ | Mitochondrial membrane potential |
| $IC_{50}$ | Half Maximal Inhibitory Concentration |
| $K_b$ | Affinity binding protein |

# 1 INTRODUCTION

## 1.1 Cancer distribution, incidence, and mortality worldwide

Cancer is considered a group of related diseases characterized by the autonomous proliferation of neoplastic cells due to innumerous epigenetic and genetic alterations (Millimouno et al. 2014) with the continuous influence of lifestyle habits (Colditz et al. 2012) and the exposure to several agents i.e., to carcinogens. The carcinogens can include: (i) biological agents, which include virus or bacterial infections; (ii) chemical agents, such as tobacco smoke components and (iii) physical agents like UV radiation (Colditz et al. 2012). Additionally, ageing is another fundamental factor in development of cancer since cellular repair mechanisms tend to be less effective with aging, leading to an accumulation of abnormalities (WHO, 2015). Nevertheless, only 5 to 10% of all cancers are due to an inherited gene defect, being breast and ovarian cancers the most common hereditary tumors (Marchina et al. 2010). For this reason, it is unquestionable that most cancers are due to lifestyle factors, such as dietary habits, smoking, alcohol consumption and infections and not by hereditary factors (Irigaray et al. 2007). As reported by the World Health Organization (WHO), it is possible that by modifying or avoiding these habits, more than 30% of cancer deaths could be prevented (WHO, 2015).

Data from the International Agency for Research on Cancer (GLOBOCAN) in 2012, estimated 14.1 million new cancer cases: 7.4 million (53%) in males and 6.7 million (47%) in females, with 8.2 million cancer deaths (Ferlay et al. 2013). Moreover, WHO projects a rise in cancer deaths to 13.1 million until 2030 (WHO, 2015). The most predominant and deadliest cancers registered worldwide, since 2012, were lung cancer, corresponding to 1.6 million deaths, liver cancer with 745 000 deaths, stomach cancer with 723 000 deaths and colorectal cancer with 694 000 deaths. The risk factors identified by WHO, as the main cause of deaths, were obesity, tobacco and alcohol consumption and sedentary lifestyle (WHO, 2015).

According to Direcção – Geral de Saúde, the incidence of cancer in Portugal in 2020 will be of 50 000 cases (Direcção-Geral de Saúde, 2014). In 2014, WHO estimated for Portugal 6 622 new cases of prostate cancer and 6 088 for breast cancer in male and female patients, respectively. Breast cancer was the deadliest cancer in females, corresponding to 16.9% deaths, and in males, the deadliest were trachea, bronchus, and lung cancers with 19.3% deaths (WHO, 2014).

## 1.2 The Molecular Biology of Cancer

### 1.2.1 Carcinogenesis Hallmarks

Carcinogenesis is a multistep process associated with sequential accumulation of genetic mutations within tissue cells leading to the dysregulation of gene activities involved in cell growth control, programmed cell death regulation and genetic stability maintenance (Ashkenazi et al. 2008).

Hanahan & Weinberg have identified six malignancies capabilities responsible for cancer development including unlimited proliferative potential, environmental independence for growth, evasion of cell death, angiogenesis, invasion, and metastasis. Simultaneously to these biological phenomena, genome instability (Hanahan & Weinberg, 2011) and inflammation are also responsible for cell phenotype changes during cancer progression (Huang, 2013). The hallmarks responsible for the cancer development are described in Figure 1.1.

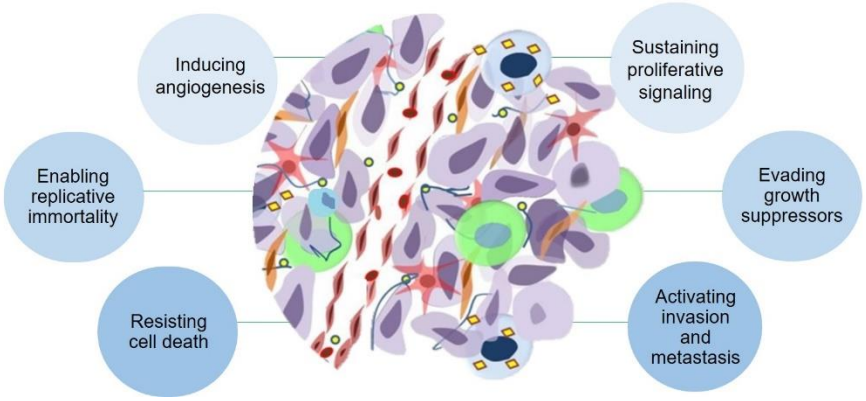


**Figure 1.1 -** Cancer hallmarks proposed by Hanahan and Weinberg. According to these authors, cancer development comprises features such as, sustaining proliferative signalling, evading growth suppressors, activating invasion and metastasis, resisting cell death, enabling replicative immortality and inducing angiogenesis. Adapted from (Hanahan & Weinberg, 2011).

To promote sustained chronic proliferation, as well as dysregulation of both cell survival and energy metabolism, cancer cells disrupt the control of production and release of growth-promoting signals. For this purpose, cancer cells are capable of producing growth factor ligands leading to an autocrine proliferative stimulation; manipulate the adjacent normal cells to supply them with various growth factors and, finally, cancer cells cause dysregulation and structural alterations of its surface receptors resulting in a hyperresponsivity to otherwise-limiting amounts of factors (Hanahan & Weinberg, 2011).

Figure 1.2 summarizes the features of the metastatic process. Cancer metastasis is responsible for approximately 90% of cancer patient mortality (Reymond et al. 2013), comprising a multistep process ordered in the following fashion: (1) local infiltration of tumor cells into the adjacent tissue; (2) transendothelial migration of cancer cells into vasculature – intravasation; (3) cell survival in the circulatory system; (4) cell extravasation and (5) the subsequent proliferation in competent organs leading to colonization at distal sites (Van Zijl et al. 2011).

The ‘‘seed and soil’’ theory, proposed by Stephen Paget in 1889, describes the organ-specific pattern of metastasis i.e., the influence of the primary tumor on site specific metastasis. Therefore, the secondary growth of cancer cells (the ‘‘seed’’) is dependent on the competence of the distal organ (the ‘‘soil’’) i.e., certain cancer cells have specific affinity for certain organs (Paget, 1889). Nowadays, this theory has been approved for various cancer types which metastasize at different and tumor-specific sites (Van Zijl et al. 2011). As mentioned, the microenvironment of the primary tumor is crucial for the metastasis success, because its needs to support tumor cell dissemination, motility, and local invasion into the vasculature, whereas the microenvironment at the secondary site needs to support cell adhesion, proliferation, and neovascularization. In addition, metastatic behavior of tumor cells can be influenced by the tumor microenvironment through (i) changes in the glycoprotein composition of the extracellular matrix (ECM) which, in turn, can influence the cell adhesion, motility, proliferation and apoptotic rates; (ii) alterations in the ECM-degrading proteinase activities within the stroma, facilitating the movement of tumorigenic cells by disrupting stromal barriers; and (iii) the release of bioactive ECM fragments and/or growth factors that can promote or suppress neoplastic progression of both stromal and tumor cells (Schedin & Elias, 2004). Besides the influence of primary tumor in metastasis process, overall, a range of biological, extrinsic chemical barriers, and physiological factors prevents this process. The biological factors are represented by the cellular microenvironment which regulates tumor dissemination by regulatory cytokines, chemokine feedback loops and by secretion of matrix metalloproteinases, while the extrinsic chemical barriers include pH, reactive oxygen species (ROS) or hypoxia, and the physiological factors correspond to intratumoral tensional forces, the composition of the basement membrane and the anatomy of capillary walls i.e., the anatomical structure and the density of lymphatic or blood vessels influencing the cancer cell spreading at distal sites of metastasis (Van Zijl et al. 2011).

Furthermore, neovascularization at tumor microenvironment is equally essential not only for the supply of nutrients, oxygen, and immune cells, but also for the removal of metabolic waste products resulting from tumor growth and metastasis. The neovascularization process, commonly designated angiogenesis, is a process highly regulated by both activator and inhibitor molecules leading to new blood vessel formation. The angiogenesis process include 4 steps: (i) destruction of the basal membrane, (ii) migration of endothelial cells (EC) activated by angiogenic factors, (iii) proliferation and stabilization and (iv) the continuing influence by angiogenic factors leading to the prolongation of the angiogenic process (Nishida et al. 2006). Curiously, the aggressiveness of the tumor cells spreading is related to the neovascularization, since this process reduces the accessibility of chemotherapeutic drugs to the tumor site (Nishida et al. 2006).

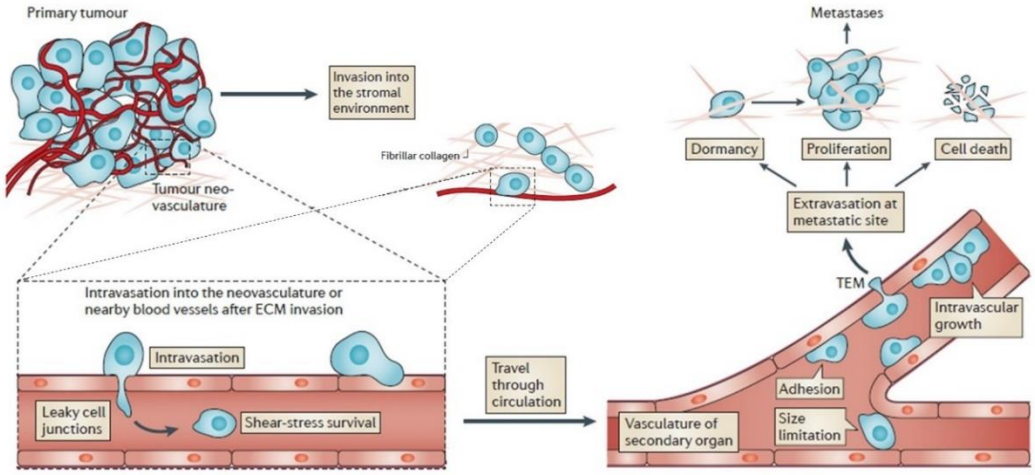


**Figure 1.2 -** The metastatic process. Some of the cancer cells from the primary tumor acquire invasive and migratory properties, allowing invasion of surrounding tissues or migration towards neighboring blood vessels. The intravasation of cancer cells i.e. the entry of these into the blood vessels through EC junctions is required for the spread throughout body and, the subsequent extravasation i.e. when cancer cells leave the circulation at potential secondary tumor sites. Then, cancer cells transmigrate through the endothelial barrier, invading the basement membrane that surrounds the blood vessels. At the new metastatic site, cancer cells can enter in a state of dormancy or proliferate. Nonetheless, most cancer cells, that extravasate at the new microenvironment, will undergo cell death. Adapted from (Reymond et al. 2013).

Cells are continually exposed to a variety of cellular stresses, which are responsible for genomic aberrations causing genomic instability. Subsequently, the accumulation of these abnormalities can often result in the development of cancers, therefore it is important the proper stress response, through cell cycle regulation and cell death, to maintain genomic integrity and protect cells from malignant transformation (Ozaki & Nakagawara, 2011). In that sense, in the following subchapters the regulation of cell cycle and cell death will be presented.

### 1.2.2 Cell Cycle Regulation

The mammalian cell cycle involves various complex and highly regulated cellular events composed by two stages: interphase and mitosis (M), leading to deoxyribonucleic acid (DNA) synthesis and segregation of replicated chromosomes into two daughter's cells, respectively. Interphase includes G1 (gap 1), S (synthesis) and G2 (gap 2) phases, whereas mitosis includes prophase, metaphase, anaphase, and telophase stages. In addition, cells can be committed to enter G1 phase, remaining in a quiescent phase i.e., the Go (gap 0), where the cells do not grow and do not multiply (Vermeulen et al. 2003).

In cancer, cell cycle dysregulation and the subsequent unlimited cell proliferation are two fundamental events resulting from mutations in proto-oncogenes and tumor suppressor genes such as retinoblastoma protein (pRB) and p53 protein, as well as, in genes encoding for cyclin-dependent protein kinases (CDKs), cyclins, CDK-activating enzymes, cyclin-dependent kinase inhibitor (CKI), CDK substrates and checkpoint proteins. In normal cells, the proto-oncogenes products act at diverse levels

along signalling pathways related to cell proliferation. When mutated i.e., activated oncogenes, can promote uncontrolled tumor growth due to the dysfunction of proteins that are normally involved in the inhibition of cell cycle progression (Vermeulen et al. 2003).

CDKs belongs to a family of serine/threonine protein kinases and with pRB and p53 pathways (Lim & Kaldis, 2013) act as the central regulators of cell cycle by maintaining the exit and entry cells into the different cell cycle phases (Kitagawa et al. 2013). Furthermore, the CDKs' catalytic activity is also modulated by interactions with cyclins and CKI leading to the orderly progression of cells through the cell cycle (Lim & Kaldis, 2013). Figure 1.3 resume the regulation of cell cycle.

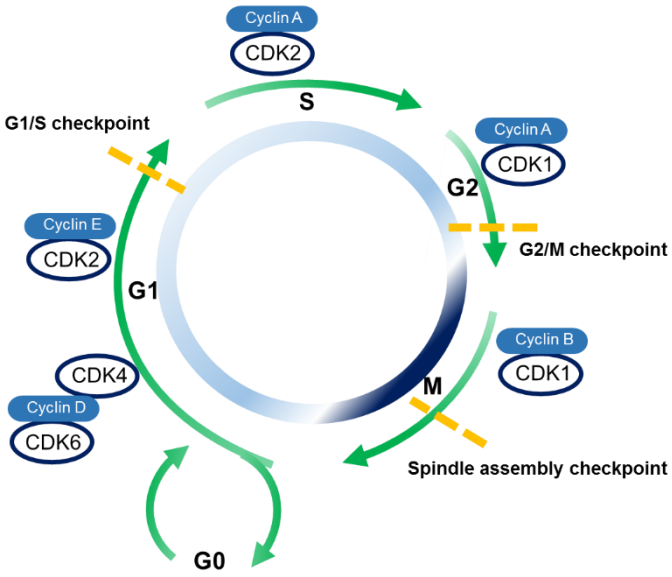


**Figure 1.3 -** Cell cycle phases and the cyclin-CDK complexes associated with each phase, as well as, the checkpoints involved in cell cycle regulation. The late G1 phase is regulated by cyclin D-CDK4 and cyclin D-CK6 complexes. The G1/S transition is associated with cyclin E-CDK2 complex the G1/S checkpoint also occurs. The complex cyclin A-CDK2 is a regulator of late S phase and before the cells progress to G2 phase, the S checkpoint also occurs. Cyclin A-CDK1 is implicated in the G2/M transition and in the checkpoint G2/M. Mitosis progression is regulated by cyclin B-CDK1 complex. Abbreviations: CDKs - cyclin-dependent protein kinases. Adapted from (Ferenbach & Bonventre, 2015).

Several exogenous and endogenous agents can cause DNA damage e.g., metabolic products, spontaneous nucleotides modifications, and physical and chemical agents. Consequently, the unrepaired DNA can potentially lead to tumor development. According to the literature, in response to DNA damage, three mainly checkpoints (G1/S, G2/M and spindle assembly) are activated to promote the correct DNA replication and growth cells. The restriction point is defined as a point of no return in G1, i.e., cells enter the quiescent phase (Vermeulen et al. 2003).

Ataxia-telangiectasia-mutated and ataxia and rad3 related are protein kinases that recognize DNA damage and, subsequently, phosphorylate the p53 protein leading to cell cycle arrest at the G1/S checkpoint in a p53-dependent manner (Vermeulen et al. 2003). At the molecular level, p53 – the guardian of the genome ─ is a nuclear transcription factor of several target genes involved in important

cellular process e.g., cell cycle, DNA repair, cell death, senescence, and angiogenesis (Ribeiro et al. 2016). Upon DNA damage, p53 is stabilized and activated through post-translational modifications with the subsequent accumulation in the cell nucleus. Depending on the damage severity (Ozaki & Nakagawara, 2011), i.e., when the stress levels are low, the p53 can induce a transient G1 cell cycle arrest allowing cells to repair their genome however, when the damages are too severe this protein can leads to the cells' senescence or death by apoptosis through the activation of genes involved in apoptotic signalling pathway (Ribeiro et al. 2016).

After cell cycle, when cyclins, CDKs and CKIs, complete their functions, they are ubiquitylated by specific E3 ligases and eliminated via the ubiquitin–proteasome pathway (Kitagawa et al. 2013).

### 1.2.3 Cell Death Signalling Pathways

A broad diversity of regulated cell death phenomena, besides the common cell death mechanisms ─ caspase-dependent apoptosis and necrosis ─ are described in the literature, including necroptosis, autophagic cell death, pyroptosis, mitotic catastrophy, among others (Galluzzi et al. 2012). Notwithstanding, the present study is mainly focused on caspase-dependent apoptosis pathway and autophagy.

#### 1.2.3.1 Caspase-dependent Apoptosis

Programmed cell death or apoptosis is a highly controlled physiological process that involves an energy-dependent cascade that culminate on the elimination of damaged cells. In addition, it is a vital pathway of various molecular processes such as normal cell turnover, embryonic development, tissue homeostasis, among other (Elmore, 2007).

Apoptosis and necrosis are two process that can occur independently, sequentially, as well as, simultaneously (Zeiss, 2003). While necrosis death follows acute cellular injury through an uncontrollable and passive process mediated by the interference with the energy supply of the cell and direct damage to cell membranes (Elmore, 2007), apoptosis is a well-established and highly controlled biochemical process divided into two pathways, namely intrinsic or extrinsic pathways (Adams & Cory, 2009). The extrinsic pathway involves ligand binding to a death receptor and the intrinsic pathway is initiated by cellular stresses resulting in the release of cytochrome-c from mitochondria (Millimouno et al. 2014; Figure 1.4). Both pathways subsequently cause activation of the caspase cascade which then triggers an ordered series of events that leads to death (Elmore, 2007).

As described in Figure 1.4, the extrinsic apoptosis pathway involves the binding of an extrinsic death-inducing ligand (FasL) to its death receptor (FAS) with an intracellular death domain resulting in the recruitment of Fas-associated death domain (FADD; Bruin et al. 2008; Millimouno et al. 2014). Subsequently, FADD protein associates with procaspase-8 forming the death-inducing signalling complex (DISC), which leads to an auto-catalytic activation of procaspase-8 and -10 (Lavrik & Krammer, 2012). Consequently, these activated caspases promote the release of active enzymes into the

cytoplasm enabling the cleavage and activating effectors of caspases such as caspase-3 and -7, initiating the cascade of events in apoptotic cell death (Ranjan et al. 2012). The intrinsic apoptotic pathway is initiated by non-receptor mediated intracellular stimuli such as irreparable DNA damage, hypoxia, temperature, nutrients deprivation, among other (Elmore, 2007). As a result of these stimuli, the p53-regulated genes products enhance the secretion of cytochrome-c from the mitochondria into the cell cytosol (Harris & Levine, 2005). Cytochrome-c binds and activates the apoptotic protease activating factor 1 (APAF-1), also a p53-regulated gene, and the procaspase-9, forming the apoptosome. Then, the apoptosome activates the procaspase-3 into caspase-3 culminating in cleavage of proteins (Galluzzi et al. 2012). The cross-talk between the extrinsic and intrinsic apoptosis pathways occurs through caspase-8 cleavage of Bid (Elmore, 2007). Figure 1.4 describe the two mainly apoptotic pathways.

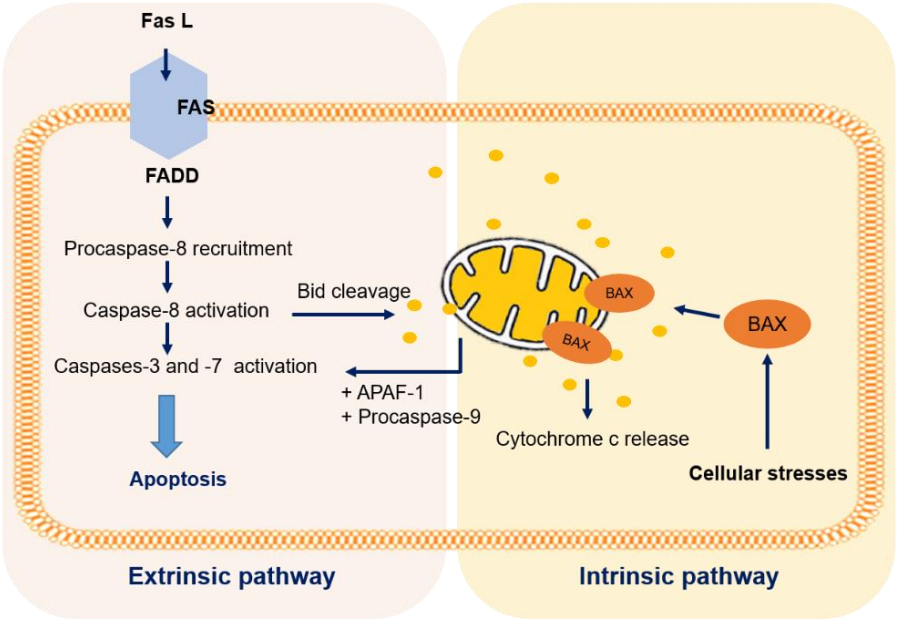


**Figure 1.4 -** Extrinsic and intrinsic pathways of apoptosis cell death. The schematic diagram describes the signalling molecules involved in the extrinsic (death receptor) and intrinsic (mitochondrial) apoptosis pathways. Abbreviations: APAF-1 - apoptotic protease activating factor 1; BAX - B-cell lymphoma protein 2 (BCL-2)-associated X protein; Bid - BH3-interacting domain death agonist; Fas L - Fatty acid synthetase ligand; FADD - Fas-associated death domain. Adapted from (Bruin et al. 2008).

During apoptosis, cells undergo several morphological changes including shrinkage, membrane budding (Kurosaka et al. 2003), phosphatidylserine (PS) externalization (Dasari & Tchounwou, 2014), nuclear condensation and DNA cleavage. These alterations culminate in the cellular fragmentation, with the cytoplasm retained in subcellular apoptotic bodies, thus allowing organelle integrity (Kurosaka et al. 2003). Subsequently, the apoptotic bodies are phagocytosed by macrophages and degraded on phagolysosomes. For these reasons, no inflammatory reaction is associated with apoptosis. However, in the absence of scavengers to clean up apoptotic cells, transition to a secondary or late stage necrosis can occur (Elmore, 2007).

### 1.2.3.2 Autophagic Cell Death

In response to nutrient starvation, hypoxia, energy depletion, endoplasmic reticulum (ER) stress and pharmacological agent treatment (Glick et al. 2010; Thost et al. 2015), eukaryotic cells activate a metabolic self-degradative process to digest their own cellular contents by a process referred to as autophagy or macro-autophagy (Thost et al. 2015).

Autophagy is a dynamic multistep process characterized by the lysosomal degradation (Thost et al. 2015) of protein aggregates, lipids, ribosomes and damaged or unnecessary organelles, through dynamic membrane rearrangements (Hamasaki et al. 2013), leading to cellular homeostasis and survival (Thost et al. 2015). Additionally, this cellular mechanism also provides macromolecules and energy (adenosine triphosphate, amino acids, etc.; Hamasaki et al. 2013). The main autophagy hallmark is the formation of double-membrane vesicles ─ autophagosomes ─ at the phagophore assembly site that sequester the subcellular components for posterior degradation. The formation of autophagosomes requires a membrane precursor such as autophagopore (Janku et al. 2011; Thost et al. 2015) derived from the lipid bilayer of ER, trans-Golgi network, mitochondrial outer membrane, or the plasma membrane, which then expands to engulf the intracellular components (Glick et al. 2010). The maturation of autophagosomes involves their fusion with lysosomes ─ autophagolysosomes ─ acquiring acidic hydrolases and leading to degradation of components (Thost et al. 2015). The resulting by-products return to the cytosol, where they can be re-used for metabolism and formation of new macromolecules (see Figure 1.5; Glick et al. 2010). For more information about molecular signalling pathway of autophagy refer to: (Janku et al. 2011; Hamasaki et al. 2013).

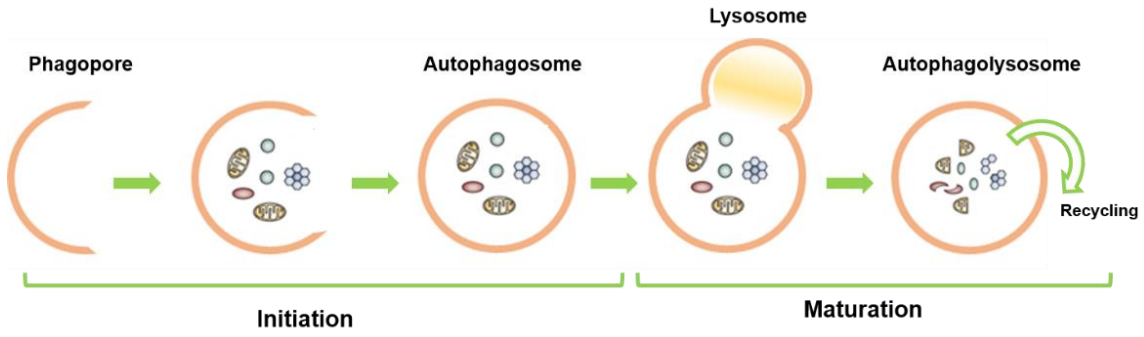


**Figure 1.5 -** Autophagy process. Briefly, the phagopore is formed resulting in an autophagosome which then fuses with the lysosome originating the autophagolysosome. Subsequently, the cargo-containing membrane compartment is lysed and degraded. Adapted from (Janku et al. 2011).

Autophagy process is known to suppress a variety of pathological conditions such as neurodegeneration, tumorigenesis, diabetes, and heart failure (Hamasaki et al. 2013). Autophagy prevents tumorigenesis by limiting necrosis and inflammation, inducing cell cycle arrest, and preventing genome instability. However, as a cell survival mechanism, other investigators have argued that autophagy may promote drug resistance and tumor cell adaptation to stress. Ultimately, the role of autophagy in cancer may be cell type- and/or stage-specific (Glick et al. 2010).

## 1.3 Cancer Therapy

### 1.3.1 Conventional treatment options for cancer therapy

Cancer treatment decisions include the determination of the benefits of adjuvant (after surgery) or neoadjuvant (before surgery) chemotherapy and radiotherapy according to each patient, since it can lead to increased toxicity; specific quality-of-life implications, and competing health issues. Furthermore, it is necessary to keep the balance between the specific circumstances and individual choices of patients and their families about therapy (Rahal et al. 2014).

Classical cancer treatment options include cytoreductive surgery, radiotherapy and chemotherapy (Vergote et al. 2011) and can be used either alone or in combination to eradicate the total tumor mass and/or diminish the possibility of invasion and metastasis (Shewach & Kuchta, 2009).

Surgery is divided into two strategies: (i) primary cytoreductive which aims to remove as much tumor as possible before the administration of chemotherapy or radiotherapy and (ii) interval cytoreductive surgery which involves the surgery after a brief period of neoadjuvant chemotherapy, usually three cycles of chemotherapy, or radiotherapy leading to the reduction of metastases confining the tumor mass (Vergote et al. 2011). Radiotherapy is a widely-used strategy for the treatment of solid and localized tumors, usually applied after surgery or used as an effective modality of palliative treatment to relieve patients from symptoms caused by the cancer (Baskar et al. 2012). Cancer chemotherapy is based on the intravenous administration of drugs (Crawford, 2013). Nevertheless, cancer cells due to their extensive genomic instability can adapt to chemotherapeutic agents by the activation of alternative pathways or enabling new genetic mutations to overcome the inhibitory effect of the drug, resulting in drug-resistant phenotypes (Mendelsohn, 2013).

Neoadjuvant therapies, are used mainly for patients with a very high rate of metastasis and in patients with a poor general condition (Vergote et al. 2011). This therapeutic approach aims to decrease the tumor size allowing complete resection (Mehren, 2008), as well as, allows the observation of the disease's biological behavior in response to a systemic therapy. This feature is extremely important in the clinical trials context, since it is possible to achieve the potential benefit by detection of the increasing response rates in the pre-operatory condition (Leal et al. 2015). In addition, patients that are only submitted to surgery i.e., without the neoadjuvant approach, can lead to poorer outcome (Mehren, 2008). On the other hand, adjuvant therapy leads to the destruction of tumor cells that may have been left behind after surgery (Baskar et al. 2012). Figure 1.6 describes some of the therapeutic approach limitations (Jabir et al. 2012).

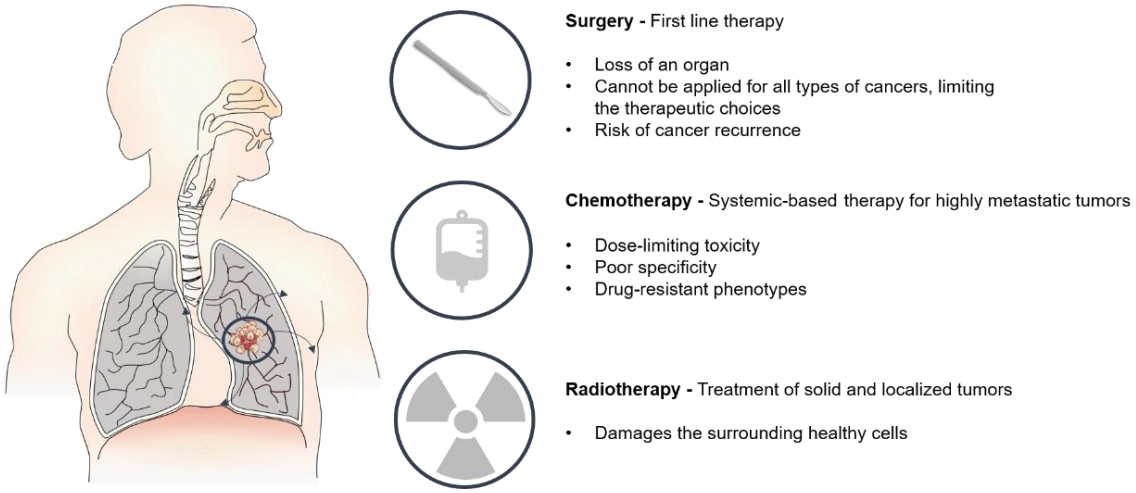


**Figure 1.6 -** Therapeutic options and their limitations. Adapted from (Jabir et al. 2012).

Unfortunately, tumor response to traditional therapeutic approaches are usually partial, brief, unpredictable and associated with high resistance (Souhami et al. 2002). To avoid these outcomes, new approaches in cancer treatment, namely immunotherapy, hyperthermia and nanoparticle targeted therapy, increase effectiveness, specificity, and capability of improving the patient's quality of life (Cabral & Baptista, 2014). However, the focus of this project is chemotherapy, which will be discussed in the following sub-chapter. For more information about the therapies mentioned before refer to: (Alderton & Bordon, 2012; Soares et al. 2012; Brannon-Peppas & Blanchette, 2012)

### 1.3.2 Chemotherapy

Chemotherapy is generally based on the use of chemical substances that target tumor cells in rapid proliferation, or other hallmark of tumor cells through its action on DNA synthesis, DNA repair systems, cell-cycle checkpoints, apoptosis, and angiogenesis. In addition, the adjustment of the damaging mechanism of the genes and the stopping of the blood supply to the cancer cells are also potential targets of chemotherapeutic drugs (Mehren, 2008). Chemotherapy drugs can be divided into five major groups according to its mode of action in tumor cells: alkylating agents, antimetabolites, anti-tumor antibiotics, topoisomerase inhibitors and mitotic inhibitors, among others (Table 1.1; Tukenova et al. 2010).

**Table 1.1 -** Main classes of chemotherapeutic drugs discriminating their main representatives, modes of action and adverse effects on patient organism.

| Agent Class | Chemotherapeutic drug | Mode of action | Adverse Effects |
|---|---|---|---|
| **Alkylating agents** | Cisplatin | Crosslinking of DNA chains | Myelosuppression, immunosuppression, nephrotoxicity |
| **Antimetabolites** | 5-Fluorouracil | Inhibition of enzymes Introduction of false substances in DNA | Myelosuppression, cardiotoxicity, alopecia |
| **Anthracyclines** | Doxorubicin | Inhibition of topoisomerase II | Cardiotoxicity, myelosuppression |
| **Mitotic inhibitors** | Paclitaxel | Antimicrotubular agent | Peripheral neuropathy |

Briefly, the alkylating agents, which include platinum drugs, act through the covalent binding of hydrocarbons or alkyl groups to cell's DNA, causing DNA cross-links and strand breaks leading to either apoptosis or necrosis. On the other hand, antimetabolites are agents that compete with physiologic molecules during the formation of cellular macromolecules through their incorporation into macromolecules framework affecting their normal functionality in cells. Most of these chemotherapeutic agents are cell-phase specific because their affect the DNA or ribonucleic acid (RNA) synthesis by either replacing a nucleotide (e.g., 6-mercaptopurine) or repressing nucleotide synthesis (e.g., methotrexate and 5-fluorouracil), resulting in the formation of truncated cellular proteins, and ultimately apoptosis (Mihlon et al. 2010). Anti-tumor antibiotics, which include anthracyclines interfere with enzymes involved in DNA replication (e.g., doxorubicin) whereas, topoisomerase inhibitors, which also include the doxorubicin, are responsible for the inhibition of the action of DNA topoisomerases I or II. Topoisomerases are enzymes that relieves the torque on the double helix of DNA allowing the strand to unwind, and then re-annealing the free ends. Doxorubicin inhibits the re-annealing reaction, and the accumulation of DNA strand breaks, ultimately leading to apoptosis or cell necrosis. Mitotic inhibitors derived from natural products (e.g., paclitaxel) have as cellular target the microtubules which are responsible for the cytoskeletal framework of a cell that allows intracellular transport of cellular components and mitosis during the cell division. Some of these anticancer agents will be discussed in more detail in the following two sub-chapters according to the malignancy in study (ovarian carcinoma; Mihlon et al. 2010).

The use of systemic chemotherapeutic drugs is associated with high tissue toxicity, unspecific biodistribution and development of multidrug resistance (MDR) patterns (Crawford, 2013). MDR is often associated with an outgrowth of one tumor cell clone that has additional genetic changes (Mehren, 2008) being an obstacle to attempt to improve the prognosis of patient (Jabir et al. 2012). The two mechanisms responsible for chemoresistance in cancer include the acquired and *de novo*. While the acquired resistance is associated with the exposure of tumor cells to therapeutic agents, *de novo* resistance is associated with the adhesion of tumor cells to ECM (Lovitt et al. 2014). In addition, the reduced drug effectiveness during treatments is related to non-specific mechanisms, such as the increase of drug

efflux from tumor cells, down- or up-regulation of a drug target, existence of cancer stem cells and the influence of tumor microenvironmental components (Figure 1.7; Lovitt et al. 2014).

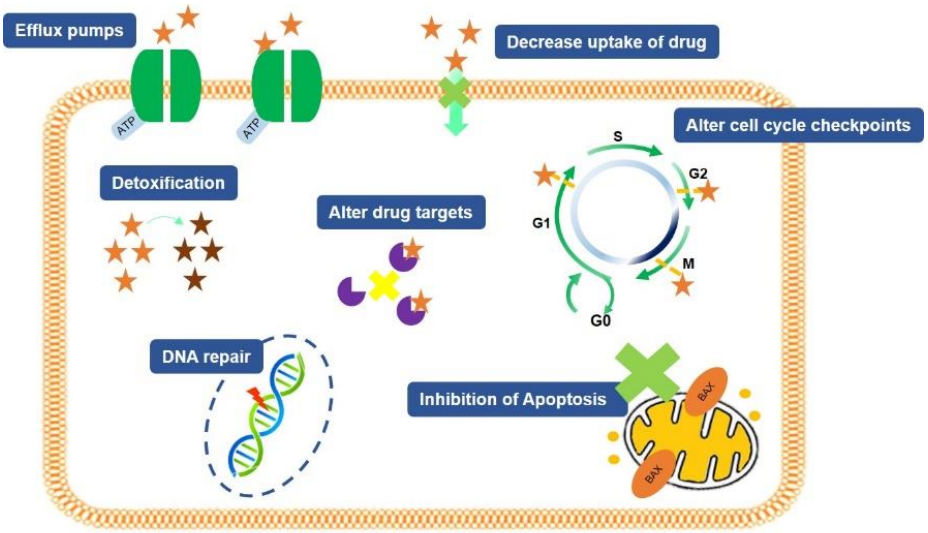


**Figure 1.7 -** Multiple mechanisms responsible for chemoresistance in tumor cells. These includes decreasing drug accumulation in tumor cells through efflux pumps, increasing cellular detoxification, altering the cell cycle checkpoints, altering the drug targets, inducing a response anti-apoptotic and, finally, increasing the mechanisms involved in DNA repair. Adapted from: (Chai et al. 2010; Kigawa 2013).

Over the past years, significant efforts have been made to improve both early detection of cancer and new therapies. In spite of that, the mortality rates associated with cancer have not significantly reduced being this malignancy the major health problem worldwide. In addition to the reasons described above, and considering the side effects of current anticancer drugs, is important the development and synthesis of new molecules with more efficiency and efficacy for cancer treatments.

#### 1.3.2.1 Ovarian Cancer: principal features and therapeutic approach

Ovarian carcinoma (OC) is the fifth leading cause of cancer-related mortality in women with more than 40 000 new cases annually in the European Union (Colombo et al. 2010). OC is a deadly and highly metastatic disease with a 30 to 92% of 5-year survival rate depending on the spread of disease at diagnosis (Yap et al. 2009). The high morbidity and mortality associated with OC is related with the late diagnosis which, in turn, is related with not explicit symptoms, where most patients show metastatic spread beyond the ovaries (Goff et al. 2000; Smith et al. 2005; Binaschi et al. 2011).

OC is a disease predominantly associated with older being 80% of diagnosed cases in postmenopausal women (aged over 50 years; Ledermann et al. 2013). Although the exact etiologic factor responsible for the development of OC remains unknown, the risk of the disease is inversely proportional to the number of lifetime ovulations. Several studies considered that the OC is more common in industrialized countries, and available epidemiologic data suggest that some environmental (e.g., obesity and cigarette smoking) and ethnicity factors may contribute to development of the cancer, although this

remains uncertain (Jelovac & Armstrong, 2011). Additionally, it is known that genetic factors have the most potent impact i.e., family history plays a very important role in the development of the disease because women with a first-degree relative have more than a twofold increase in risk of OC compared with women with no family history of OC. Additionally, hereditary OC results in the earlier development of the disease, approximately 10 years earlier, than women with non-hereditary ovarian cancer (Ledermann et al. 2013).

Standard treatment for OC include debulking surgery and six cycles of platinum/taxane-based chemotherapy (i.e., the combination of cisplatin or carboplatin and paclitaxel or docetaxel) resulting in a complete clinical remission in most of the patients (Smolle et al. 2013; American Cancer Society, 2016). Platinum-drugs (e.g. cisplatin and carboplatin) forms inter- and intra-strand crosslinks on DNA which are then recognized by the cellular machinery that either repairs the lesion or induces apoptosis. The mechanism by which platinum-drugs lead to apoptosis is through inhibition of transcription i.e., the RNA polymerases stalls at the platinum cross-link, recruiting then the transcription-coupled repair machinery and being unable to repair the lesion, the cell evokes a programmed cell death pathway (Agarwal & Kaye, 2003; Johnstone et al. 2014). Paclitaxel and docetaxel (taxanes) are anti-microtubule agents that irreversibly binds to the protein β-tubulin promoting the microtubule stabilization which results in G2–M arrest and apoptosis, via both p53-dependent and -independent pathways (Agarwal & Kaye, 2003; Jimenez et al. 2011).

Besides the efforts for the adequate primary treatment, patients evidence an overall unfavourable prognosis in part caused by the early development of chemotherapy resistance, a main factor in cancer-associated mortality, and ultimately death by recurrent disease (Chien et al. 2013; Vergote, 2014). The length of the disease-free period following response to platinum-based chemotherapy can be used to categorize patients into three groups based in clinical evidence: platinum refractory, platinum-resistant, and platinum-responsive (Figure 1.8; Chien et al. 2013).

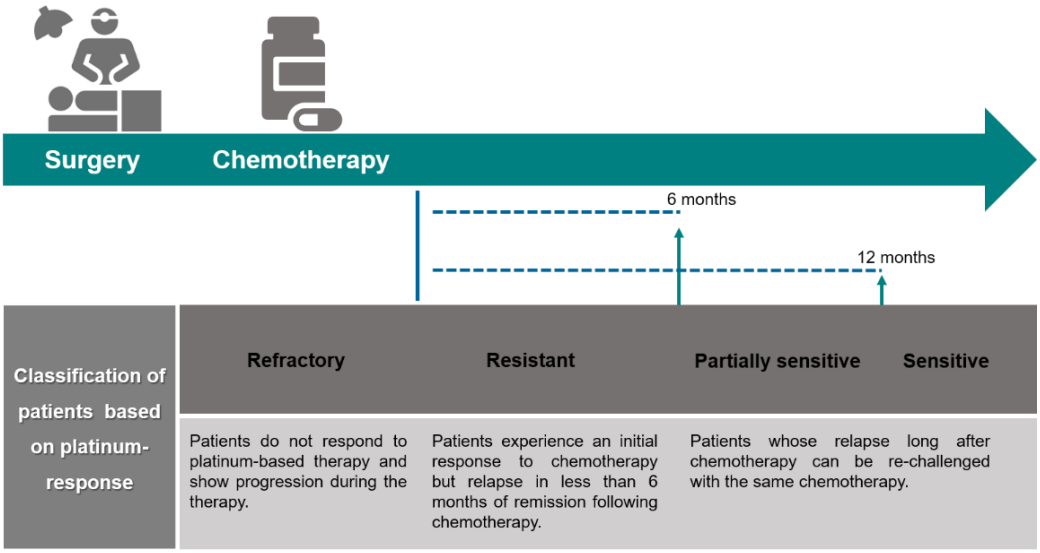


**Figure 1.8 -** Classification of ovarian carcinoma patients according with their platinum-response. Second-line treatment is needed for the most of patients. Platinum sensitivity is a good predictor of response. Platinum refractory disease and platinum-resistant disease has a bad prognosis while platinum sensitive patients have a long interval between diagnosis and recurrence show a better survival. Adapted from (Chien et al. 2013; Smolle et al. 2013).

Considering all outcomes described above it is urgent to develop more effective and targeted therapies, since the biology of OC is very heterogenous, leading to the overall improvement of OC patient's quality of life (Vergote, 2014). The development of molecular targeted therapies, including small-molecule inhibitors and monoclonal antibodies that target multiple crucial cancer characteristics – angiogenesis, survival, cell growth and metastases have been recently described (Yap et al. 2009; Coward et al. 2015).

### 1.3.3 Derivatives of spirooxindoles in cancer therapy

Spirooxindoles are important compounds composed by a spiro system fused at the 3-position (C3) a varied of heterocyclic motifs (Figure 1.9), found in many natural products with pharmacological interest (Galliford & Scheidt, 2007). In drug discovery, spirooxindole scaffold represents a crucial structure for the synthesis of synthetic and natural compounds with biological activity since they incorporate both oxindoles and other heterocyclic moieties simultaneously (Yu et al. 2015).

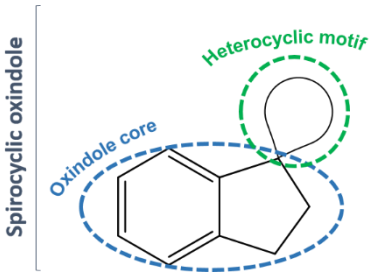


**Figure 1.9 -** Spirocyclic oxindoles scaffold. Adapted from (Yu et al. 2015).

At the moment, spirooxindole derivatives are under intense research due to their vast range of bioactive properties such as anticancer, murine double minute 2 (MDM2) antagonists, ion channel blockers, antimicrobial and antimalarial activities (Santos, 2014). The Santos' group has been studying the *in vitro* antitumoral activity of a series of novel spiropyrazoline oxindole derivatives against human cancer cell lines, including the compound in study (5-bromo-2',4',5'-triphenyl-2',4'-dihydrospiro[indoline-3,3'-

pyrazol]-2-one (AM130); Monteiro et al. 2014; Ribeiro et al. 2016; Nunes 2016). The overall research development by the team demonstrated that these agents are able to inhibit the growth of cancer cells with high selectivity. Additionally, the loss of cell viability, as a result of these agents' action, is associated with the p53 stabilization and transactivation, the induction of apoptosis, as well as the inhibition of the interaction between p53 and MDM2. Considering that the p53 tumor suppressor is the "guardian of the genome" that plays a significant role in the regulation of several biological processes, restoring its function in cancer cells represents a valuable anticancer approach, that has been immensely study by Santos' group. In this sense, the present project arises as a continuation of the study developed by Nunes, 2016.

### 1.4 Rationale and aims

There is a growing demand for chemotherapeutic agents that can selectively inhibit tumor growth with the subsequent reduction of deleterious effects in healthy tissue and capable to avoid the development of drug resistance profiles (Silva et al. 2014). Considering this, the present study aims to explore the cytotoxic potential and mode of action of a novel anticancer agent, referred as AM130 synthetized for the first time by Santos' group (Monteiro et al. 2014). To accomplish these aims after compound synthesis, several biological assays were performed as described in Figure 1.10.

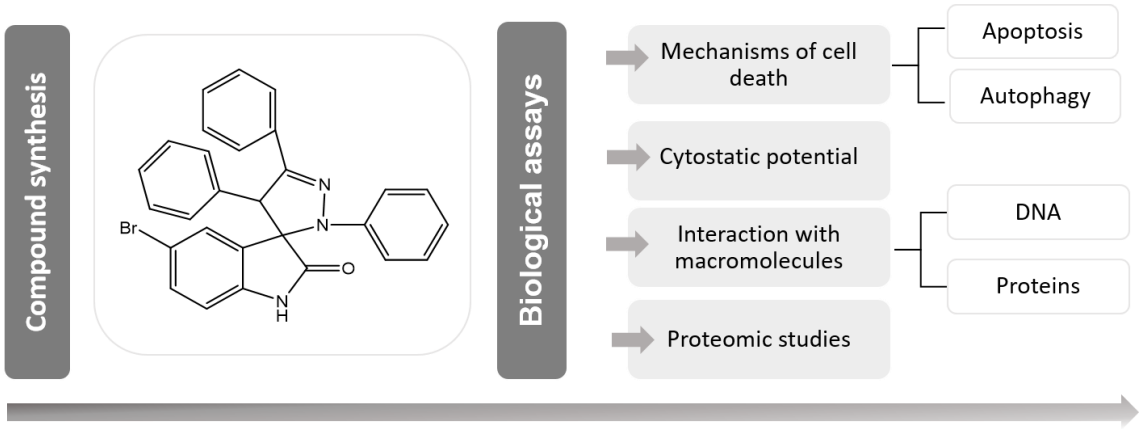


**Figure 1.10 -** Workflow process for AM130 chemotherapeutic agent study in cancer cells and healthy cells.

# 2 MATERIALS AND METHODS

## 2.1 Compound characteristics

### 2.1.1 Synthesis

The 5-bromo-2',4',5'-triphenyl-2',4'-dihydrospiro[indoline-3,3'-pyrazol]-2-one named during this project by AM130 compound was synthesized at Faculdade de Farmácia (Universidade de Lisboa) according to the procedure described by Monteiro et al. 2014.

#### 2.1.1.1 Synthesis of (*E)*-3-benzylidene-5-bromoindolin-2-one

A solution of 5-bromoindoline-2,3-dione (1.3 x $10^{-3}$ mol; 300 mg; 1.0 equiv.), ethylene glycol (2.2 mL) and hydrazine monohydrate (3.8 x $10^{-3}$ mol; 0.15 mL; 2.5 equiv.) was heated under reflux for 4 h under nitrogen atmosphere. The resulting brown solution was filtrated. The resulting 5-bromoindolin-2-one was dissolved in ethanol (11 mL), and then benzaldehyde (1.6 x $10^{-3}$ mol; 164 µL; 1.6 equiv.) and piperidine (1.5 x $10^{-3}$ mol; 145 µL; 1.0 equiv.) were added. After 1 h 30 min at reflux, the reaction was placed at -20ºC to obtain a precipitate, which was filtrated and dried in vacuo overnight. The residue was purified by flash column chromatography using ethyl acetate/n-hexane 1:2 as eluent, followed by purification using silica gel preparative chromatography (yield 16.3%; 65.8 mg; Sun et al. 1998).

#### 2.1.1.2 Synthesis of AM130

*(E)-3*-benzylidene-5-bromoindolin-2-one (2.4 x $10^{-4}$ mol; 36.7 mg; 2.0 equiv.) was dissolved in dry dichloromethane (20 mL) and *(Z)-N*-phenylbenzohydrazonoyl chloride (5.6 x $10^{-3}$ mol; 56.4 mg; 2.0 equiv.) and triethylamine (7.3 x $10^{-4}$ mol; 56.8 µL; 3.0 equiv.) were added. The reaction was stirred at room temperature (RT) for 9 h. Then, distillated water (20 mL) was added to the reaction, the phases were then separated and the aqueous phase was extracted three times with ethyl acetate (10 mL). The combined organic phases were dried and concentrated. After flash column chromatography (eluent: ethyl acetate/n-hexane 1:2), the product was washed with diethyl ether resulting in a white solid (yield 18%; 10.8 mg) – 5-bromo-2',4',5'-triphenyl-2',4'-dihydrospiro[indoline-3,3'-pyrazol]-2-one (AM130). The $^{1}$H nuclear magnetic resonance spectroscopy of compound were was in accordance, with the one reported (Monteiro et al. 2014).

### 2.1.2 General preparation of AM130 for biological assays

For biological studies, AM130 compound was dissolved in dimethyl sulfoxide (DMSO, Sigma, St. Louis, EUA) obtaining a final concentration of 100 mM and divided in aliquots with 100 mM or 10 mM. DMSO is the most common organic solvent used due to its good solvating ability, relative chemical inertness and, high boiling and freezing points. The samples dissolved in this solvent can be stored either at RT or in a frozen state and thawed when needed (Cheng et al. 2003). The compound dissolved in DMSO and in powder was stored at -20°C.

#### 2.1.2.1 Effects of freezing and sonication of an AM130 solution in DMSO

The spectra of AM130 in DMSO was analyzed by UV–Visible spectroscopy (230–600 nm) in an Evolution 300 UV–Vis spectrophotometer (Thermo Fisher Scientific, Madison, USA) using a quartz cuvette of 1 cm path length. Initially, a range of dilutions was made from a stock solution with 100 mM (10; 25; 50; 75; 100 and 200 µM) under two conditions: immediately after its solubilization in DMSO i.e., without freezing the solubilized compound and 1 week after freezing (-20°C). In addition, to verify the effects of sonication (sonicator Elma, D-78224 Singen/Htw, Germany) in compound solubility, AM130 UV-Vis spectra was also analyzed with 100 µM after 72 h of freezing through two conditions: sonicated and not sonicated.
Compound stability was previously performed in phosphate buffered saline (PBS) at 37ºC for 72 h by Nunes, 2016.

## 2.2 Human cell lines culture

### 2.2.1 Cell line characteristics

Human cancer cell lines are an integral part of drug discovery practices and for that, during the present project three types of adherent human cancer cell lines, HCT116 (colorectal carcinoma), MDA-MB-453 (breast adenocarcinoma) and A2780 (ovarian carcinoma), were used to characterize the antiproliferative potential of AM130 compound described in Section 2.1. In addition, to evaluate the cytotoxic effect of the compound in normal cells, a culture of normal human fibroblast was also used. All cells lines used in this study were obtained from American Type Culture Collection (ATCC®). Cell lines used, source, cells morphology and growth medium are summarizing in Table 2.1.

**Table 2.1 -** HCT116, MDA-MB-453 and A2780 cell lines and normal human fibroblast used during this project and respective typical characteristics namely source, morphology, and growth medium. DMEM - Dulbecco's Modified Eagle Medium (Invitrogen, New York, EUA); RPMI - Roswell Park Memorial Institute medium (Invitrogen, New York, EUA); FBS – Fetal Bovine Serum (Invitrogen, New York, EUA); Penicillin/Streptomycin (antibiotic) + Antymicotic (Invitrogen, New York, EUA); MEM non-essential amino acid 100x (Sigma, St. Louis Missouri, EUA). Cells Source: ATCC – The Global Bioresource Center, 2015.

| Cell line | Source | Morphology | Growth medium % (v/v) |
|---|---|---|---|
| **HCT116** | Colorectal carcinoma | Epithelial | DMEM<br>FBS 10%<br>Pen/Strep 1%<br>MEM 1x |
| **MDA-MB-453** | Breast adenocarcinoma | Epithelial | DMEM<br>FBS 10%<br>Pen/Strep 1%<br>MEM 1x |
| **A2780** | Ovarian carcinoma | Epithelial | RPMI<br>FBS 10%<br>Pen/Strep 1%<br>MEM 1x |
| **Fibroblasts**[a] | Human dermis | Sindle-shaped/ bipolar and refractile | DMEM<br>FBS 10%<br>Pen/Strep 1%<br>MEM 1x |

[a] Healthy culture

### 2.2.2 Cell culture maintenance

HCT116 and MDA-MB-453 cell lines were grown in DMEM and A2780 cells in RPMI, supplemented with 10% (v/v) FBS, MEM 100x and 1% (v/v) antibiotic/antimycotic solution (Pen-Strep+antimycotic: 10000 units/mL of penicillin, 10000 µg/mL of streptomycin and 25 µg/mL of Fungizone® Antimycotic), which is named by complete culture medium recipe (CCR; see Table 2.1). Normal human fibroblasts were cultivated in the same growth conditions of HCT116 and MDA-MB-453 cell lines. HCT116 and A2780 cell lines were maintained in 75 $cm^2$ vented cell culture flasks and MDA-MB-453 cells and normal human fibroblast in 25 $cm^2$ vented cell culture flasks (SPL Life Sciences, Korea) in an incubator (SANYO $CO_2$ Incubator, Electric Biomedical Co., Osaka, Japan) with controlled atmosphere (5% (v/v) $CO_2$ and 99% (v/v) humidity) at 37°C.

Upon reaching 80% cell confluency (Olympus CXX41 inverted microscope, Tokyo, Japan), cells were subcultured to avoid absence of nutrients in the growth medium and loss of growth due to contact inhibition. For this purpose, initial medium was discarded and replaced by 3 mL and 2 mL (for 75 and 25 $cm^2$ flasks, respectively) of Tryple™ Express (Invitrogen, New York, EUA), a trypsin analogous whose function is to help cells to detach from the culture flaks, and incubated at RT. After 10 min, Tryple™ Express action was neutralized by addition of 3 mL and 2 mL (for 75 and 25 $cm^2$ flasks, respectively) of fresh CCR medium. The total cell suspension was transferred to 15 mL Falcons tubes (SPL Life Sciences, Korea) and centrifuged for 5 min under 500 x g at 15°C (Sigma 3-16K 10280, Tuttlingen, Germany). The supernatant obtained, which includes Tryple™ Express, old medium and cellular debris, was discarded and the remaining pellet was resuspended in 1 mL of fresh CCR medium.

Cells were counted using the trypan blue exclusion method in an hemocytometer (Hirschmann, Eberstadt, Germany) from a mixture of 350 µL of CCR medium, 100 µL of 0.2% (v/v) trypan blue (Sigma, St. Louis, EUA) and 50 µL of cellular suspension obtained during the subculturing process. Trypan blue is known to dye to cells with loss of membrane permeability thus, excluding unviable cells from count. The cells were observed using Olympus CXX41 inverted microscope, Tokyo, Japan. The final assessment of cell density (in cells/mL) is obtained by multiplying the number of total cells counted, the volume of the hemocytometer ($10^4$ $mL^{-1}$) chamber and the dilution factor (10) divided by the number of squares counted, as represented in the following Equation (1):

$$\textbf{Total cells/mL} = \frac{\textbf{Total cell counted x 10 x } 10^4}{\textbf{Number of squares}}$$

**Equation 1**

Applying the Equation (1), it was possible to estimate the appropriate volume of the cell suspension to add in a new 75 and 25 $cm^2$ vented cell culture flasks with 13 mL and 5 mL, respectively, of fresh CCR medium. Cells were incubated at 37°C in a controlled atmosphere of 5% (v/v) $CO_2$ and 99% (v/v) humidity.

### 2.3 *In vitro* cytotoxicity assessment

Cell viability assay was performed in HCT116, MDA-MB-453 and A2780 cell lines as well as in healthy cells using a homogeneous, colorimetric method applied to determine the number of viable cells in proliferation – CellTiter 96 Aqueous Non-Radioactive Cell Proliferation Assay (Promega, Madison, USA; Silva et al. 2012). The CellTiter 96® AQueous Assay is composed by two solutions: *[3-(4,5-dimethylthiazol-2-yl)-5-(3-carboxymethoxyphenyl)-2-(4-sulfophenyl)-2Htetrazolium]*, inner salt (MTS) and phenazinemethosulfate, an electron coupling reagent (Promega, 2012).

A control experiment to study the interference of the compound with the MTS reagent was performed. Additionally, the cytotoxic potential of common chemotherapeutic agents, such as cisplatin and doxorubicin (Sigma, St. Louis, EUA), was also assessed.

#### 2.3.1 Cell culture

For the dose-response curves, the cell density (in cells/mL), determined by the exclusion method (Section 2.2.2; Equation 1), was diluted to 0.75 x $10^5$ cells/mL using the appropriated CCR medium and seeded in a 96-well plate (SPL Life Sciences, Korea). After 24 h of incubation at 37°C in a 5% $CO_2$ (v/v) and 99% (v/v) humidity atmosphere, the cells plated were observed using the inverted microscope and their adherence were confirmed.

#### 2.3.2 Compound exposure

CCR medium was removed after 24 h and replaced by fresh CCR medium containing: 0.5, 1, 5, 10, 25, 50 and 75 µM of AM130 compound or 0.1% (v/v) DMSO (vehicle control). The 96-well plates were

incubated under the same conditions during 48 h. A total of three biological experiments with technical duplicates were performed for each condition.

### 2.3.3 Cell Viability assay

After 48 h of cell incubation in the presence or absence of compound, cell viability was evaluated through CellTiter 96® AQueous Non-Radioactive Cell Proliferation Assay. Briefly, the medium was removed and 100 µL of a solution mixture of fresh CCR medium and MTS reagent (20 µL reagent to 100 µL of CCR medium) was added to each well. Then 96-well plates were incubated during, approximately, 45 min under the same conditions described above. Afterwards, the absorbance at 490 nm was measured with Tecan Infinite F200 Microplate Reader (Tecan, Männedorf, Switzerland). Obtained data were normalized relatively to control samples (DMSO) to obtain cell viability for each concentration with Equation (2):

$$\textbf{Cell Viability}\ (\%) = \frac{\textbf{Samples absorvance}\ (\textbf{490 nm})}{\textbf{Control absorvance}\ (\textbf{490 nm})}\ \textbf{x 100}$$

**Equation 2**

Results are expressed as relative $IC_{50}$ values, determined using the *GraphPadPrism 6* software (Graph Pad Software Inc., San Diego, Ca, USA). Relative $IC_{50}$ corresponds to the halfway point from maximum viability plateau and minimum viability plateau from an inhibition curve, not always corresponds to a 50% of cell viability, being the accepted concept for the study. However, the absolute $IC_{50}$ value corresponds to a compound concentration that causes 50% of cell metabolic inhibition (Neubig et al. 2003).

## 2.4 Assessment to cell death

### 2.4.1 Cells staining with Hoechst 33258 – Propidium Iodide

A2780 cells treated with AM130 compound were evaluated by nucleic acid staining with Phenol, *4-[5-(4-methyl-1-piperazinyl) [2,5'-bi-1H-benzimidazol]-2'-yl]-, trihydrochloride 23491-45-4* (Hoechst 33258) and propidium iodide (PI; Sigma, St. Louis Missouri, EUA). Hoechst 33258 and PI staining methods, with the analysis of apoptotic and necrotic cells, respectively, through fluorescence microscopy, constitutes a preliminary assay to evaluate viability loss due to compound' action. Briefly, cells were collected by the procedure described in Section 2.2.2 and plated in 2-well cells culture slide (SPL Life Sciences, Korea) at 0.75 $x10^5$ cells per mL diluted in fresh CCR medium and incubated in a humidified atmosphere at 37°C. After 24 h of incubation, depleted CCR medium was replaced by AM130 compound with $IC_{50}$ concentration (8.5 µM) or 0.1% (v/v) DMSO (vehicle control) diluted in fresh CCR medium. Following 48 h of incubation at the same conditions described previously, medium was discarded once more and cells were washed twice with PBS 10x (Invitrogen, New York, EUA) supplemented with 5% (v/v) FBS. Afterwards, cells were readily fixed to microscope slides with 4% (v/v) paraformaldehyde (PFA; Invitrogen, New York, EUA), at RT in the absence of light for 20 min. For cell staining, PFA was removed and cells were washed three times with PBS 10x supplemented. For nuclei detection, 400 µL solution of Hoechst 33258 and PI was added, containing Hoechst 33258 (5 µg/mL), PI (25 µg/mL) in

PBS 10x supplemented and incubated in the absence of light, at RT, for 15 min, followed by three times washing with PBS 10x supplemented. Before lamellae preparation with a droplet of glycerol, cells were washed again with PBS 1X.

Fluorescent nuclei were analyzed based on the chromatin condensation degree and characteristics. Normal nuclei showed non-condensed chromatin uniformly distributed over the entire nucleus, whereas apoptotic nuclei showed condensate or fragmented chromatin with a bright non-homogenous blue fluorescence. In addition, some cells formed apoptotic bodies. On the other hand, nuclei of necrotic cells showed a bright pink fluorescence. The samples were photographed in an Olympus BX51 fluorescent microscope with an attached Olympus DP50 (Olympus) camera and the photographs were acquired with Infarview software, and three random microscopic fields per sample with *ca.* 50 nuclei were counted. Mean values were expressed as the percentage of apoptotic nuclei.

### 2.4.2 Annexin V-FITC and PI double-staining assay

The annexin V-binding assay using flow cytometry is considered one of the most sensitive and reliable technique to detect and distinguish between early apoptosis and late apoptosis, as well as necrosis (Henry et al. 2013). However, due to the staining difficulties of A2780 cells, we performed the assay with the HCT116 cell line (also with a low $IC_{50}$) instead of the A2780 cell line.

To quantify AM130-induced cell death in HCT116 cells a double-staining with fluorescein isothiocyanate (FITC) label and annexin V and PI was performed. HCT116 cells were seeded in 35 mm culture dishes (VWR, Europe) at $1x10^5$ cells/mL and incubated in the conditions described in section 2.2.2. Culture medium was removed after 24 h and replaced with 1 mL of fresh CCR medium containing either $IC_{50}$ compound concentration or 0.1% (v/v) DMSO (vehicle control). Cells were incubated for 48 h, collected by trypsinization and centrifuged at 1000 x g for 5 min at RT. The obtained pellet was rinsed twice with 1 mL of cold PBS 1x intercalated with 5 min of centrifugations at 1000 x g. Following centrifugations, 100 µL of annexin binding buffer 1x, 5 µL of annexin V-FITC and 2 µL of PI (Annexin V-FITC Apoptosis Detection Kit; Invitrogen, USA) was added to all samples and incubated for 15 min at RT, in the absence of light. Afterwards, to these cellular suspensions were added 400 µL of annexin binding buffer 1x and 500 µL of cold PBS 1x. The analysis and quantification of apoptotic events and necrosis were performed by flow cytometry on Attune® Acoustic Focusing Flow Cytometer (Life Technologies, Carlsbad, California) using an *Attune® Cytometric* software (Life Technologies), with the acquisition of at least 10 000 events per sample. Data presented here are from two independent experiments.

### 2.4.3 Measurement of mitochondrial membrane potential ($\Delta\Psi_M$)

The mitochondrial membrane potential ($\Delta\Psi_M$) is an important parameter of mitochondrial function and, because of that, is an indicator of cell health (Christensen et al. 2013). To measure $\Delta\Psi_M$ a lipophilic cationic dye — 5*,5',6,6'-tetrachloro-1,1',3,3'- tetraethylbenzimi-dazolyl-carbocyanine iodide* was used (JC-1; Abnova Corporation, Walnut, CA, USA).

A2780 cell lines were seeded into 8-well cells culture slide (SPL Life Sciences, Korea) at 0.75 × $10^5$ cells/well density and incubated during 24 h in the same conditions described in Section 2.2.2. After incubation, A2780 cells were treated with 8.5 µM of AM130 compound or 0.06% (v/v) DMSO (vehicle control) diluted in CCR fresh medium and incubated for 48 h. For the measurement of the fluorescence intensity, cells were stained with JC-1 staining solution for 20 min at 37°C in dark condition, followed by their visualisation with Olympus Bx51 microscope equipped with Olympus DP50 camera using the same exposition time for all samples. By *ImageJ* software (National Institutes of Health (NIH), Bethesda, MD, USA), green to red fluorescence ratio of each sample was determined. Experiments were repeated two times using two independent biological experiments.

### 2.4.4 Analysis of AM130-regulated apoptotic proteins by Western Blot

#### 2.4.4.1 Sample Preparation

For whole protein extraction, A2780 cells were seeded in 75 $cm^2$ vented cell culture flasks at a cell density of 4 x $10^6$ cells, in the same conditions mentioned in section 2.2. After 24 h, depleted medium was removed and fresh CCR medium was added with the $IC_{50}$ corresponding compound concentration (8.5 µM) or with 0.1% (v/v) DMSO (vehicle control). After 48 h, cell samples were washed twice with PBS 1x and collected with a scrapper to a microtube on ice. All samples were centrifuged at 500 x g, for 5 min at 4ºC, and the supernatant discarded. Then, the pellets were washed one more time with PBS 1x and centrifuged at 900 x g for 5 min at 4ºC, and to ensure that all PBS was removed to not dilute cell lysis solution, a final spin was performed. Additionally, samples were resuspended in 100 µL of cell lysis solution containing NaCl-Tris-EDTA buffer (150 mM NaCl; 50 mM Tris, pH=8; 5 mM EDTA), phosphatase inhibitors 1x (PhosStop, Roche), protease inhibitors 1x (complete ULTRA Tablets, Mini, EASYpack, Roche, Switzerland), 0.1% (w/v) dithiothreitol (DTT; AMRESCO, USA), 1 mM of phenylmethylsulfonyl fluoride (PMSF; Sigma, St. Louis, EUA), and 2% (w/v) Nonidet P-40 (Thermo Scientific, MA, EUA) and samples were stored at -80ºC, until further processing. After thawing, all samples were submitted to 2 min 30 s of continue pulses at ultrasonicate bath in ice and maintained on ice for 1 min to overcome protein loss and overheating. Cell lysates were centrifuged 8000 x g for 10 min at 4ºC and supernatants were recovered.

For total protein quantification, Pierce Protein Assay kit (Thermo Scientific, MA, USA) was used. Initially, a calibration curve was established with several standard BSA solutions from 0 to 1000 µg/mL (Thermo Scientific, MA, USA) and the protein extracts were diluted in 1:10 proportion in ultrapure water (18.2 $M\Omega.cm^{-1}$ at 25°C). Sequentially, 150 µL of Pierce reagent were added followed by 5 min of incubation at RT in absence of light. Absorbance was measured with with Tecan Infinite F200 Microplate Reader at 660 nm. After quantification, exactly 50 µg were transferred to another microtube together with Sodium dodecyl sulfate (SDS) Loading Buffer 4X and 3% (w/v) DTT, boiled for 1 min, and immediately put on ice. Before loaded the samples into the gel 1 µL of 30% (w/v) DTT was added to samples.

#### 2.4.4.2 SDS-PAGE and transfer to nitrocellulose membrane

A SDS-PAGE gel was prepared, and ran at 120 V and 50 mA during 1 h. After the SDS-PAGE was complete, electrotransfer to a nitrocellulose membrane was performed. For that, a sandwich was prepared with the gel in contact with the membrane, between a pair of filter paper sheets and sponges. The wet transfer was set up, and the tin was filled with cold 1x transfer buffer (25 mM Tris, 192 mM Glycine, 20% (v/v) methanol, pH ~8.3) until the sandwich was fully covered. The transfer process occurred overnight at 40 V at 4ºC and, to finish the process, 1 h at 100 V.

#### 2.4.4.3 Primary and secondary antibody incubation

The membrane was incubated for 1 h with fresh 5% non-fat milk in 1x TBST buffer (50 mM Tris, 150 mM NaCl and 0,1% (v/v) Tween 20, pH ~7.5) to block non-specific protein bidding. Then, each nitrocellulose membrane was exposed to different primary antibody in 5% non-fat milk in TBST, namely anti-Bax (1:5000; Abcam, United Kingdom), anti Bcl-2 (1:1000; Sigma, St. Louis, EUA) and anti-PARP (1:500; Thermo Scientific, MA, USA) and was left to incubate for 1 h at RT, with constant agitation. Concluded this incubation, the membrane was washed three times with 1x TBST buffer with agitation for 5 min at RT. The same procedure above was also employed to the membrane incubation with the secondary antibody (1:3000, Anti-mouse IgG, horseradish peroxidase (HPR)-linked Antibody or 1:2000, Anti-rabbit IgG, HPR-linked Antibody; Cell Signalling Technology, USA). All membranes were stripped with stripping buffer (0.1M glycine, 20 mM magnesium acetate and 50 mM potassium chloride) and, then, re-incubated with anti-ß actin (1:5000; Sigma, St. Louis, EUA) as a control for further normalization of the results.

To detect the protein bands on the membrane, a WesternBright ECL subtract (Advansta, USA) was prepared. ECL is an enhanced chemiluminescent substrate for detection of HRP activity from secondary antibodies. The membrane was then totally covered in substrate and incubated for 5 min. Sequentially, the film was exposed to the membrane, on a dark room. The quantification of proteins was determinate by densitometry using *Image J* software. BAX and BCL-2 data are from two independent experiments whereas PARP cleavage is from one assay.

### 2.4.5 Measurement of production of intracellular reactive oxygen species

Reactive oxygen species (ROS) Detection Reagents (Life Technologies, Invitrogen™, USA) was used to detect the accumulation of intracellular ROS in A2780 cell lines through the oxidation of dichlorofluorescein-diacetate ($H_2$DCF-dA). $H_2$DCF-dA when oxidized by peroxides is converted into a high fluorescent component named 2,7-dichloroflurescein (DCF), which in turn is directly proportional to amount of ROS in cells (Marchi et al. 2012). Briefly, for the $H_2$DCF-dA staining assay, A2780 cells were seeded in the same conditions describe in 2.4.3 section. After the incubation period, the medium was removed and replaced by fresh CCR medium containing 8.5 µM of compound, 0.03% (v/v) DMSO (vehicle control), CCR medium for the corresponding untreated cells and 25 µM of $H_2O_2$ for considering 100% of ROS generation. After 48 h of exposure to the treatments mentioned, cells were washed gently

three times with PBS 1x and stained with 100 mM of $H_2$DCF-dA in a pre-warmed PBS 1x and incubated for 20 min at 37°C, protected from light. The unbound $H_2$DCF-dA was removed by washing the cells three times with PBS 1x and, then, fixed with 4% (v/v) PFA and incubated at RT during 20 min. The fluorescence of DCF was visualized and images were captured using the fluorescence microscopy (Olympus BX51 fluorescent microscope). Mean fluorescence intensity (MFI), an index of the amount of ROS produced in A2780 cells, was analyzed by *ImageJ* software. Measurements were from two independent experiments.

### 2.4.6 Assessment to autophagic potential

The CYTO-ID® Autophagy Detection Kit (Enzo Life Sciences, UK) was used for the detection of autophagy in A2780 cells by fluorescence microscopy. Before seeding A2780 cells, the lamellae (VWR, Europe) were dipped in 70% (v/v) ethanol and dried, followed by PBS 1x wash. Cancer cell line were plated in lamellae in 24-well plates (VWR, Europe) at a density of 75.000 cells/well diluted in 500 µL of fresh CCR medium. They were allowed to adhere for 24 h at 37°C in an incubator with 5% (v/v) $CO_2$ and 99% (v/v) humidity atmosphere. After incubation, the culture medium was removed and cells were treated with the previously-determined $IC_{50}$ concentration (8.5 µM) or 0.1% (v/v) DMSO as a negative control, and incubated at the same conditions described previously. After 12 h, an autophagy inductor i.e., rapamycin (50 mM), was added to the corresponding well. Following 48 h of incubation, the supernatant was removed and the cells were washed twice with 200 µL of PBS 10x supplemented with 5% (v/v) FBS and stained with an autophagy staining solution which consists of Hoechst 33342 (1 mg/L), Cyto-ID® Green (Enzo Life Sciences, USA) and PBS 10x supplemented. The staining solution was removed after 30 min of incubation at 37˚C in a humidified incubator and cells were washed again with 200 µL of PBS 10x supplemented three times. For the cells fixation to lamellae it was used 4% (v/v) PFA, at RT in the absence of light for 20 min, followed by three times wash with 200 µL of PBS 10x supplemented. Before microscope slide preparation with a droplet of glycerol, cells were washed with PBS 1X and then visualized and photographed in an Olympus BX51 fluorescent microscope with an attached Olympus DP50 (Olympus) camera. Photographs were acquired with Infarview software. The autophagic activity of AM130 was measure through counting the cells with autophagosomes or autophagolysosomes from two independent experiments.

## 2.5 Cell cycle Progression Assay

Cell cycle arrest, as a possible AM130 compound effect, was determined by DNA content analysis using PI staining – fluorescent intercalating agent with high affinity to nucleic acids – (Kim & Sederstrom, 2016) and analyzed by flow cytometry. Additionally, cell cycle synchronization was achieved by a double block with thymidine, a common S-phase blocker used to arrest and synchronize cells in the early S-phase (Bostock et al. 1971). However, as with apoptosis quantification (Section 2.4.2) due to difficulties in analyzing A2780 cell cycle progression, we proceed the study with HCT116 cell line (instead of A2780 cell line).

HCT116 cancer cells were seeded and incubated at 37ºC, 99% (v/v) humidity and 5% (v/v) $CO_2$ with a cell density of 1 x $10^5$ cells/mL. After 8 h of seeding, the first thymidine block was performed by the addition of 2 mM thymidine (Sigma, St. Louis, USA) in culture medium. Cells were incubated during 16 h and afterwards the old medium was depleted and replaced with fresh CCR medium without thymidine for an additional 10 h of incubation at same conditions described before. The second blockage was performed by adding 2 mM thymidine followed by a 14 h of incubation period. Finished the double block procedure, the medium was replaced by fresh CCR medium with AM130 $IC_{50}$ concentration or 0.1% (v/v) DMSO (vehicle control), and was left incubating during 4, 9, 12 and 24 h. After each time point, cells were collected by trypsinization with TrypLE™ Express and centrifuged for 5 min, 1000 x g at 4ºC. Supernatant was removed and the pellet was resuspended in cold PBS 1x. An additional centrifugation was performed in the previous mentioned conditions. Subsequently, supernatant was discarded and the pellet was resuspended in 1 mL of cold PBS 1x followed by 1 mL of 80% (v/v) ethanol solution cautiously with constant vortex agitation. Cell samples were then maintained on ice for a period of 30 min, and then stored at 4ºC for at least 18 h prior to analysis. In addition, cells from another disk were collected after thymidine block procedure and fixed, in the same conditions described previously, for synchronization control. Afterwards, cells were centrifuged for 5 min at 1000 x g at 4ºC. Supernatant was removed and resuspended in 50 μg/mL RNase A in PBS 1x and incubated at 37ºC for 30 min. PI was added to a final concentration of 2.5 μg/mL and DNA content was analyzed on Attune® Acoustic Focusing Flow Cytometer (Applied Biosystems) and the data collected were treated with *FCS Express 6 Flow Cytometry* software. The results are from two independent experiments.

### 2.6 Assessment to AM130 interaction with DNA

#### 2.6.1 Interaction with genomic DNA

The possible interaction between AM130 and genomic DNA in cell living context with the possibility of DNA fragmentation was assessed. For this purposed, A2780 cell line was collected by the proceed described in Section 2.2.2 and seeded in 25 $cm^2$ vented cell culture flasks at a density of 9 x $10^5$ cells/flask and incubated at 37°C in a 5% $CO_2$ (v/v) and 99% (v/v) humidity atmosphere. After 24 h incubation, CCR medium was removed and replaced with 5 mL of fresh medium containing AM130 $IC_{50}$ concentration with a control solution of 0.4% (v/v) of DMSO. All samples were incubated in the same conditions described in Section 2.2.2. The followed steps involved the trypsinization of cells with TrypLE™ Express and the genomic DNA extraction using the High Pure PCR Template Preparation Kit (Roche, Germany) according to the manufacture's procedure. To verify if the interaction of AM130 compound with DNA causes fragmentation, electrophoresis (BioRad PowerPac Basic, Berkley, California) was performed with an 0.8% (w/v) agarose gel, stained with 2% (v/v) GelRed nucleic acid stain (1000x; Biotium, Hayward). Samples were loaded with 5 μL of 6x loading dye, under 80 Volts (V) for 1 h 40 min with λ DNA/HindIII (Ferments, Maryland, EUA) as a molecular weight marker. Sequentially, the results were visualized using Molecular Imager® Gel Doc™ XR, System with Image Lab™ Software (BioRad, Berkley, California) and the image was obtained with GelDoc software. Results were confirmed with three independent assays.

### 2.6.2 Plasmid DNA cleavage assay

#### 2.6.2.1 *Escherichia coli* culture and DNA extraction

AM130 compound interaction with plasmid UC18 (pUC18; Ferments, Maryland, EUA) was also assessed. Plasmid DNA (pDNA) was obtained from *Escherichia coli* transformed cells, grown overnight in a Luria–Bertani (LB) liquid medium (AppliChem, Darmstadt, Germany) supplemented with 100 µg/mL of ampicillin (Bioline, London, UK), at 37°C. Plasmid extraction and purification were performed using a NZYMiniprep kit (NZYTech, Lisbon, Portugal) according to the manufacturer's instructions. The concentration of pDNA was determined by measuring the absorbance at 260 to 280 nm with a NanoDrop2000 spectrophotometer. The purity of plasmid DNA was verified by monitoring the ratio absorbance at 260/280 nm and 260/230 nm in the range 1.8-1.9.

#### 2.6.2.2 Plasmid DNA Electrophoretic procedure

*In vitro* interaction between AM130 and DNA was performed in a microtube containing 100 ng of pUC18 and AM130 at different concentrations (0 to 100 µM), diluted in 5 mM Tris–HCl, 50 mM NaCl, pH 7.0 buffer to a final volume of 20 µL and incubated for 24 h at 37°C. Control samples consisted of DMSO in the same proportion used for the compound in 5 mM Tris–HCl, 50 mM NaCl, pH 7.0 buffer incubated in the same conditions mentioned previously. The same procedure was done for pUC18 in a mixture with buffer Hind III (Ferments, Maryland, EUA), pUC18, restriction enzyme *Hind III* (10 U/µL; Ferments, Maryland, EUA), which was used for the digestion of the supercoiled DNA, and ultrapure water (18.2 $M\Omega.cm^{-1}$ at 25°C), incubated for 2 h at 37°C. The restriction enzyme *Hind III* after incubation reactions were stopped by adding 5 µL of loading buffer (25mM Tris-HCl, 25 mM EDTA (pH 8.0), 50% glycerol, 0.1% bromophenol blue). The samples were subjected to electrophoresis on 0.8% (w/v) agarose stained with 2% (v/v) GelRed nucleic acid stain under 80V for 2 h. The molecular weight marker used contained λ DNA/HindIII. The gels obtained were visualized and acquired with Molecular Imager® Gel Doc™ XR, System with Image Lab™ Software (BioRad, Berkley, California) and GelDoc software. Data were confirmed with three independent experiments.

### 2.6.3 UV-visible titrations

In the present study, the interaction between AM130 compound and calf thymus DNA (CT-DNA; Invitrogen, New York, EUA) was assessed by UV–Visible spectroscopy (300–700 nm) using a quartz cuvette of 1 cm path length, to verify if the cytotoxic effect of the compound in cancer cells is due to its capability to bind to DNA.

CT-DNA concentration (monomer units) was previously determined using NanoDrop2000 (Thermo Scientific, MA, USA) by reading its absorbance at 260 nm. The solution of CT-DNA gave a ratio of UV absorbance at 260 and 280 nm approximately 1.8, indicating that DNA was free from protein. The concentration of the DNA was determined using the Lambert Beer's law (Equation 3):

$$A = \varepsilon \times \ell \times C$$

**Equation 3**

where A is the absorbance at 260 nm, ε is the molar extinction coefficient of DNA (6 600 $M^{-1}$ $cm^{-1}$), $\ell$ is the optical path in cm and C is the CT-DNA concentration in M.

The absorption spectra of a CT-DNA solution in the absence and presence of AM130 compound were acquired using a fixed amount of compound concentration (100 μM) in absence or presence of increasing concentrations of CT-DNA (between 0 and 25 μM). All samples were prepared in 5 mM Tris–HCl, 50 mM NaCl, pH 7.0 buffer and incubated at 37°C for 24 h. The baseline was the corresponding buffer solution and ultrapure water (18.2 MΩ.$cm^{-1}$ at 25°C). The absorbance values obtained were corrected to DMSO values and fitted in Equation 4. Additionally, was used the UV titration data at 381 nm to obtain intrinsic binding constant ($K_b$):

$$\frac{[DNA]}{(\varepsilon_a - \varepsilon_f)} = \frac{[DNA]}{(\varepsilon_b - \varepsilon_f)} + \frac{1}{K_b\,(\varepsilon_b - \varepsilon_f)}$$

**Equation 4**

where [DNA] is the concentration of CT-DNA (per nucleotide phosphate) and $\varepsilon_a$, $\varepsilon_f$, and $\varepsilon_b$ are the apparent, free and bound complex extinction coefficients, respectively (Aslanoglu, 2006). $\varepsilon_f$ was determined by a calibration curve of the isolated compound in aqueous solution; following the Lambert Beer's law, $\varepsilon_a$ was determined as the ratio between the measured absorbance and the compound concentration. From the graphical analysis of [DNA] / ($\varepsilon_a - \varepsilon_f$) versus [DNA], it is known that (1 / ($\varepsilon_b - \varepsilon_f$)) corresponds to the slope and Y intercept equal to (1 / Kb ($\varepsilon_b - \varepsilon_f$)). $K_b$ corresponds to the ratio between slope and the Y intercept (Shahabadi et al. 2011). For the calculation of $K_b$, it was necessary to assume that only one type of interaction occurs between the CT-DNA and AM130 compound in the aqueous solution resulting in the formation of one type of complex. It is also presumed that the substrate and the ligand follow Beer's law for the absorbance light (Agarwal et al. 2013). Results are from one independent experiment. To confirm the UV-Visible results, circular dichroism (CD) was performed.

### 2.6.4 Circular Dichroism

The interaction between AM130 and CT-DNA was also assessed by circular dichroism (CD), being the all CD spectra recorded in Chirascan™ (AppliedPhotophysics, United Kingdom) at RT in the range of 230–600 nm. For the measurements, a quartz cell with a path length of 1 cm was used and the data collected were automatically corrected for background contributions. The concentration of AM130 compound in the experiment was 100 μM in the absence or presence of increasing concentrations of CT-DNA (5, 12.5, 17.5 and 25 μM). All samples were prepared in 5 mM Tris–HCl, 50 mM NaCl, pH 7.0 buffer and spectra were recorded after incubation at 37˚C for 24 h. The baseline was the corresponding buffer solution. The results are from two independent experiments and averages were calculated.

### 2.7 Assessment to AM130 interaction with serum proteins

AM130 capability to interact with proteins was assessed through UV-Vis spectroscopy. Bovine serum albumin (BSA) is considered a standard protein model for studying drug–protein interaction *in vitro* (Seetharamappa & Kamat, 2004) and for that it was chosen for the mentioned assays. Some preliminary studies were carried out to select AM130 concentrations for AM130–protein interaction. Based on these preliminary experiments, BSA concentration was kept fixed at 2 µM and AM130 concentration varied from 2, 4 and 6 µM. Thus, to assessed AM130-BSA interaction, several solutions were prepared containing a constant BSA concentration (Sigma, St. Louis, USA) and a range of AM130 concentrations diluted in 10 mM pH 7 phosphate buffer/0.15 M NaCl buffer. Reference solutions containing only AM130 compound in the same proportions was used (2, 4 and 6 µM) and subtracted automatically. The UV-Vis spectrum for the AM130-BSA interaction was obtained (from 250 to 420 nm) as mentioned in section 2.6.3, after 1 h of incubation at 4ºC. Data were from two independent experiments.

### 2.8 Proteome profiling: Two-Dimensional Gel Electrophoresis

#### 2.8.1 Protein sample preparation, precipitation and purification

A2780 cancer cells were seeded in 75 $cm^2$ vented cell culture flasks, at a cell density of 4 x $10^6$ cells/flask and incubated in the conditions described in section 2.4.4.1. Cell lysates were centrifuged 8000 x g for 10 min at 4ºC and supernatants were recovered. For whole protein precipitation and purification 2-D Clean-Up Kit (GE Healthcare, United Kingdom) was used accordingly with manufacturer's protocol (Healthcare, 2009) with exception for wash additive and wash buffer step, where cell lysates were incubated overnight at -20ºC. Moreover, an additional wash step was also performed, where 25 µL of ultrapure water (18.2 $M\Omega.cm^{-1}$ at 25°C) were added to disperse pellet. Wash buffer and wash additive were added in the same proportions according to the manufacturer's protocol. After centrifugation, 130 µL of re-hydration buffer (7 M urea (BDH Prolabo, VWR International), 2 M Tiourea (Merck, Frankfurt, Germany), 2% (w/v) 3-[(3-Cholamidopropyl) dimethylammonio]-1 propanesulfonate (GE Healthcare, United Kingdom), phosphatase inhibitors 1x, protease inhibitors 1x, bromophenol blue (Merck, Frankfurt, Germany), 0.1% (w/v) DTT and 1 mM PMSF) were added to protein extract, and allowed to react overnight at RT. After a 10 min centrifugation under 8000 x g at RT, the resulting supernatants were recovered. For total protein quantification, Pierce Protein Assay kit was used, as described in section 2.7.

#### 2.8.2 2-D Gel Electrophoresis: Isoelectric Focusing and SDS-PAGE

Isoelectric focusing (IEF), was performed by in-gel active rehydration using the Ettan IPGphor3 IEF System (GE Healthcare, United Kingdom). 90 µg of whole protein sample was uniformly distributed into each 7 cm Immobilized pH gradient (IPG) strip holder (GE Healthcare, United Kingdom), resuspended in 125 µL of rehydration solution supplemented with 0.5% IPG (GE Healthcare, United Kingdom) and 0.5% of destreak (GE Healthcare, United Kingdom), Immediately after, a 7 cm long Immobiline DryStrip pH 3-10 NL (GE Healthcare, United Kingdom) was placed over the sample, ensuring that no bubbles

were formed between the gel and the sample. Additionally, 750 µL of Drystrip Cover Fluid (GE Healthcare, United Kingdom) were added over the strip to protect the strip from drying. IEF method was performed in Ettan IPGphor3 IEF System (GE Healthcare, United Kingdom), according to protocol mentioned in Table 5.1 (Appendix A). After IEF, IPG strips were incubated into two equilibrium solutions to assure the protein's primary structural conformation. Initially, strips were loaded onto an equilibrium solution (70 mM Tris-HCl pH 8.8, 6M Urea, 30% (v/v) glycerol and 2% (w/v) SDS (GE Healthcare, United Kingdom)) supplemented with 1% (w/v) DTT for 15 min at RT, followed by a second solution further supplemented with 2.5% (w/v) iodoacetamide (GE Healthcare, United Kingdom), incubated for another 15 min under constant stirring.

For the second-dimension, a 12.5% (v/v) polyacrylamide gel was prepared – 4.8 mL of a 30 % (w/v) acrylamide/bis-acrylamide mix, 4.2 mL of ultrapure water (18.2 $M\Omega.cm^{-1}$ at 25 °C), 3 mL of Tris-HCl buffer (Merck) 1.5 M pH 8.8, 90 µL of a 10% (v/v) ammonium persulfate (APS; Biorad, California, USA) and 12 µL of tetramethylethylenediamine (Sigma, St. Louis, EUA). After gel polymerization, IPG Strips were placed on top of polyacrylamide gel and sealed with a 0.5% (v/v) agarose solution diluted in running buffer (3.79 g/L Tris, 18 g/L glycine, 1.25 g/L SDS, and bromophenol blue traces). Molecular weight protein marker used was NZY Colour Protein Marker II (NZYTech, Lisbon, Portugal). SDS-PAGE Mini-PROTEAN® 3 System was used to perform electrophoresis run, with an initial run of 30V to assure all protein transfer to polyacrylamide gel followed by a 120V run. The system was switch off prior the bromophenol blue band exits from the gel.

### 2.8.3 Detection and Digital Imaging

Polyacrylamide gel staining was performed using 3 PhasTGelTM Blue R tablets (Coomassie R350; GE Healthcare) diluted in 1 L, 10% (v/v) acetic acid. Afterwards a 30 min incubation at 50ºC followed by another 30 min incubation at RT was performed and gels were rinsed with ultrapure water (18.2 $M\Omega.cm^{-1}$ at 25 °C) until protein spots were clearly observable. Images of the 2-DE gels were acquired using Magic Scan software in Tiff and Lab Scan format, and protein spot analysis was performed using *Melanie 7.0* software (GeneBio, Genebra, Switzerland). Protein spots of control gel and AM130-treated cells gel were compared to evaluate possible abundance levels variation. An intensity ratio between homologous spots of the two gels was carried out. Abundance levels inferior to ≤ 0.7 (protein subexpression) and superior to ≥ 1.5 (protein overexpression) were considered significant.

## 2.9 Statistical analysis

All data were expressed as Mean ± SEM from at least three independent experiments unless otherwise indicated. *GraphPad Prism 6* software was used to analyse the results through One or Two-way ANOVA or Student's t-test for comparing the control group with treatment groups for statistical significance. $p < 0.05$ was considered to indicate a statistically significant difference.

# 3 RESULTS AND DISCUSSION

## 3.1 Chemistry

Spirooxindole framework is found in many natural products and due to its different biological activities ranging from MDM2 antagonists, ion channel blockers and anti-inflammatory agents to antimalarial has been the subject of huge interest by industry and academia for the development of novel spirooxindoles (Santos, 2014). Additional, the prevalence of the pyrazoline scaffold, a five-membered heterocyclic ring with two adjacent nitrogen atoms within the ring, in bioactive molecules has also sparked interest (Shaaban et al. 2012; Monteiro et al. 2014).

In the last years, Santos's group (iMed.ULisboa) has reported the synthesis and characterization of several spiropyrazoline oxindoles derivatives containing a five membered ring (pyrazoline), including the compound in study (Monteiro et al. 2014). Figure 3.1 describes the synthesis of 5-bromo-2',4',5'-triphenyl-2',4'-dihydrospiro[indoline-3,3'-pyrazol]-2-one (AM130) by 1,3-dipolar cycloaddition reaction (Santos, 2014), between *(E)*-3-benzylidene-5-bromoindolin-2-one **4** obtained by aldolic condensation of 5-bromoindolin-2-one **2** with benzaldehyde in the presence of piperidine and *(Z)-N*-phenylbenzohydrazonoyl chloride **5**.

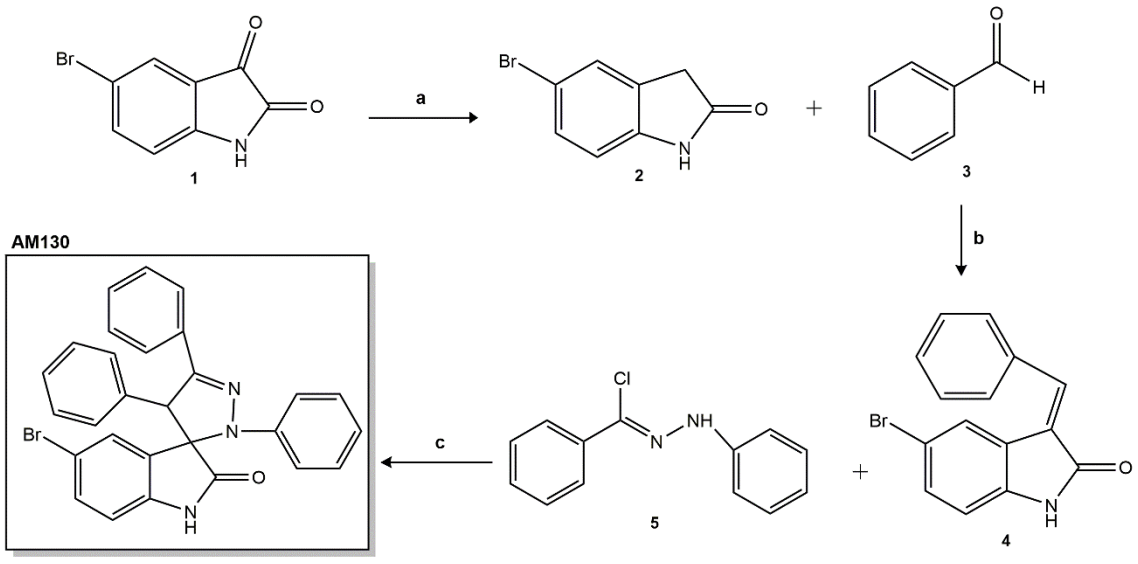


**Figure 3.1 -** Synthesis of 5-bromo-2',4',5'-triphenyl-2',4'-dihydrospiro[indoline-3,3'-pyrazol]-2-one **5** (AM130) by 1,3-dipolar cycloaddition reaction. Reagents and conditions: (a) $C_2H_6O_2$, $NH_2.NH_2.H_2O$, reflux, 4 h; (b) EtOH, $C_7H_6O$, $C_5H_4N$, reflux, 1 h 30 min; (c) $CH_2Cl_2$, $Et_3N$, RT, 9 h.

Many compounds under investigation in drug discovery have low solubility. The common procedure for dissolving these compounds for cell-based assays is the use of DMSO. Unfortunately, this does not mean that compounds will necessary have good aqueous solubility (Lipinski et al. 2012). Considering this, compounds' solubility in DMSO and buffers has been emerged as a critical issue since their low solubility affects bioassays causing an underestimated activity and variable data. Several studies have described some strategies to optimize the bioassays to overcome solubility issues, including the early

screening for solubility, improve storage, handling of DMSO stocks and ensure that low-solubility compounds are fully solubilizes for bioassays. Additional, has been also demonstrated that repeated freeze-thaw cycles can enhance compound precipitation, a cause that leads to its loss (Kozikowski, 2003; Oldenburg et al. 2005; Di & Kerns, 2006). In this regard, during the present study the issues mentioned above have been considered and, firstly the stock solution was divided into aliquots with the necessary amount for each bioassay. In addition, the AM130 spectra in DMSO were tested through UV–Visible spectroscopy (230–600 nm) with a range of dilutions from stock solution at 100 mM under two conditions: immediately after its solubilization in DMSO and 1 week after freezing (-20°C) with or without sonicated. Data from UV–Visible spectroscopy demonstrated that AM130 has low solubility in DMSO precipitating when stored at -20°C (results not shown). To overcome this issue, before compound administration to cells, each aliquot was submitted to sonication resulting in a homogeneous suspension.

### 3.2 Cytotoxicity of AM130 against human cancer and healthy cells

The MTS colorimetric assay is based on the bioreduction of the MTS reagent into a soluble product ─ formazan ─ by the intracellular dehydrogenase enzymes found in metabolically active cells in the presence of an electron coupling reagent. With the methodology described above, it was possible to determine the number of viable cells, since the amount of formazan measured is directly proportional to the number of living cells in a culture (Wang et al. 2010; Riss et al. 2013). A pharmacological parameter such as relative $IC_{50}$ was calculated from dose-response curves resorting to *GraphPadPrism 6* Software (Figures 3.2 and 3.3 and Appendix A), with a confidence interval of 95%.

*In vitro* antiproliferative activity of AM130 compound was evaluated against a series of human cancer cell lines enabling the determination in which cancer cell line the compound induces a more pronounced growth inhibition. Previously studies developed by Monteiro et al. 2014; Nunes, 2016, tested the cytotoxic potential of the compound in human breast cancer cell lines (MCF-7 and MDA-MB-231), carcinoma colorectal cell line wild-type for p53 (HCT116 $p53^{(+/+)}$) or lacking p53 (HCT116 $p53^{(-/-)}$), as well as in healthy human embryonic kidney 293 cells (Hek-293T). Taking this into account, during the present project, the antiproliferative activity of the compound was tested in different cell lines namely A2780, HCT116 and MDA-MB-453, as well as in normal human fibroblasts and applied in range concentrations of 0.5 to 75 µM with an exposure period of 48 h.

The MTS control assay allowed to confirm to that the AM130 compound does not interfere with the MTS reagent. Overall, AM130 shows a broad-spectrum antiproliferative activity with a varying degree of cytotoxicity in all cancer cell lines screened ($IC_{50}$ < 12 µM; Table 3.1). Furthermore dose-response curves, displayed in Figures 3.2 and 3.3 and Appendix A, highlighted the ability of the compound to inhibit cell proliferation in a dose-dependent manner. On the other hand, for normal human fibroblast the cell viability was almost unchanged, except with concentration above of 50 µM, declining substantially after, suggesting that AM130 toxicity in normal cells is lower than all tested cancer cells. Among all the tested cancer cell lines, AM130 elicited a higher inhibitory effect on the proliferation of A2780 cell line, exhibiting a relative $IC_{50}$ of 8.5 µM, followed by HCT116 and MDA-MB-453 cancer cell

lines with $IC_{50}$ values of 10.5 and 11.3 µM, respectively (see Table 3.1 and Figures 6.1 and 6.2, Appendix A). By showing a greater cytotoxic effect in A2780, this cell line was chosen for the further biologic assays.

**Table 3.1 -** *In vitro* cytotoxicity of AM130 (relative $IC_{50}$) against several human cancer cell lines and normal human fibroblasts. Compounds' inhibitory activity was assessed after 48 h of exposure. Data expressed as mean ± SEM of three independent biological assays.

| | Relative $IC_{50}$ (µM) | | | |
|---|---|---|---|---|
| **Cell line** | **A2780** | **HCT116** | **MDA-MB-453** | **Fibroblasts** |
| **AM130** | 8.5 ± 0.7 | 10.5 ± 0.1 | 11.3 ± 0.1 | 55.2 ± 0.5 |

In order to compare the cytotoxic potential of the compound to well-known anticancer drugs e.g., cisplatin and doxorubicin, their antiproliferative activity were also determined against A2780 cancer cell line. Cisplatin presents a relative $IC_{50}$ of 1.9 ± 0.2 µM whereas doxorubicin shows a $IC_{50}$ value of 0.6 ± 0.03 µM for A2780 carcinoma cell line (Figure 6.3 and Figure 6.4, Appendix A). These values demonstrated that compound in study has a lower cytotoxicity in A2780 compared to the common chemotherapeutic drugs mentioned.

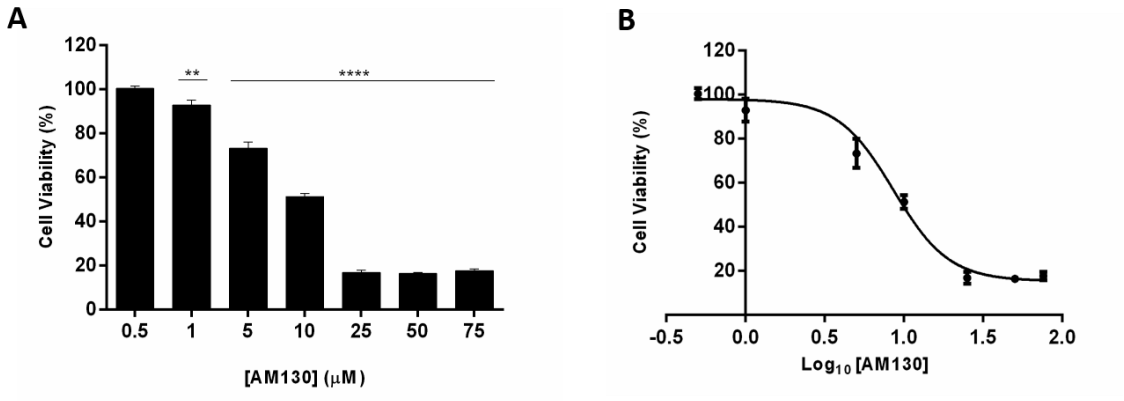


**Figure 3.2 -** Dose dependent cytotoxicity (A) and the correspondent dose-response curve (B) of AM130 in A2780 cells followed by 48 h of incubation. Cell viability values were tested and function of the control (cells + 0.1 % (v/v) DMSO), which were set to 100 %. Data are the average of three independent assays and error bars correspondent to SEM (* $p \leq 0.05$, ** $p \leq 0.01$, *** $p \leq 0.001$, **** $p \leq 0.0001$). Relative $IC_{50}$ was calculated from dose-response curves resorting to the *GraphPad Prism 6* software.

The cytotoxic potential in healthy cells was performed, indicating a good selectivity of AM130 for cancer cells since it demonstrates lower toxicity in normal human fibroblasts ($IC_{50}$ of 55.2 µM; 6.5 times higher compared with A2780 cell line). In this regard at its $IC_{50}$ (8.5 µM) AM130 mainly affects A2780 cells without inducing, toxicity into healthy cells.

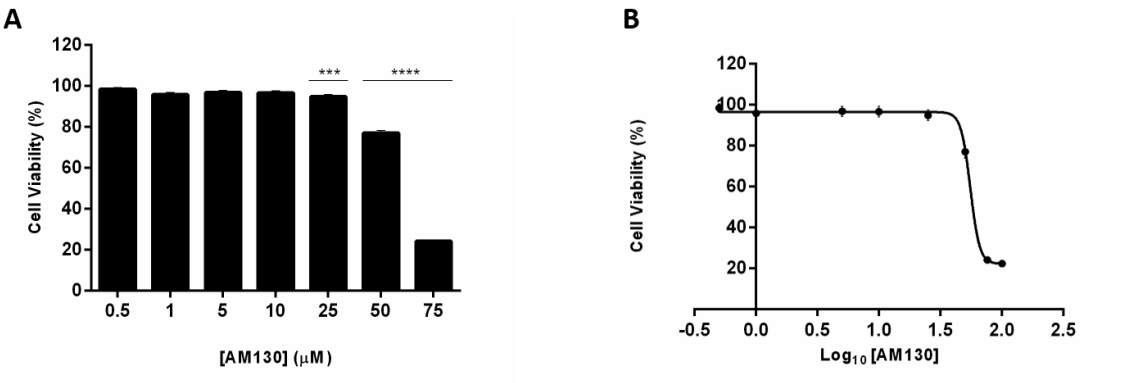


**Figure 3.3 -** Dose dependent cytotoxicity (A) and the correspondent dose-response curve (B) of AM130 in healthy cells (normal human fibroblast) followed by 48 h of incubation. Cell viability values were tested and function of the control (cells + 0.1 % (v/v) DMSO), which were set to 100%. Data are the average of three independent assays and error bars correspondent to SEM (* $p \leq 0.05$, ** $p \leq 0.01$, *** $p \leq 0.001$, **** $p \leq 0.0001$). Relative $IC_{50}$ was calculated from dose-response curves resorting to the *GraphPad Prism 6* software.

## 3.3 Evaluation of cell death

### 3.3.1 Hoechst 33258: nuclear morphology alterations

Nuclear double-staining with Hoechst 33258 and PI was used to analyze and determine, as much as possible, the type of cell death induced in A2780 cells by AM130. Hoechst 33258 fluorescence is sensitive to DNA conformation and chromatin state in cells and, due to its high affinity for DNA, allows the detection of nuclear changes, e.g. chromatin condensation and nuclear fragmentation, therefore being a good indicator of apoptosis (Cao et al. 2011). On the other hand, PI is a cell impairment DNA-binding dye, which can only stain cells' nuclei when plasma membrane permeability and integrity are lost, indicating late apoptosis or necrosis (Brun et al. 2012).

In control cells, the nuclei have homogeneous distribution of blue fluorescence (Hoechst 33258 dye) indicating the presence of uncondensed and disperse chromatin through the whole nucleus. It was also observed cells in mitosis, both evidences suggestive of viable cells (Silva et al. 2012; Silva et al. 2014). On the other hand, A2780 cells exposed to $IC_{50}$ concentration (8.5 µM) of AM130 exhibit two nuclear morphological alterations typically associated with apoptosis, namely, chromatin condensation and fragmentation (Silva et al. 2014), as indicated by the bright non-homogenous fluorescence. Considering that PI stains the nuclei of death cells bright pink and observing Figure 3.4, probably the compound in study does not cause necrosis in cancer cells, since no cells were stained by PI. Indeed, there is a clear decrease in cell density in AM130-treated cells when compared to the control group, which is associated with increasing cell death by apoptosis.

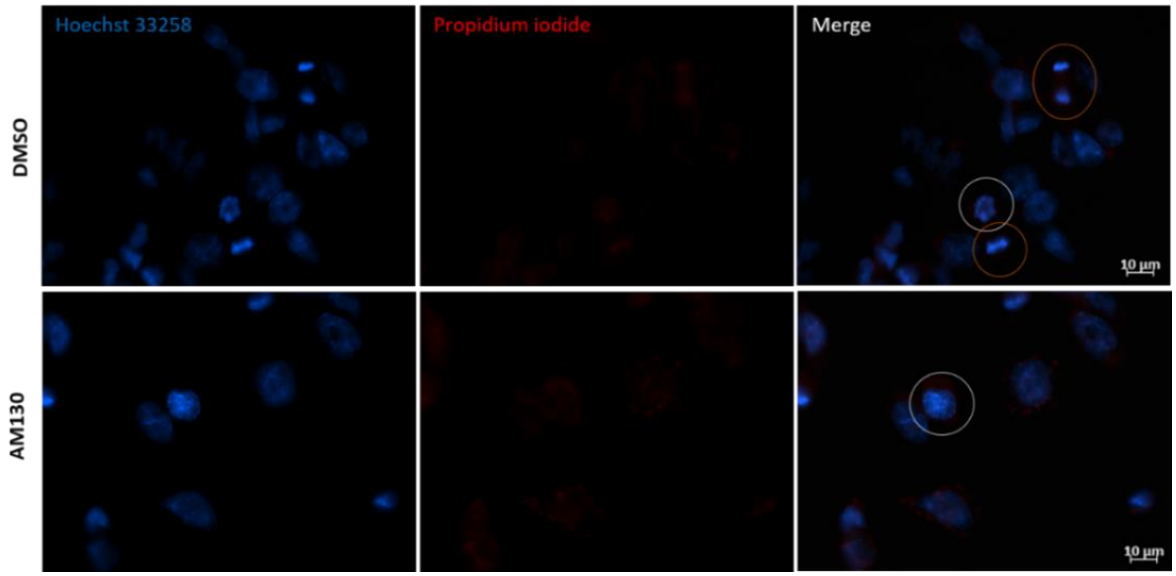


**Figure 3.4 -** Fluorescence microscopy images showing nuclei morphological alterations in A2780 cells. A2780 cells were exposed to 8.5 µM or 0.1% (v/v) DMSO (vehicle control) for 48 h. Orange circles indicate mitosis events, whereas the white circles indicate an initial event of apoptosis i.e., chromatin condensation. Results are from three independent experiments. The images were edited with *ZEISS Microscope Software ZEN* software.

Counting the cells with nuclear changes, such as, chromatin condensation and fragmentation, A2780 cells exposed to $IC_{50}$ concentration exhibited 31% ± 6 of apoptosis, a 3.8-fold increase when comparing to control group (Figure 3.5). Overall, these preliminary results show that AM130 is able to trigger apoptosis in the cancer cell line. However, the molecular targets involved are to be deciphered.

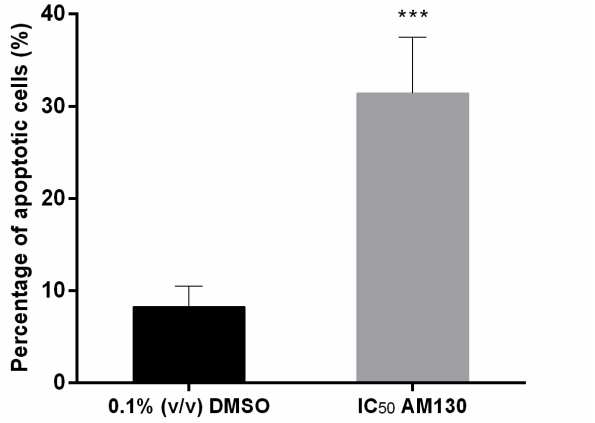


**Figure 3.5 -** Mean values expressed as the percentage of apoptotic nuclei in A2780 cells. Data are represented as means ± SEM and statistics was performed by t-student test compared to control with $p \leq 0.05$ of three independent assays (* $p \leq 0.05$, ** $p \leq 0.01$, *** $p \leq 0.001$, **** $p \leq 0.0001$) using the *GraphPad Prism 6* software.

The detection of apoptotic features by fluorescence microscopy in the present bioassay was not simple, since the nucleus morphology by itself is irregular, causing some difficulties in the distinction between normal and apoptotic cells. To confirm the present results, the quantification of A2780 cell death was assessed using flow cytometry and annexin V-FITC/PI.

### 3.3.2 Annexin V-FITC/PI staining

The previous fluorescence microscopy results did not allow to clearly identify and quantify the apoptosis hallmarks. Therefore, flow cytometry double staining with annexin V-FITC/PI in HCT116 cells was achieved instead of the A2780 cells, as explained in the method procedure. The double staining with annexin V-FITC and PI was used to distinguish between apoptotic and necrotic cell death. They are easily differentiated through the morphological characteristics and biochemical changes (Invitrogen, 2011). Annexin V binds to PS that is translocated to the outer membrane leaflet as a consequence of an early event of apoptosis (Brumatti et al. 2008). On the other hand, cells in late apoptosis and necrosis shows alterations in the integrity of cell membrane, which allows the PI to enter the nucleus and binds to DNA molecule (Brun et al. 2012). With this staining methodology it is possible to use flow cytometry to quantify cells according with (i) annexin V-negative and PI-negative (viable cells), (ii) annexin V-positive and PI-negative (early apoptotic cells), (iii) annexin V-positive and PI-positive (late apoptotic cells) and (iv) annexin V-negative and PI-positive (necrotic cells; Henry et al. 2013).

The exposure of HCT116 cancer cells to compound reveals a slight increase in the percentage of early apoptotic cells, 34% compared to the control that exhibits 29%, and an increase of apoptotic cells in later stages. The presence of AM130 did not result in necrotic cells (Figure 3.6). Annexin V analysis suggests that AM130 can induce apoptosis in cancer cells without inducing necrosis, which is in line with the previous results obtained by Hoechst staining (Section 3.3.1). However, since this bioassay was performed in other cell line instead A2780, which could influence the results, the evaluation of functional activity of mitochondrial was performed in A2780 cells (see Section 3.3.3) to confirm the mentioned conclusions.

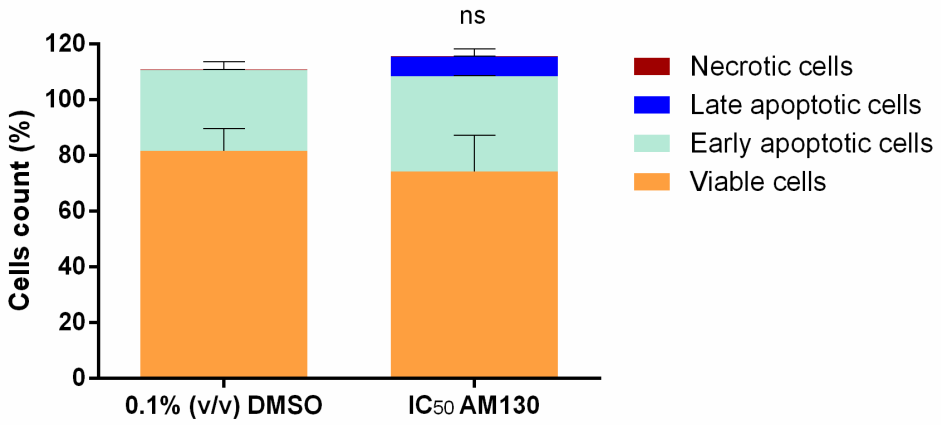


**Figure 3.6 -** Evaluation and quantification of apoptosis and necrosis by flow cytometry with annexin V-FITC and PI double staining. HCT116 cells were treated with 0.1% (v/v) DMSO (vehicle control) and the compound at $IC_{50}$ concentration for 48 h. Viable cells (FITC-/PI-); early apoptotic cells (FITC+/PI-); late apoptotic cells (FITC+/PI+); necrotic cells (FITC-/PI+). Data are presented as the mean ± SEM and statistics was performed by Two-way ANOVA compared to control with $p \leq 0.05$ of two independent experiments (ns - statistically non-significant) using the *GraphPad Prism 6* software.

### 3.3.3 Measurement of changes in mitochondrial membrane potential ($\Delta\Psi_M$)

To examine the functional activity of mitochondria, changes of the $\Delta\Psi_M$ in AM130-treated cells, was analysed. In healthy cells, due to the negative potential of the inner mitochondrial membrane i.e., with a high $\Delta\Psi_M$, the positively charged lipophilic JC-1 spontaneously forms aggregates with intense red fluorescence in the matrix of mitochondria. On the other hand, in apoptotic or unhealthy cells with low $\Delta\Psi_M$, JC-1 remains in its monomeric form (green fluorescence) indicating that electrochemical gradient is necessary for both formation and maintenance of the J-aggregates in mitochondria. Thus, the depletion of this normal gradient decreases the $\Delta\Psi_M$, leading to the loss of red fluorescence and the increase of cytoplasmic green fluorescence, being the $\Delta\Psi_M$ an appreciated indicator of cells' health and functional status (Smiley et al. 1991; Petit et al. 1995; Perelman et al. 2012).

Figure 3.7, shows the changes of A2780 cell fluorescence as a result of compound treatment. Untreated A2780 cells loaded with JC-1 exhibited less but heterogeneous distribution of green fluorescence (JC-1 monomers) and an intense red fluorescence (JC-1 aggregates). These results are similar to A2780 exposed to 0.06% (v/v) of DMSO (vehicle control). On the other hand, the exposure of A2780 cells to the $IC_{50}$ concentration of AM130 resulted in changes in cell staining with the decrease of red fluorescence regions intensity, while green fluorescence intensity in the cytoplasm increased, indicating that AM130 can induce mitochondrial dysfunction. Curiously some cells, more visible in AM130-tretated cells, exhibited both green and red fluorescence. According with Smiley et al. 1991, the co-existence of green and red fluorescence in the same cell or mitochondria possibly reflect the physiological modulation of mitochondria activity (Smiley et al. 1991).

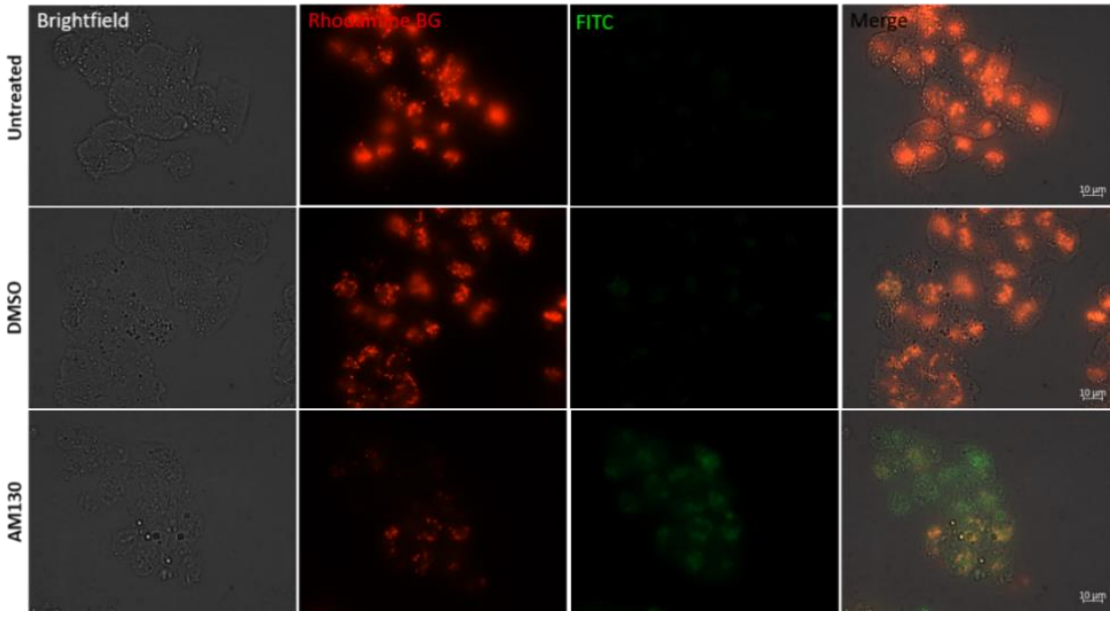


**Figure 3.7 -** Effect of AM130 compound on mitochondrial membrane potential ($\Delta\Psi_M$) in A2780 cells. Cells were incubated in the absence or presence (8.5 µM) compound or 0.06% (v/v) DMSO (vehicle control) for a period of 48 h. Results are from two technical duplicates and two biological assays. Images were edited with *ZEISS Microscope Software ZEN* software.

The changes of the green/red fluorescence intensity reflect $\Delta\Psi_M$ alterations in A2780 cells. In untreated and control cells, the fluorescence ratio green/red was 0.05 ± 0.03 and 0.07 ± 0.03, respectively, indicating that overall cells in those conditions were healthy (Figure 3.8). However, when exposed to the compound, the ratio increased up to 1.25 ± 0.22, corroborating the results obtained by fluorescence microscopy (Figure 3.7).

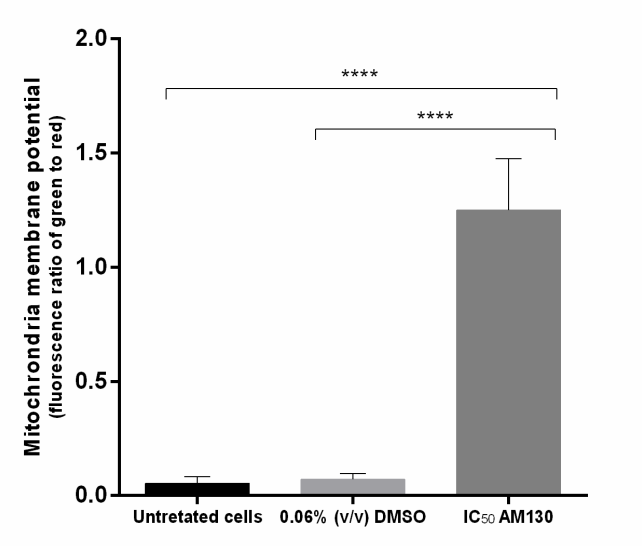


**Figure 3.8 -** Fluorescence ratio green to red of $\Delta\Psi_M$, represented as mean ± SEM. Cells were incubated in the absence or presence (8.5 µM) compound or 0.06% (v/v) DMSO for 48 h. Statistics analysis was performed by One-Way ANOVA (* $p \leq 0.05$, ** $p \leq 0.01$, *** $p \leq 0.001$, **** $p \leq 0.0001$) and graph was made using the *GraphPad Prism 6* software. Results are from two technical duplicates and two biological assays.

Overall, the observed changes in the cells fluorescence suggest that the decrease of JC-1 aggregates in mitochondria, with the subsequent diffusion into the cytosol, can be due to the permeability of the mitochondrial membrane increase, causing the collapse of $\Delta\Psi_M$. Mitochondrial membrane permeabilization is a “point-of-no-return” event in cell death process as consequence of multiple cell death stimuli, which leads to the release of various apoptogenic proteins that normally are located in the intermembrane space (Wang, 2001; Penninger & Kroemer, 2003). To verify if the $\Delta\Psi_M$ depletion is accompanied with the increase of mitochondria membrane permeabilization and, subsequently, the release of cytochrome-c leading to apoptosis through intrinsic pathway, the expression of BAX and BCL-2 proteins was examined by western blot (Section 3.3.4).

### 3.3.4 Effects of AM130 in the levels of pro- and anti-apoptotic proteins

The Bcl-2 family proteins includes both anti–apoptotic (e.g., BCL-2) and pro–apoptotic (e.g., BAX) proteins, and their expression levels, interaction and ratio determine the fate of the cell. Therefore, the increase of expression of BAX protein is associated with the induction of apoptosis whereas the increase of expression of BCL-2 protein is associated with the inhibition of apoptosis and cell survival mechanisms (Katiyar et al. 2005). The interplay between these mitochondrial related proteins results in the release of cytochrome c from mitochondria, which then activates effector caspases, a hallmark of apoptosis, that, in turn, cleave several important cellular target proteins, including poly(ADP-ribose)

polymerase (PARP), resulting in apoptosis (Li & Dou, 2000). PARP is a family of proteins involved in DNA repair and programmed cell death (Chaitanya et al. 2010). Western blot analysis was performed to examined the expression levels of pro- and anti-apoptotic Bcl-2 family proteins, as well as, PARP.

As shown in Figure 3.9 A, the exposure to AM130 markedly increased the expression level of BAX and PARP, while reducing the expression level of BCL-2. Moreover, there was a strong increase in BAX to BCL-2 ratio (Figure 3.9 B), which is known to determine the apoptotic response of the cell (Katiyar et al. 2005) suggesting that the induction of apoptosis involving the mitochondria could be the mechanism of cell death induced by AM130 in cancer cells. In addition, the increased expression levels of PARP could be an indication of extent of DNA degradation, preventing its DNA repair action, resulting in cell death.

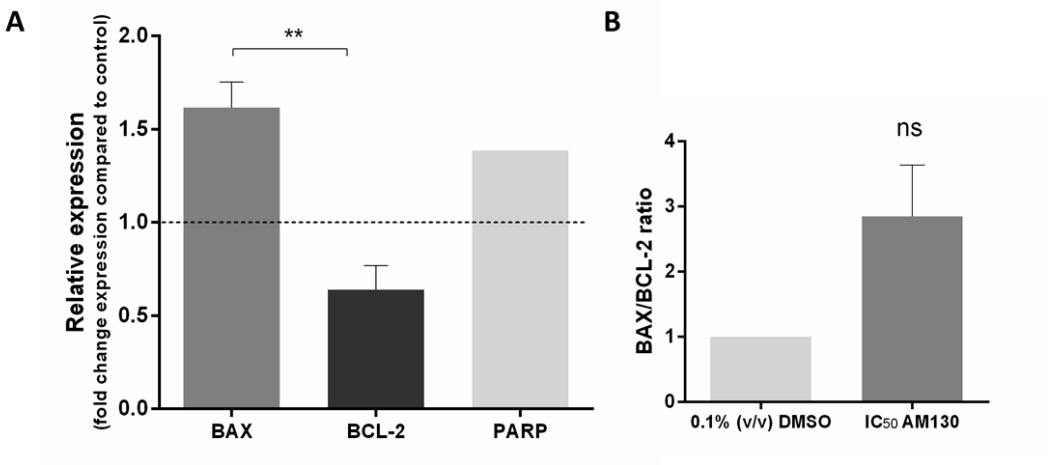


**Figure 3.9 –** Relative expression changes of apoptotic related proteins induced by AM130. (A) Analysis of BAX, BCL-2 and PARP proteins expression in AM130-treated cells compared to control. (B) Ratio of BAX/BCL-2 protein expression levels. Membranes were probed with anti-BAX, anti-BCL-2 and anti-PARP antibodies followed by peroxidase-conjugated appropriate secondary antibodies, and visualized by ECL detection system. Membrane was striped and re-probed with anti–β-actin for loading control. Statistics analysis was performed by One-Way ANOVA (* $p \leq 0.05$, ** $p \leq 0.01$, *** $p \leq 0.001$, **** $p \leq 0.0001$, ns - statistically non-significant) using the *GraphPad Prism 6* software. BAX and BCL-2 data are from two independent experiments whereas PARP cleavage is from one assay.

Data confirm that AM130 causes cancer cell death by apoptosis, as demonstrated in Section 3.3.1, through mitochondria-mediated apoptotic pathway. In fact, A2780 cells exposed to AM130 suffer mitochondrial damages resulting in a decrease of $\Delta\Psi_M$ (Section 3.3.3), which leads to both condensation and fragmentation of chromatin (early apoptotic events), culminating in cell death.

### 3.3.5 Measurement of production of intracellular reactive oxygen species

Even though AM130 is able to induce apoptosis in ovarian cancer cells, as a mechanism of action, the capability of AM130 to induce reactive oxygen species (ROS), was also assessed. Intracellular ROS were determined using $H_2$DCF-dA, a cell-permeable non-fluorescent compound that accumulates within cells upon de-acetylation and reacts with ROS, turning highly fluorescent (Invitrogen, 2006). Figure 3.10 and Figure 3.11 shows that the exposure of A2780 cell line to AM130 do not change the green

fluorescence intensity comparing to control cells treated with 0.06% (v/v) DMSO. Based on these results, it appears that the compound does not induce generation of ROS.

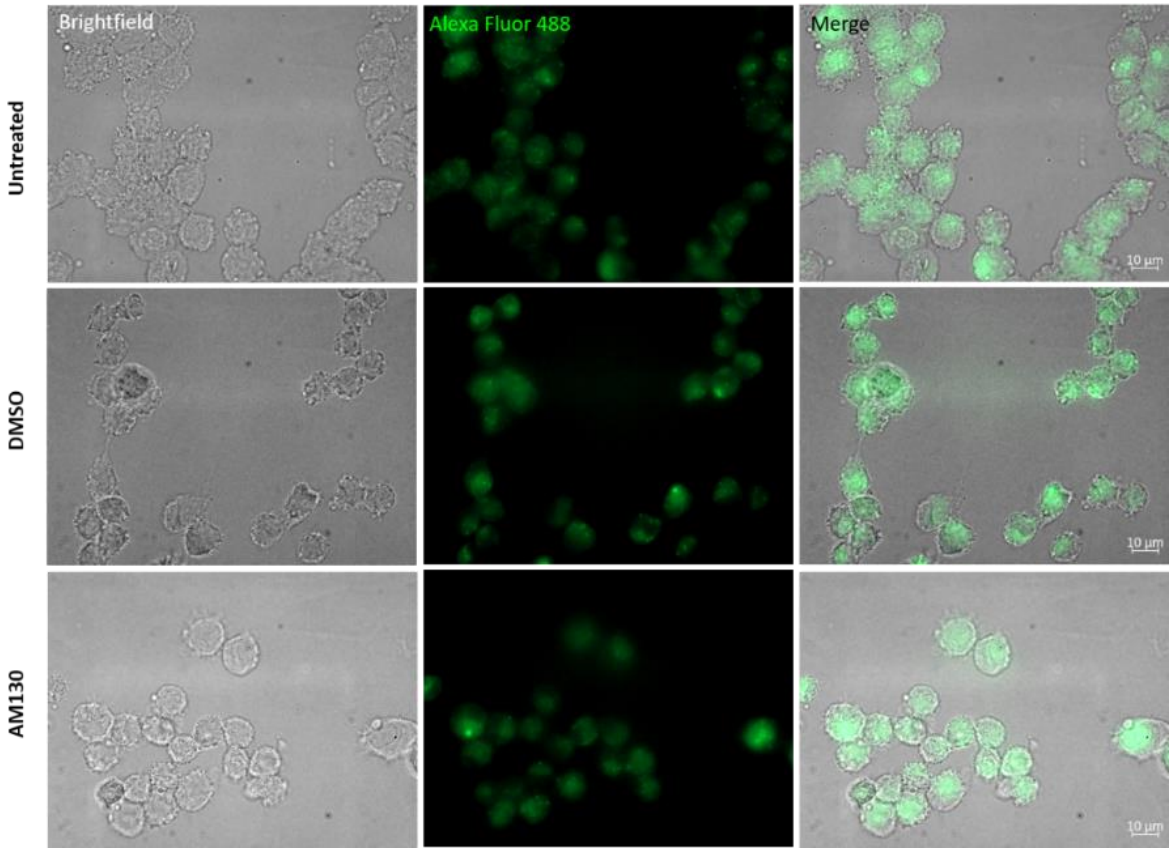


**Figure 3.10 -** Representative images of fluorescence microscopy to assess AM130 effect in ROS production. A2780 cells were culture with 8.5 µM of compound or 0.03% (v/v) DMSO (vehicle control) for 48 h and detected using the $H_2$DCF-dA assay. $H_2O_2$ (25 µM) was used as a positive control for ROS induction. Images are representative of two independent experiments. The images were edited with *ZEISS Microscope Software ZEN* software.

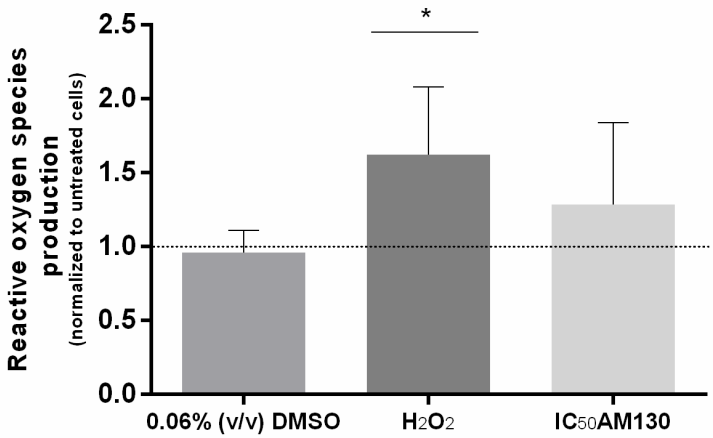


**Figure 3.11 -** Quantification of the fluorescence intensity of $H_2$DCF-DA dye in A2780 cells. Results are presented as the mean ± SEM and normalized to untreated cells. $H_2O_2$ (25 µM) was used as a positive control for ROS induction. Data are from two independent experiments. Statistics analysis was performed by One-Way ANOVA (* $p \leq 0.05$, ** $p \leq 0.01$, *** $p \leq 0.001$, **** $p \leq 0.0001$) and graph was made using the *GraphPad Prism 6* software.

### 3.3.6 Assessment to AM130 effect in autophagic cell death

The assessment of autophagic cell death in A2780 cells was also analyzed to verify if AM130 induces other type of cell death besides apoptosis. For this purpose, fluorescence microscopy was performed using two dyes: Hoechst 33342 dye, which is a cell permeable nucleic acid dye usually used to identify chromatin condensation and fragmentation (Rahman et al. 2013) and Cyto-ID® Green dye, a 488nm-excitable green fluorescent reagent which becomes brightly fluorescent in vesicles produced during autophagy (Enzo Life Sciences, 2016).

Cell exposure to rapamycin and AM130 showed accumulation of Cyto-ID® Green dye in the cytoplasm (Figure 3.12). To quantify dye accumulation, the cells with autophagic vacuoles were counted. As shown in Figure 3.13, AM130-treated cells exhibited similar effects in the induction of autophagy compared with the inductor of autophagy with 58% and 62% of autophagy, an increase of 34% and 38% over the control group, respectively. The exposure to AM130 compound apparently induces autophagic cell death in A2780 cancer cells.

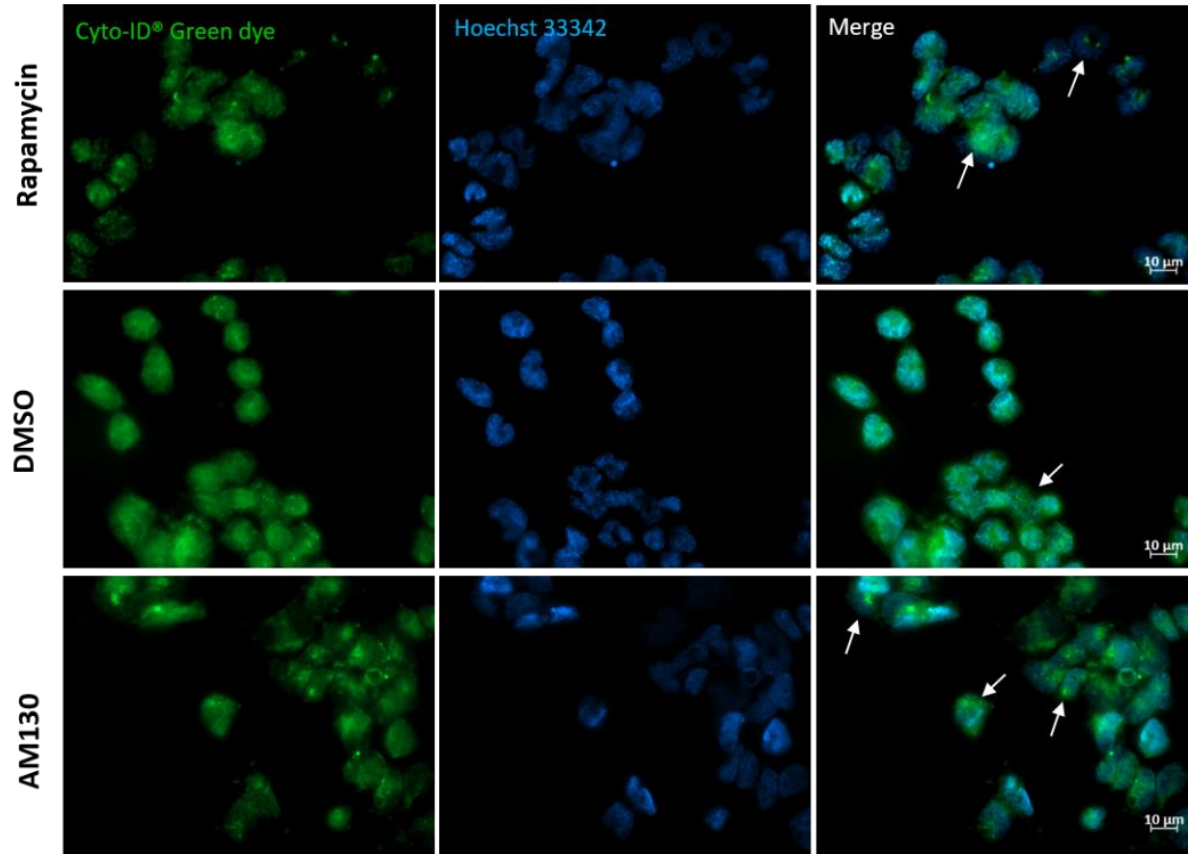


**Figure 3.12 -** Hoechst 33342 and Cyto-ID® Green dye double-staining in A2780 cells to assess autophagic cell death. Cells were exposed during 48 h to rapamycin (an inductor of autophagy), 0.1% (v/v) of DMSO (vehicle control) and AM130 compound ($IC_{50}$ concentration). Data are from two independent experiments. White arrows appoint to autophagy hallmarks i.e., autophagosomes and autophagolysomes. Images were edited with *ZEISS Microscope Software ZEN* software.

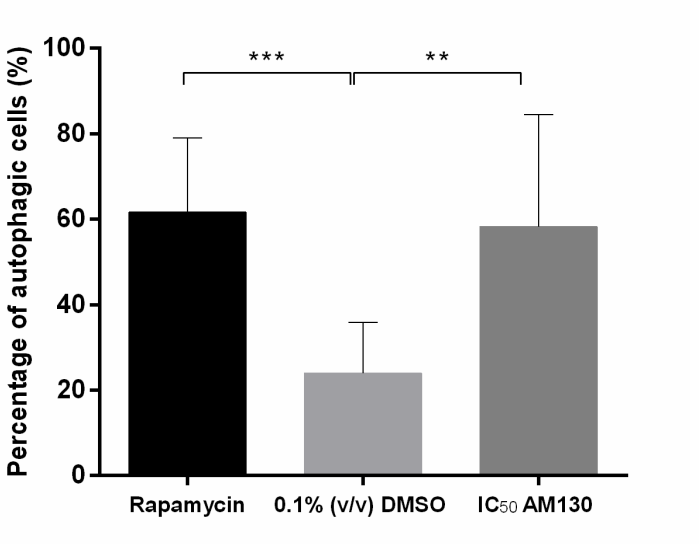


**Figure 3.13 -** Percentage of cells with autophagic vacuoles. Results are expressed as mean ± SEM from two independent experiments. Graph and statistics analysis using One-Way ANOVA (* $p \leq 0.05$, ** $p \leq 0.01$, *** $p \leq 0.001$, **** $p \leq 0.0001$) were performed by *GraphPad Prism 6* software.

The results displayed in Figures 3.12 and 3.13 suggests that the AM130 compound can induce a non-apoptotic cell death in cancer cells such as autophagy. This is particularly interesting because this non-common type of programed cell death is associated with resistance to anticancer therapies by cancer cells (Janku et al. 2011), demonstrating that AM130 could inhibit the growth of these cells, increasing the therapy efficiency. Curiously, these results corroborate the previous western blot results about the increased levels of PARP since this protein is also related with the induction of autophagy (Chaitanya et al. 2010; Figure 3.9 A). Overall, the results discussed so far suggest that AM130 possibly trigger A2780 cell death through mitochondria-mediated apoptotic pathway and autophagy without inducing ROS.

### 3.4 Effects of AM130 on cell cycle progression

Growth inhibition in cancer cells by anticancer drugs could be a result of induction of apoptosis, cell cycle arrest or both. Considering the observed cytotoxic potential of AM130 in cancer cells it was important to assess cell cycle progression. Cell cycle analysis was performed through quantification of DNA content using the PI fluorescent dye for each phases of the cell cycle by flow cytometry. The fluorescence intensity of the stained cells at certain wavelengths will correlate with the amount of DNA. However, due to difficulties in assessing A2780 cell cycle progression, we decided to use HCT116 cell line instead of this cell line. For that purpose, HCT116 cells were synchronized at G1/S phase and then incubated with AM130 in media lacking thymidine for 4, 9, 12 and 24 h, the cell cycle was allowed to continue and cells analyzed. The proportion of cell cycle and content of DNA diploid are shown in Figure 3.14 and Table 6.1 (Appendix B). Cell cycle distribution analysis of HCT116 cells showed that AM130 compound had no effect on cell cycle progression, since did not occurred any cell cycle arrest, on the other hand the cell cycle continues to progress. However, DNA interaction studies may be useful to confirm that this macromolecule is not the principal intracellular target of the compound.

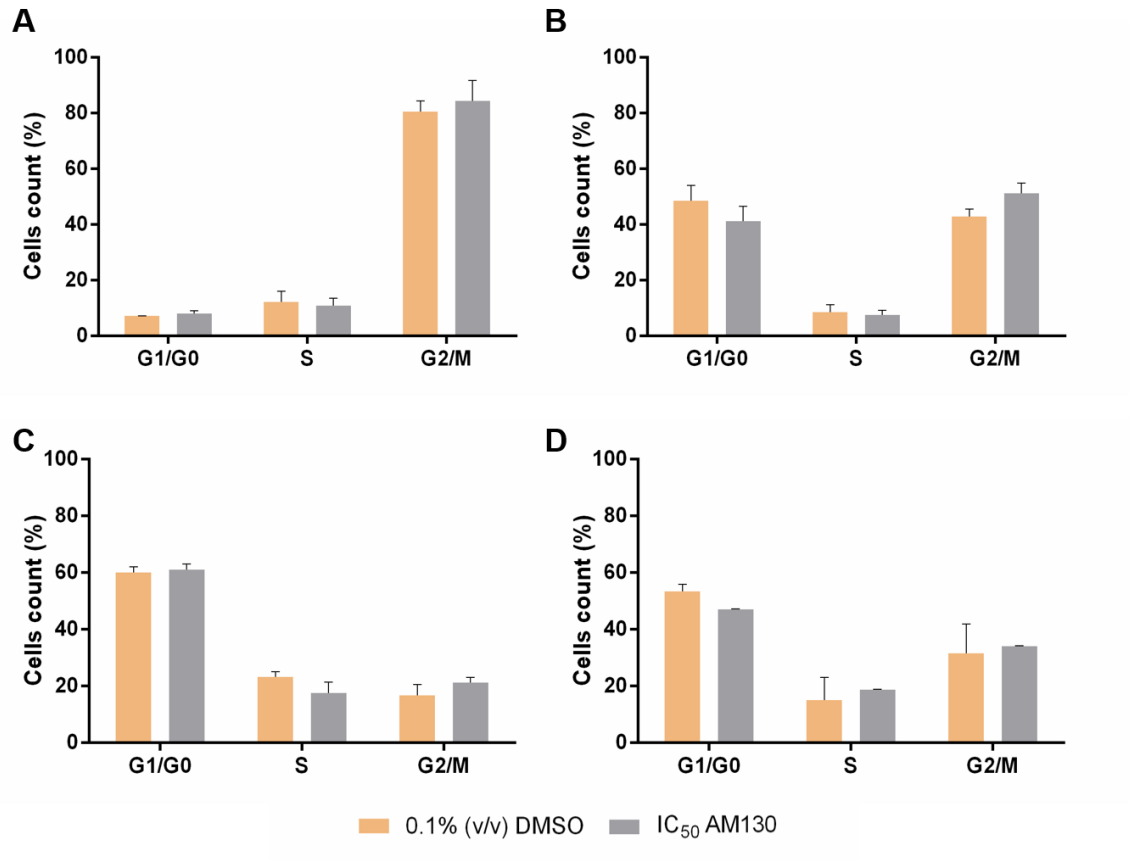


**Figure 3.14 -** Effect of AM130 compound or DMSO in the cell cycle progression of HCT116. Cells were synchronized and exposed to a 0.1% (v/v) DMSO solution (vehicle control) or $IC_{50}$ of compound (8.5 µM) for 4 h (A), 9 h (B), 12 h (C) and 24 h (D) and DNA was stained with PI, and overall content was analyzed by flow cytometry. The data are represented as means ± SEM of two independent experiments.

### 3.5 Assessment to DNA cleavage as an AM130 effect

DNA is the most common pharmacological target of many drugs. Targeting DNA with the aim to regulate cell functions through the modulation of gene expression and protein synthesis or by interfering with replication seems a logical and promising therapeutic approach (Sirajuddin et al. 2013).

To assess whether AM130 interacts with DNA, thus constituting a potential intracellular target and justifying the compound's cytotoxicity, electrophoretic mobility assays were performed using A2780 genomic DNA and plasmid DNA (pUC18). A2780 cell lines were incubated with AM130 $IC_{50}$ concentration or 0.4% (v/v) of DMSO (vehicle control) for 48 h while pUC18 was exposed to increasing concentrations of AM130 or 0.02% (v/v) DMSO for 24 h with the subsequent analysis through agarose gel electrophoresis (Figure 3.15). This assay allows the observation of both cleavage and conformational changes in the supercoiled form (Form I) of pUC18 and fragmentation of genomic DNA (Keck & Lippard, 1992; Gümüs et al. 2009).

The electrophoresis results of both genomic and plasmid DNA displayed in Figure 3.15 A and B, demonstrates that AM130 does not cause fragmentation of genomic DNA or any changes in the

conformation or cleavage of Form I of pUC18. The non-fragmentation of genomic DNA, agrees with the previous ROS results. Indeed, the enhancement of free radical species levels can cause oxidative damages on DNA e.g., several modifications in the nucleotide bases or its degradation, which can be easily observed by electrophoresis, resulting in cell death (Sahin & Depinho, 2010; Sharma et al. 2012).

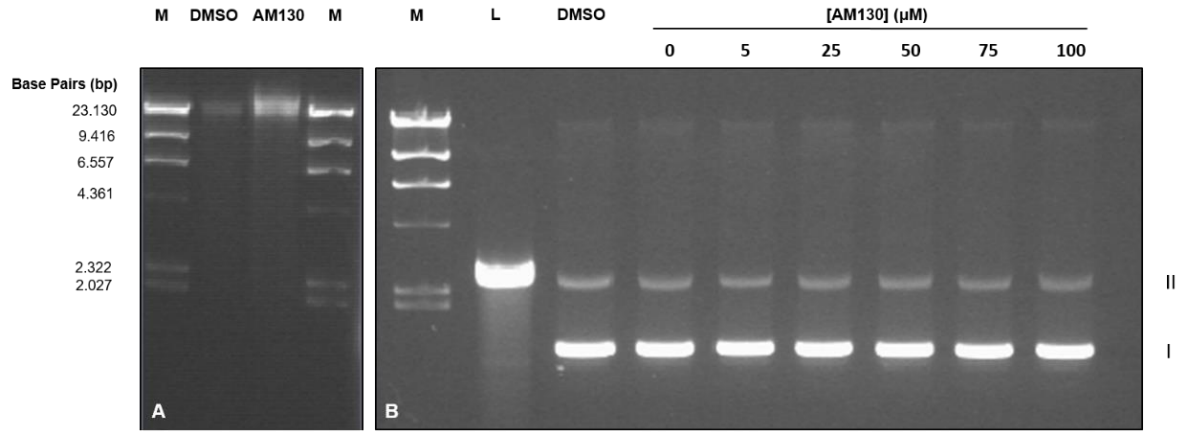


**Figure 3.15 -** Agarose gel electrophoresis concerning the incubation of A2780 DNA genomic and plasmid DNA with AM130. (A) Interaction of AM130 compound with A2780 genomic DNA. Cells were exposed to $IC_{50}$ concentration (8.5 μM) and 0.4% (v/v) of DMSO (vehicle control) for 48 h at 37ºC. (B) Exposure effect of 100 ng of pUC18 DNA to either 0.02% (v/v) DMSO or to increasing concentrations of AM130 (0 to 100 μM) in 5 mM Tris-HCl 50mM NaCl buffer pH 7.0, for 24 h at 37ºC. Resulting products were submitted to electrophoresis in agarose gel 0.8% (w/v) at 80V during 1 h 40 min. Data were from three independent experiments. M - λ-HindIII (molecular weight marker); DMSO – Control; AM130- Compound; L – Linearized pUC18 with *HindIII*; I – Supercoiled isoform; II – Circular isoform.

### 3.6 Spectroscopic studies of the effects of anticancer AM130 interaction with DNA

The interaction between AM130 and CT-DNA in 5 mM Tris-HCl buffer with 50 mM NaCl (pH 7.2) was also assessed using UV-Visible absorption spectroscopy and CD spectroscopy.

#### 3.6.1 UV-Visible spectra measurement

UV–Visible absorption spectroscopy is the most commonly technique for the study of the DNA stability and its interactions with small ligand molecules. Monitoring the changes in the absorption properties of the compound or the DNA allows the study of drug–DNA interactions (Sirajuddin et al. 2013). To understand if AM130 can interact with DNA, titration of compound with CT-DNA was monitored by UV-Vis absorption spectroscopy. Doxorubicin, which interact with DNA through an intercalative mode, was used as compound reference. According to the literature, there are four different ways by which therapeutics interact with DNA: (i) electrostatic or surface binding i.e., external binding to DNA double helix without selectivity; (ii) groove binding involving hydrogen bonding or van der Waals interaction in the major or minor groove of the DNA helix; (iii) intercalative binding mode where small molecules intercalate into the stacked base pairs of DNA and (iv) covalent binding mode (Sirajuddin et al. 2013).

The absorption spectra of AM130-CT-DNA complex in Tris-HCl buffer solution are represented in Figure 3.16. The absorption spectrum of the synthesized AM130 indicates three absorption bands attributed to π → π* at 265, 308 and 381 nm (results not shown). The absorption band at 381 nm was chosen to determine the interaction of this compound with DNA.

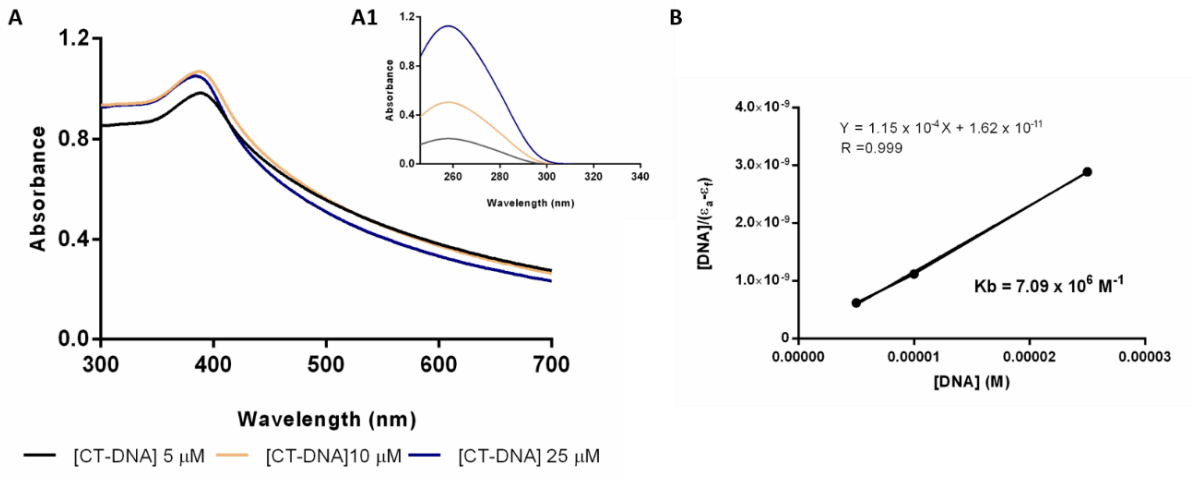


**Figure 3.16 -** Analysis of AM130–CT-DNA interaction by UV-Vis spectroscopy. Solutions were incubated 24 h at 37°C in 5 mM Tris-HCl buffer with 50 mM NaCl pH=7.2. (A) Absorbance spectrum resultant from the interaction between AM130 and CT-DNA at different concentrations (5, 10 and 25 μM). (A1) CT-DNA spectrum at 5, 10 and 25 μM. (B) Linear regression used to calculate binding affinity constant ($K_b$) of AM130 compound with CT-DNA. Data are from one experiment.

Results demonstrated that with each addition of CT-DNA to AM130 solution, the entire absorption spectrum undergoes a hyperchromic effect i.e., an increase of the absorbance with the increase of DNA concentration in solution, accompanied by a hypsochromic shift. According to the literature, the hyperchromic effect results from damages on the DNA double-helix structure after ligand–DNA complex formation, followed by an outstanding increase of the DNA absorbance (Sirajuddin et al. 2013; Jayamani et al. 2014). In addition, the magnitude of the hypsochromic shift could be interpreted as an indicator of the strength of the interaction between the DNA and the compound (Sirajuddin et al. 2013). The affinity constant was determined based on the above-mentioned absorbance increase as a result of DNA–compound interaction in order to evaluate the interaction strength. The revealing value was 7.09 x $10^6$ $M^{-1}$ (Figure 3.16 B), similar to doxorubicin, a common and strong DNA intercalator (Luís et al. 2014).

Overall, based in the absorption spectra changes of compound and in the interaction studies with pDNA, the interaction between AM130 and DNA can be attributed to a non-intercalative binding mode i.e., might be groove binding in a strong fashion. These results are supported by two facts: firstly, the binding of small molecules to minor or major groove can causes damages to DNA at the exterior phosphate backbone (Jayamani et al. 2014; Kazemi et al. 2015), leading to a hyperchromic effect and, secondly, as demonstrated before, compound is not able to cause both cleavage or reduction in the migration of the supercoiled form with increasing concentrations of the compound (Figure 3.15 B).

### 3.6.2 Circular dichroism spectra measurement

Circular dichroism (CD) absorption spectroscopy, which is sensitive to local conformational changes in the secondary structure of DNA, is highly useful for the study of the interaction between small ligands and DNA. This technique measures the difference between the absorption of left-handed polarized light and right-handed polarized light due to structural asymmetry (Chang et al. 2012; Qiao et al. 2015). The CD spectrum of CT-DNA consists in a negative band at 245 nm due to helicity of DNA and a positive band at 275 nm due to base stacking, which is characteristic of DNA in right-handed B form (Figure 3.17 A; Jangir et al. 2011).

To establish in more detail whether binding of the compound brings about any significant conformational change on the DNA double helix, CD spectra of CT-DNA were recorded by keeping the concentration of AM130 at 100 µM or 0.1% (v/v) DMSO (vehicle control) with increasing concentrations of DNA in a buffer solution 5 mM Tris-HCl 50 mM NaCl, pH 7.0. As seen in Figure 3.17 B, the CD spectra of AM130-DNA complex exhibits a positive peak between 280 and 290 nm due to the base stacking and a negative peak between 240 and 250 nm due to right-handed helicity. AM130 has not intrinsic CD signal, however being a chiral molecule any CD signal below 300 nm can be attributed to the interaction of compound with DNA (results not shown). Based on CD results the presence of the AM130 leads to conformational changes on DNA with the increase of the positive band and the decrease of the negative band (shifting to zero levels), both accompanied by a slight red shift about 3 nm compared to control group.

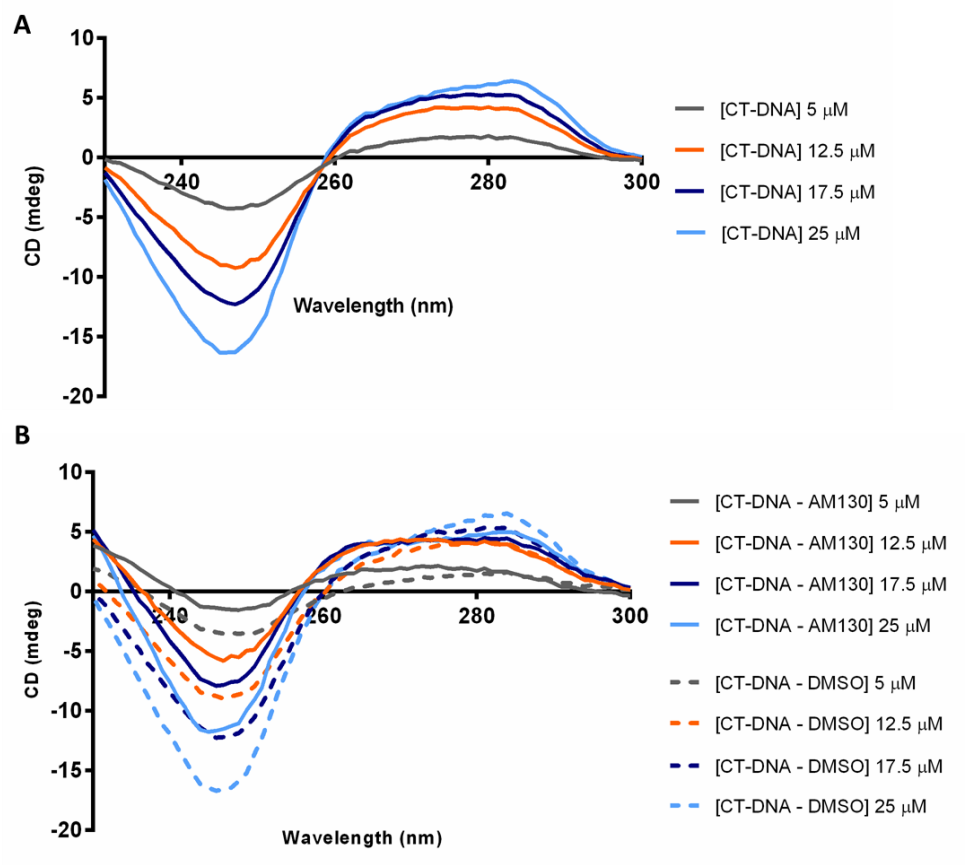


**Figure 3.17 -** The interaction of AM130 with calf thymus DNA in 5 mM Tris-HCl 50 mM NaCl, pH 7.0 buffer at 37ºC by circular dichroism (CD). (A) CD spectra of CT-DNA at 5, 12.5, 17.5, and 25 µM. (B) Interaction CD spectra of AM130 compound at 100 µM and 0.1% (v/v) DMSO (vehicle control) in the presence of increasing concentrations of CT-DNA (5, 12.5, 17.5 and 25 µM). Data are from two independent experiments.

The CD results pointed to a possible interaction of the compound with DNA through a non-intercalative binding mode, corroborating the UV-Visible results (Figure 3.16). The enhancement of the CD signal at 275 nm is possibly due to distortions in the DNA structure whereas the reduction of intensity of the signal at 245 nm can be due to the packaging of the double helix of DNA. The overall results about interaction between AM130 and CT-DNA confirm that the compound interacts with DNA via groove binding. These results are supported by literature research which indicate that compounds that interact with DNA by groove binding cannot induce distinct conformational changes in DNA. This is true because compounds can adjust its structure to the minor groove of DNA and follow the twisting of this molecule along the central axis (Geierstanger & Wemmer, 1995; Armitage, 2005). AM130 compound did not show a genotoxic effect in A2780 cells (Figure 3.15), leading to the conclusion that its reactivity observed by direct exposure *in vitro* to DNA (Figures 3.16 and 3.17) may not have a significant effect in the cellular context. For this reason, AM130 compound may interact preferentially with other cellular components, namely proteins, and, thus, being prevented from reaching the nucleus. Interaction with serum albumin (a major component of blood; Chakraborty & Basu 2009) and comparative proteomics may reveal some clues on this mechanism (Section 3.7 and Section 3.8).

### 3.7 Bovine serum albumin interaction

UV–visible absorption spectroscopy allows to investigate conformational changes in proteins, variations in hydrophobicity and the interaction between drugs and proteins (Guo et al. 2009).
In blood, drug transport is carried out by reversible binding to serum albumin proteins (Chakraborty & Basu, 2009). The binding ability of drugs to serum albumin in blood has impact on its distribution, free concentration and metabolism influencing their biological activity (Chakraborty & Basu, 2009). Bovine serum albumin (BSA) is the major binding protein for several physiological substances and is used as a model for studying drug–protein interaction *in vitro* due to its structural homology to human serum albumin (HSA) and lower cost (Seetharamappa & Kamat, 2004; Chakraborty & Basu, 2009).

The UV-Visible absorption spectrum of BSA include two absorption peaks at 220 nm and at 280 nm, corresponding to the absorption of the backbone of BSA and aromatic amino acids (tryptophan, tyrosine, and phenylalanine), respectively (Xu et al. 2013). Figure 3.18 display the changes in UV-Visible absorption spectra of BSA with increasing amount of AM130 compound. As shown, the absorption intensity of BSA at 278 nm increased regularly with increasing concentrations of the compound, also associated with a blue shift from 278 to 276 nm. Simultaneously, the absorption peak at 360 nm arises as a result from the interaction between AM130 and BSA protein, wherein increasing compound concentrations increases its intensity. Both evidences imply the formation of AM130-BSA complex with changes in protein structure and in the hydrophobicity of BSA (Buddanavar & Nandibewoor, 2016).

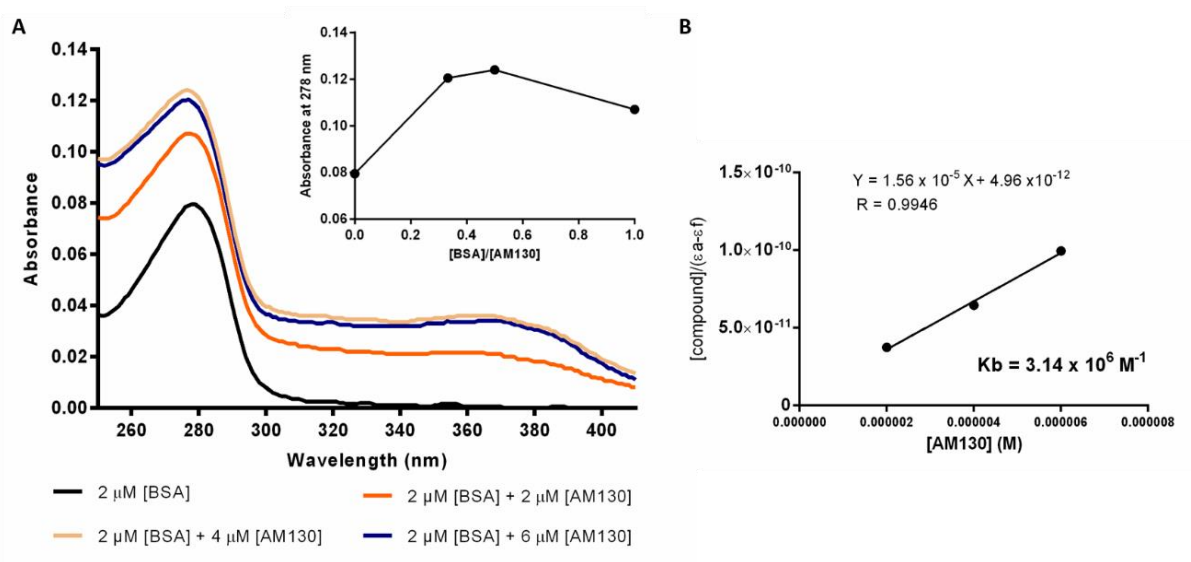


**Figure 3.18 -** Absorption spectrum showing the formation of AM130 – BSA complex by UV-Vis spectroscopy. (A) Interaction of AM130 at different concentrations (2, 4 and 6 μM) with BSA (2 μM). (B) Linear regression used to calculate $K_b$ of AM130 compound with BSA. Solutions were incubated 1 h at 4˚C in 10 mM phosphate buffer 0.15 M NaCl pH 7.0. Data are from two independent experiment.

In the upper right corner of Figure 3.18 is represented the [BSA]/[AM130] ratio. As demonstrated the absorbance intensity increased until reach the maximum [BSA]/[AM130] ~ 0.5, with a slight increase of intensity when ratio is from 0.3 to 0.5. This indicates that BSA has various binding sites for AM130, and redistribution took place when two molecules of the compound binds to one of BSA protein.

Nevertheless, the change in $\lambda_{max}$ in the present study indicates that AM130-BSA complex induces alterations in polarity of the microenvironment around the tryptophan and tyrosine residues of BSA, as well as, in BSA conformation (Buddanavar & Nandibewoor, 2016). To evaluate the bond strength between compound and BSA protein, the $K_b$ was obtained from the plot log[($I_o$-I)/I] *vs.* log[Q], namely 3.14 x $10^6$ $M^{-1}$ (Figure 3.18 B). According to previously studies, the $K_b$ values in the range of $10^4$ to$10^6$ $M^{-1}$ indicate an efficient and optimal interaction between drugs and proteins (Tarushi et al. 2014). For this range, $K_b$ value, besides promoting the binding of the compound to the serum albumin proteins, also ensures that a significant amount of compound gets transported and distributed through the organism. At the same time, these values allow the compound release once it reaches its target (Rajendiran et al. 2007; Tarushi et al. 2014). Overall, the present results demonstrate that AM130 compound is capable to efficiently interact with the serum albumin proteins with the advantage of increasing its systemic biodistribution (Luís et al. 2014).

### 3.8 Proteomics

The comparative proteome profile of AM130-treated cancer cells was established for a better understanding of the molecular mechanisms underlying the biological activity of this spirooxindole derivative compound, including insights into its cytotoxicity, allowing the correlation between altered protein expression and potential targets. The 2D-gels obtained were compared with HCT116 cell line reference 2D-gel (Figure 6.5 Appendix C) to determine the variation in abundance levels of identified proteins i.e. values above 1.5, over-expressed proteins, and below 0.7, under-expressed proteins, were considered as biologically significantly different. HCT116 cells were used as reference in this study since it is the cell line with a higher number of identified proteins available in our research group. Mass spectroscopy analysis was not achieved due to time limitations however, a latter spots characterization and confirmation will be performed.

A total of 273 and 263 proteins were identified in A2780 cells exposed to 0.1%(v/v) DMSO (vehicle control) and $IC_{50}$ concentration of AM130, respectively. Additionally, 40% of the analyzed proteins exhibited significant differences in abundance ($p < 0.05$), including 19% over-expressed, 21% under-expressed, and 60% of proteins with no significant variation (Figure 3.19).

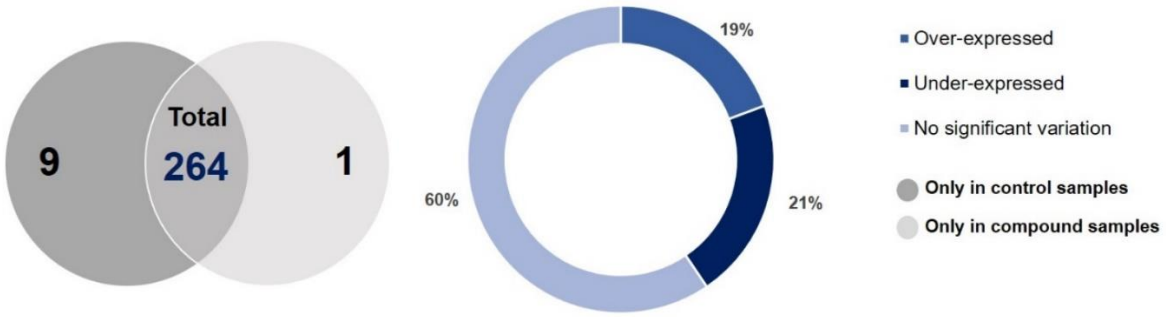


**Figure 3.19 -** Protein overlaps among AM130-treated A2780 cancer cells compared to control. In the left is represented the Venn diagram of protein overlaps between two biological assays in which 264 proteins are common between A2780 exposed to DMSO (vehicle control) and to compound, 9 proteins are only expressed in DMSO and 1 protein appears in cells exposed to AM130. For these proteins was not possible to match with the reference 2D-gel but in Figure 3.20 the spots were identify with colors. On the other hand, in the right is indicated the percentage of under- (< 0.7-fold) and over- (>1.5-fold) expressed proteins as well as, the proteins without significant abundance (0.7 ≤ fold ≤ 1.5).

In this study, given the extensive number of proteins with substantial differences in abundance levels, only a few will be addressed here like proteins known to be involved in apoptosis, cytoskeleton maintenance, cell cycle progression and cellular stress. The total number of proteins that were possible to identify by previous characterized gels and that exhibited significant differences in abundance are depicted in Figure 3.20 and Table 3.2. The proteins with altered intracellular levels in A2780 cells that matched with the HCT116 gel reference were subjected to analysis using STRING 10.5 database. Furthermore, the proteins without match with the gel reference will be excised from the 2D-gel and, then characterize by Maldi-Tof MS/MS in the Instituto de Tecnologia Química e Biológica António Xavier. The majority of the identified proteins were associated with the regulation of apoptosis (59%), regulation of response to stress (63%) and protein folding (27%). Additionally, was also predicted that most of the proteins were from the cytosol and nucleus.

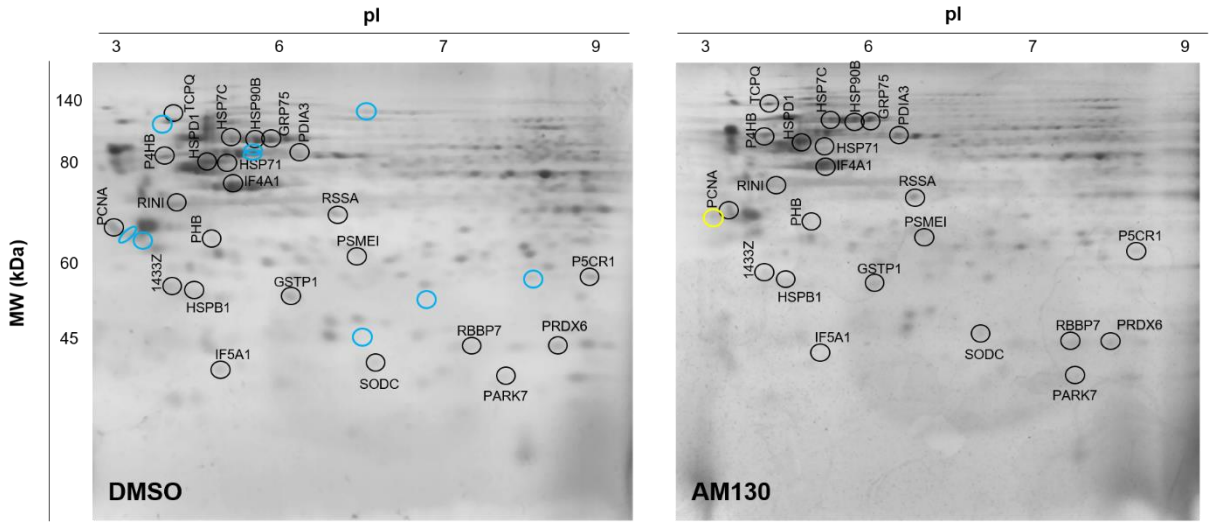


**Figure 3.20 -** Representative two-dimensional gel electrophoresis for total protein extracts from A2780 cell line. Cell were exposed to 0.1% (v/v) DMSO or $IC_{50}$ compound concentration and incubated for 48 h. Proteins were separated by 7 cm 3–9 NL IPG-Strips and loaded on SDS-PAGE gels. Proteins with different abundance are shown as proteins' abbreviation spots, which are also presented in Table 3.2. The blue circles presented in the left 2D-gel indicates the proteins that were only expressed in A2780 exposed to DMSO and absents in AM130-treated cells (2D-gel in the right), and the same for the yellow circle indicated in the AM130 2D-gel (see Figure 3.19). The protein spots were identified using *Melanie 7.0* software.

**Table 3.2 -** Proteome evaluation of AM130-treated A2780 cells compared to control. Proteins whose abundance variance levels were considered significantly altered were highlighted. Fold variation under 0.7 (red) was consider as under-expression and fold variation over 1.5 (green) was considered as over-expression.

| **Human Protein identification** (abbreviation) | **Expression level** | **Molecular Function** |
|---|---|---|
| Superoxide dismutase [Cu-Zn] (SODC) | 0.5 | Component turnover/Detox |
| Pyrroline-5-carboxylate reductase 1 (P5CR1) | 0.6 | Stress response |
| Glutathione S-transferase P 1 (GSTP1) | 2.4 | Detoxification |
| Peroxiredoxin-6 (PRDX6) | 1.8 | Component turnover/Detox |
| Glutamate dehydrogenase 1, mitochondrial (DHE3) | 1.6 | Metabolic activity |
| Histone-binding protein RBBP7 (RBBP7) | 1.8 | Chromatin remodeling factor |
| T-complex protein 1 subunit theta (TCPQ) | 2.4 | Cytoskeleton mobility |
| Protein disulfide isomerase family A member 3 (PDIA3) | 1.8 | Protein binding/Folding |
| Protein disulfide-isomerase (P4HB) | 2.3 | Protein binding/Folding |
| Proteasome activator complex subunit 1 (PSME1) | 0.6 | Endopeptidase activator activity |
| Prohibitin (PHB) | 1.6 | Regulation of mitochondrial activity |
| 14-3-3 protein zeta/delta (1433z) | 1.9 | Signal transduction |
| Proliferating cell nuclear antigen (PCNA) | 1.6 | Transcriptional/ translational machinery |
| Eukaryotic translation initiation factor 5A-1 (IF5A1) | 2.4 | Transcriptional/ translational machinery |
| Eukaryotic initiation factor 4A-I (IF4A1) | 1.8 | Transcriptional/ translational machinery |

| **Human Protein identification** (abbreviation) | **Expression level** | **Molecular Function** |
|---|---|---|
| Ribonuclease inhibitor (RINI) | 1.6 | Transcriptional/ translational machinery |
| Heat shock 60kDa protein 1 (HSPD1) | 2.0 | Chaperone/ Stress response |
| Heat shock 27kDa protein 1 (HSPB1) | 1.9 | Chaperone/ Stress response |
| Heat shock 70 kDa protein 9 (GRP75) | 1.7 | Chaperone/ Stress response |
| Heat shock cognate 71 kDa protein (HSP7C) | 2.2 | Chaperone/Stress response |
| Heat shock protein HSP 90-beta (HSP90B) | 1.8 | Chaperone/Stress response |
| Protein DJ-1 (PARK7) | 1.7 | Stress response |
| 40S ribosomal protein SA (RSSA) | 0.6 | Ribosome binding |

Ovarian carcinoma cells exposed to AM130 showed an increase in abundance levels of Disulfideisomerase (P4HB) and disulfide-isomerase A3 (PDIA3), members of the ER stress signaling pathway, revealing a cellular response to stress as a consequence to the exposure to the compound (Pressinotti et al. 2009; Pierrard et al. 2012). In addition, it also shows an increase in Glutathione S-transferase P 1 (GSTP1) and Peroxiredoxin-6 (PRDX6) with a decrease in Superoxide dismutase [Cu-Zn] (SODC) level. These three enzymes are involved in cellular protection against oxidative injury (Chang et al. 2007; Karsani et al. 2014) suggesting that A2780 cell line is considerably less prone to damage induction by ROS when exposed to AM130.

Proteasome activator complex subunit 1 (PSME1) is a protein required for efficient antigen processing, and influences the function of the 26S and 20S proteasome when it interacts with the proteasome activator complex subunit 2 (PSME2). The proteasome is a multicatalytic proteinase complex responsible for the degradation of proteins, namely crucial proteins involved in cell cycle regulation and programmed cell death (Voorhees et al. 2003). The proteomics analysis of AM130 2D-gel compared to DMSO 2D-gel presented showed a decrease in abundance of PSME1, whereas the proteasome activity increases in most cancers.

The adapter protein 14-3-3 protein beta/alpha (1433Z) is involved in the regulation of several signaling pathways including cell proliferation, cell apoptosis and angiogenesis. Moreover, it has been associated with malignant tumor growth and progression. The over-expression of 1433Z can be positively correlated with cancer progression, metastasis and worse survival in ovarian carcinoma patients (Hodgkinson et al. 2012; Kaneko et al. 2016). Thus, 1433Z might be associated with resistance to neoadjuvant chemotherapy, as previously demonstrated by several research groups (Liu et al. 2006; Chuthapisith et al. 2007). However, although in the present study AM130 showed an antiproliferative potential against A2780 cells, further studies must be performed to verify the involvement of this protein in chemotherapy resistance.

Prohibitin (PHB) is a regulatory protein with essential functions in the cell proliferation and apoptosis and its over-expression leads to cell death through intrinsic apoptotic pathway (Coates et al. 2001; Zhang et al. 2012). This explains the results obtained about the mechanism of cell death induced in A2780 cancer cells by AM130. The proliferating cell nuclear antigen (PCNA) protein acts as molecular platform for enzymes responsible for the DNA replication and repair (Cazzalini et al. 2014). During DNA

injuries, as a consequence of the increase in oxidative stress, the PCNA is recruited to repair DNA (Tsai et al. 2017). This explains the increased expression of PARP analyzed by western blot (Figure 3.9 A). Although the overall DNA interaction studies did not demonstrate that AM130 is capable to induce damages in DNA (Figure 3.15) and its involvement in ROS production (Figure 3.11), proteomics analysis revealed that some DNA damage in A2780 cancer cells occurs when exposed to compound.

Proteomic analysis revealed changes in the expression of proteins related to the carcinogenesis process namely, Eukaryotic translation initiation factor 5A-1 (IF5A1), Eukaryotic translation initiation factor 4A-2 (IF4A2) and 40S ribosomal protein SA (RSSA). IF5A1 and IF4A2 are two proteins involved in the translation machinery by mRNA binding. IF5A1 is a regulator of p53/TP53 dependent apoptosis and TNF-α mediated apoptosis with elevated abundancy in cancer cells. Ovarian carcinomas cells exhibit over-expression of this protein when exposed to AM130, which could explain the levels of apoptosis obtained by Hoechst staining and flow cytometry assays (Figure 3.5 and 3.6, respectively). Additionally, A2780 cancer cells exposed to the compound also showed a decreased in RSSA protein, which plays important functions in cell adhesion to the basement membrane, fate determination and tissue morphogenesis.

RINI is a ribonuclease inhibitor involved in the inhibition of RNASE1, RNASE2 and ANG which, in turns, leads to the inhibition of RNA cleavage (Yao et al. 2013). The over-expression pattern of this protein suggests that protein synthesis is interrupted. AM130-treated cells also exhibited over-expression of heat shock proteins (HSP) namely HSPD1, GRP75, HSP7C, HSP90B, HSP71 and HSPBI. The HSP are a heterogeneous group of chaperones whose functions include the protection of cells from environmental stress damage through a protein quality control mechanism and the cooperation in newly synthesized polypeptides transport to target organelles (Sarto et al. 2000). The high intracellular levels of GRP75, HSP7C, HSP90B and HSP71 could indicate a possible accumulation of radicals in the cells, culminating in cell death. Although these findings suggest the involvement of oxidative stress in AM130 related cancer cell death, the obtained results, namely the measure of ROS and DNA interaction studies, demonstrated that the main mechanism of AM130 action does not involves the production of ROS. In addition, the over-expression of HSPD1 protein is related with the activation of procaspase 3, contributing to apoptotic cell death (Sarto et al. 2000; Ciocca et al. 2013), which is correlated directly to the previous results.

HSPB1 is a “survival protein” that interferes with several cell death pathways, specifically in upstream events (e.g., the release of cytochrome-c) of the apoptotic cascade in response to chemotherapy to counter the antiproliferative action of antitumoral agents. The high intracellular levels of this protein in cancers is associated with the increase of resistance to radiotherapy or to common antitumoral agents like cisplatin and doxorubicin (Gibert et al. 2011). Furthermore, the increased levels of Protein DJ-1 (PARK7) is also related to cell protection against oxidative stress and cell death (Chen et al. 2010). Thus, its over-expression represents a defense mechanism by cancer cells against the damages induced by AM130.

Overall, the proteomic study proved that A2780 cancer cells treated with AM130 reveals two types of response: the first one corresponds directly to an antitumoral response by the compound, leading to an increase of pro-apoptotic proteins like HSPD1 and the second one involves cell survival mechanisms activated by the damages induced by the compound.

# 4 CONCLUSIONS AND FUTURE PERSPECTIVES

Over the past years, despite the significant efforts in cancer treatment to increase therapy efficiency without promoting healthy cells toxicity and cancer cells resistance, cancer remains one of the major causes of death worldwide. To overcome this fatality, both genomics and proteomics progresses in the identification of unique cellular and biochemical features of each tumor and the knowledge of the molecular mechanisms and biological targets of anticancer agents, have, together, brought up the necessity for both synthesis and evaluation of new compounds with more promising antiproliferative potential with specific intracellular targets in cancer cells.

The potential antitumoral agent studied, a spiropyrazoline derivative – 5-bromo-2',4',5'-triphenyl-2',4'-ihydrospiro[indoline-3,3'-pyrazol]-2-one, was firstly synthesized and then, its putative effects in intracellular pathways were investigated in ovarian carcinoma using the A2780 cell line as a model. The low yields obtained during the synthesis of AM130 were due to my inexperience in organic chemistry, making it impossible to obtain considerable amounts of the final product. These losses occurred mostly during the purification processes.

During the present study, it was demonstrated that the AM130 compound presented an effective antiproliferative potential against human cancer cell lines, namely A2780, HCT116 and MDA-MB-453 at concentrations that do not affect the survival and growth of normal human fibroblasts, hence demonstrating some selectivity for those cancer cell lines. Notably, data demonstrated by the altered nuclear morphology, which identifies apoptotic features, flow cytometry, mitochondrial potential changes and western blot, indicates that possible the mitochondria-mediated apoptotic pathway was, at least in part, responsible for AM130-induced A2780 cell death, probably without ROS contribution. Additionally, the exposure of A2780 cancer cells to the compound seems to induce other non-apoptotic mechanism of cell death, such as autophagy. However, the mechanism of cell death induced by the compound possibly may not result from complex-induced DNA damages as demonstrated by various methods, despite the affinity constant value for CT-DNA obtained, which was similar to the common DNA-interacting antitumor agent – doxorubicin. A specific interaction with BSA was observed by UV-visible spectroscopy with a $K_b$ value of $3.14 \times 10^6\ M^{-1}$, indicating that AM130 can be efficiently transported by serum proteins in the bloodstream. This reversible interaction with BSA can promote the delivery of compound to the tumor mass and, as much as possible, improve compound solubility. For future projects will be needed the confirmation of this interaction using HSA through fluorescence spectroscopy, since is the most abundant plasma carrier protein involved in the binding and transport of drugs in the blood showing, also, a low immunogenicity.

The study of A2780 cell line proteome revealed changes in the levels of several proteins involved in various biological pathways e.g., apoptosis, stress response and protein folding. HSP proteins are normally associated with a resistance to apoptosis, e.g., HSPB1, on the other hand, the HSPD1 can activate the procaspase 3 leading to programmed cell death. Other proteins e.g., GSTP1 and PRDX6, were involved in the protection of the cells against oxidative stress. Additionally, 2D-gel analysis showed an increase of proteins involved in the protection of cells against ROS. However, the measurement of

ROS in AM130-treated cells did not revealed the involvement of this radical in the cell death induced by the compound. To confirm these findings, mass spectrometry (Maldi-Tof MS/MS) analysis will be performed later. Considering the activation of some proteins involved in drug resistance mechanisms, it would be interesting to study the proteome of the cells incubated for different time periods to evaluate the variation of the expression of these, confirming the cellular adaptation mechanisms, as well as to get more concrete answers about the mechanism of action of the AM130. Overall, the proteomic analysis confirmed the results, namely that AM130 is able to induce apoptosis, possibly due to an intrinsic apoptosis pathway.

Ultimately, the results are promising features for *in vivo* studies. Regarding the antiproliferative activity of AM130 and the identification of its possible intracellular pathways in cancer cells, the proposed aims for the present project were achieved. Notwithstanding, the toxicity and selectivity for cancer cells, which makes the compound in study an auspicious anticancer agent, due to its low solubility the *in vivo* studies must be avoided. To overcome this issue, it would be interesting for future projects to proceed to two different approaches: change the compound' structure or the design of a delivery system, e.g., nanoparticles using the efficient interaction between AM130 and serum proteins as effective carriers for this spirooxindole derivative compound.

**Table 4.1 -** Summary of each biological assay performed in AM130-treated cells and its respective biological effects.

| Assays performed in AM130-treated cells | Biological effects |
|---|---|
| **Assessment to cytotoxic potential** | Selective antiproliferative activity against cancer cells<br>Greater cytotoxic effect in A2780 cancer cells |
| **Assessment to cell death mechanisms** | |
| • Hoechst and PI staining | Induction of chromatin condensation and fragmentation resulting in 31% of apoptosis<br>Absence of necrotic cells |
| • Annexin V-FITC/PI staining | Increase in the percentage of early and late apoptotic cells without necrotic cells |
| • Mitochondrial function | Mitochondrial dysfunction leading to the $\Delta\Psi_M$ collapse |
| • Relative expression levels of BAX, BCL-2 and PARP proteins | Increase in BAX and PARP levels and decrease in BCL-2 levels<br>Increase in BAX/BCL-2 ratio |
| • Autophagy | Accumulation of autophagosomes and autophagolysomes with 58% of autophagic cells |
| • Oxidative damages – ROS contributions | Absence of ROS accumulation |
| **Assessment to cytostatic potential** | Absence of cell cycle arrest |
| **Intracellular targets** | |
| • **DNA interaction studies** | |
| • UV-titrations | AM130-CT-DNA complex formation with a $K_b$ value of $7.09 \times 10^6\ M^{-1}$ |
| • CD | Complex formation leads to conformational changes on DNA<br>Interaction by a non-intercalative binding mode – groove binding |
| • Genomic and plasmid DNA: electrophoretic studies | Absence of genomic DNA fragmentation<br>Absence of both plasmid DNA cleavage and changes in the electrophoretic mobility |
| • **Proteins interaction studies** | Interaction with BSA through an efficient binding with a $K_b$ value of $3.14 \times 10^6\ M^{-1}$<br>AM130-BSA complex causes changes in BSA conformation and hydrophobicity |
| **Proteomic studies** | Most of the identified proteins were associated with the regulation of apoptosis (59%), regulation of response to stress (63%) and protein folding (27%).<br>From cytosol and nucleus |

## 5 REFERENCES


Adams, J.M. & Cory, S. 2009. The Bcl-2-regulated apoptosis switch: mechanism and therapeutic potential. *October*, 19(5): 488–496.

Agarwal, R. & Kaye, S.B. 2003. Ovarian cancer: strategies for overcoming resistance to chemotherapy. *Nature reviews Cancer*, 3(7): 502–516.

Agarwal, S., Jangir, D.K. & Mehrotra, R. 2013. Spectroscopic studies of the effects of anticancer drug mitoxantrone interaction with calf-thymus DNA. *Journal of Photochemistry and Photobiology B: Biology*, 120(2013): 177–182.

Alderton, G.K. & Bordon, Y., 2012. Tumour immunotherapy — leukocytes take up the fight. *Nature Reviews Immunology*, 12(4): 237–237.

Armitage, B.A. 2005. Cyanine Dye–DNA Interactions: Intercalation, Groove Binding, and Aggregation. In *DNA Binders and Related Subjects*, 253: 55–76.

Ashkenazi, R., Gentry, S.N. & Jackson, T.L. 2008. Pathways to tumorigenesis--modeling mutation acquisition in stem cells and their progeny. *Neoplasia (New York, N.Y.)*, 10(11): 1170–82.

Aslanoglu, M. 2006. Electrochemical and spectroscopic studies of the interaction of proflavine with DNA. *Analytical sciences : the international journal of the Japan Society for Analytical Chemistry*, 22(3): 439–43.

Baskar, R. et al. 2012. Cancer and radiation therapy: current advances and future directions. International Journal of Medical Sciences, 9(3): 193–199.

Binaschi, M. et al. 2011. Maintenance therapy in ovarian cancer: Molecular basis and therapeutic approach. *Experimental and therapeutic medicine*, 2(2): 173–180.

Bostock, C.J., Prescott, D.M. & Kirkpatrick, J.B. 1971. An evaluation of the double thymidine block for synchronizing mammalian cells at the G1-S border. *Experimental Cell Research*, 68(1): 163–168.

Brannon-Peppas, L. & Blanchette, J.O. 2012. Nanoparticle and targeted systems for cancer therapy. *Advanced Drug Delivery Reviews*, 64(2012): 206–212.

Bruin, J.E. et al. 2008. Increased pancreatic beta-cell apoptosis following fetal and neonatal exposure to nicotine is mediated via the mitochondria. *Toxicological Sciences*, 103(2): 362–370.

Brumatti, G., Sheridan, C. & Martin, S.J. 2008. Expression and purification of recombinant annexin V for the detection of membrane alterations on apoptotic cells. *Methods*, 44(3): 235–240.

Brun, P. et al. 2012. In vitro response of osteoarthritic chondrocytes and fibroblast-like synoviocytes to a 500-730 kDa hyaluronan amide derivative. *Journal of Biomedical Materials Research - Part B Applied Biomaterials*, 2012 (100B): 2073-2081.

Buddanavar, A.T. & Nandibewoor, S.T. 2016. Multi-spectroscopic characterization of bovine serum albumin upon interaction with atomoxetine. *Journal of Pharmaceutical Analysis*, 2016: 1–8.

Cabral, R.M. & Baptista, P. V. 2014. Anti-cancer precision theranostics: a focus on multifunctional gold nanoparticles. *Expert review of molecular diagnostics*, 14(8): 1041–52.

Cao, P. et al. 2011. Growth inhibition and induction of apoptosis in SHG-44 glioma cells by chinese medicine formula “pingliu Keli.” *Evidence-based Complementary and Alternative Medicine*, 2011: 958243.

Cazzalini, O. et al. 2014. CBP and p300 acetylate PCNA to link its degradation with nucleotide excision repair synthesis. *Nucleic Acids Research*, 42(13): 8433–8448.

Chai, S., To, K.K. & Lin, G. 2010. Circumvention of multi-drug resistance of cancer cells by Chinese herbal medicines. *Chinese medicine*, 5: p.26.

Chaitanya, G., Alexander, J.S. & Babu, P. 2010. PARP-1 cleavage fragments: signatures of cell-death proteases in neurodegeneration. *Cell Communication and Signaling*, 8(1): 31.

Chakraborty, B. & Basu, S. 2009. Interaction of BSA with proflavin: A spectroscopic approach. *Journal of Luminescence*, 129(1): 34–39.

Chang, X. et al. 2007. Research article Identification of the functional role of peroxiredoxin 6 in the progression of breast cancer. *Breast Cancer Research*, 9(6): 1–15.

Chang, Y.M., Chen, C.K.M. & Hou, M.H. 2012. Conformational changes in DNA upon ligand binding monitored by circular dichroism. *International journal of molecular sciences*, 13(3): 3394–413.

Chen, J., Li, L. & Chin, L. 2010. Parkinson disease protein DJ-1 converts from a zymogen to a protease by carboxyl-terminal cleavage. *Human Molecular Genetics*, 19(12): 2395–2408.

CHENG, X. et al. 2003. Studies on Repository Compound Stability in DMSO under Various Conditions. *Journal of Biomolecular Screening*, 8(3): 292–304.

Chien, J. et al. 2013. Platinum-sensitive recurrence in ovarian cancer: the role of tumor microenvironment. *Frontiers in oncology*, 3(251): 1–6.

Christensen, M.E. et al. 2013. Flow cytometry based assays for the measurement of apoptosis-associated mitochondrial membrane depolarisation and cytochrome c release. *Methods*, 61(2): 138–145.

Chuthapisith, S. et al. 2007. Proteomic profiling of MCF-7 breast cancer cells with chemoresistance to different types of anti-cancer drugs. *International Journal of Oncology*, 30(6): 1545–1551.

Ciocca, D.R., Arrigo, A.P. & Calderwood, S.K. 2013. Heat shock proteins and heat shock factor 1 in carcinogenesis and tumor development: an update. *Archives of Toxicology,* 87(1): 19–48.

Coates, P.J. et al. 2001. Mammalian Prohibitin Proteins Respond to Mitochondrial Stress and Decrease during Cellular Senescence. *Experimental Cell Research*, 265(2): 262–273.

Colditz, G.A., Wolin, K.Y. & Gehlert, S. 2012. Applying What We Know to Accelerate Cancer Prevention. *Biophysical Chemistry*, 4(127): 127rv4.

Colombo, N., et al. 2010. Newly diagnosed and relapsed epithelial ovarian carcinoma: ESMO Clinical Practice Guidelines for diagnosis, treatment and follow-up. *Annals of Oncology*, 21(5): 23–30.

Coward, J.I.G., Middleton, K. & Murphy, F. 2015. New perspectives on targeted therapy in ovarian cancer. *International Journal of Women's Health*, 7: 189–203.

Crawford, S. 2013. Is it time for a new paradigm for systemic cancer treatment? Lessons from a century of cancer chemotherapy. *Frontiers in Pharmacology*, 4(68): 1–18.

Dasari, S. & Tchounwou, P.B. 2014. Cisplatin in cancer therapy: Molecular mechanisms of action. *European Journal of Pharmacology*, 740(0): 364–378.

Di, L. & Kerns, E.H. 2006. Biological assay challenges from compound solubility: strategies for bioassay optimization. *Drug Discovery Today*, 11(9–10): 446–451.

Elmore, S. 2007. Apoptosis: A Review of Programmed Cell Death. *Toxicologic Pathology*, 35(4): 495–516.

Enzo Life Sciences, 2016. CYTO-ID® Autophagy Detection Kit. Available at: http://static.enzolifesciences.com/fileadmin/files/manual/ENZ-51031_insert.pdf.

Ferenbach, D.A. & Bonventre, J.V. 2015. Mechanisms of maladaptive repair after AKI leading to accelerated kidney ageing and CKD. *Nature Publishing Group*, 11(5): 264–276.

Ferlay J, Soerjomataram I, Ervik M, et al. 2013. GLOBOCAN 2012 v1.0, Cancer Incidence and Mortality Worldwide: IARC CancerBase No. 11 [Internet]. Lyon, France: International Agency for Research on Cancer. Available at: http://www.cancerresearchuk.org/health-professional/cancer-statistics/worldwide-cancer/incidence#ref-0, [Accessed September 1, 2016].

Galliford, C. V. & Scheidt, K.A. 2007. Pyrrolidinyl-spirooxindole natural products as inspirations for the development of potential therapeutic agents. *Angewandte Chemie - International Edition*, 46(46): 8748–8758.

Galluzzi, L. et al. 2012. Molecular definitions of cell death subroutines: recommendations of the Nomenclature Committee on Cell Death 2012. *Cell Death Differ*, 19(1): 107–120.

Geierstanger, B.H. & Wemmer, D.E. 1995. Complexes of the Minor Groove of DNA. *Annual Review of Biophysics and Biomolecular Structure*, 24: 463–493.

Gibert, B. et al. 2011. Inhibition of heat shock protein 27 (HspB1) tumorigenic functions by peptide aptamers. *Oncogene*, 30(34): 3672-81.

Glick, D., Barth, S. & Macleod, K.F. 2010. Autophagy: cellular and molecular mechanisms. *Journal of Pathology*, 221(1): 3–12.

Goff, B. A., et al. 2000. Ovarian carcinoma diagnosis. *Cancer*, 89(10): 2068–2075.

Gümüs, F. et al. 2009. Synthesis, Cytotoxicity, and DNA Interactions of New Cisplatin Analogues Containing Substituted Benzimidazole Ligands Synthesis , Cytotoxicity , and DNA Interactions of New Cisplatin Analogues Containing. *Journal of Medicinal Chemistry*, 52(5): 1345–1357.

Guo, X. et al. 2009. Spectroscopic studies on the interaction between sodium ozagrel and bovine serum albumin. *Journal of Molecular Structure*, 928(1–3): 114–120.

Hamasaki, M., Shibutani, S.T. & Yoshimori, T. 2013. Up-to-date membrane biogenesis in the autophagosome formation. *Current Opinion in Cell Biology*, 25(4): 455–460.

Hanahan, D. & Weinberg, R.A. 2011. Hallmarks of cancer: The next generation. *Cell*, 144(5): 646–674.

Harris, S.L. & Levine, A.J. 2005. The p53 pathway: positive and negative feedback loops. *Oncogene*, 24(17): 2899–2908.

Healthcare, 2009. 2-D Clean-Up Kit. pp.2–5.

Henry, C.M., Hollville, E. & Martin, S.J. 2013. Measuring apoptosis by microscopy and flow cytometry. *Methods*, 61(2): 90–97.

Hodgkinson, V.C. et al. 2012. Proteomic identification of predictive biomarkers of resistance to neoadjuvant chemotherapy in luminal breast cancer: A possible role for 14-3-3 theta/tau and tBID? *Journal of Proteomics*, 75(4): 1276–1283.

Huang, S. 2013. Genetic and non-genetic instability in tumor progression: Link between the fitness landscape and the epigenetic landscape of cancer cells. *Cancer and Metastasis Reviews*, 32(3–4): 423–448.

Invitrogen, 2011. Annexin V Conjugates for Apoptosis Detection. Available at: https://tools.thermofisher.com/content/sfs/manuals/mp13199.pdf.

Invitrogen, 2006. Reactive Oxygen Species (ROS) Detection Reagents. Available at: https://tools.thermofisher.com/content/sfs/manuals/mp36103.pdf.

Irigaray, P. et al. 2007. Lifestyle-related factors and environmental agents causing cancer: An overview. *Biomedicine and Pharmacotherapy*, 61(10): 640–658.

Jabir, N.R. et al. 2012. Nanotechnology-based approaches in anticancer research. *International Journal of Nanomedicine*, 7: 4391–4408.

Jangir, D.K. et al. 2011. FTIR and circular dichroism spectroscopic study of interaction of 5-fluorouracil with DNA. *Journal of Photochemistry and Photobiology B: Biology*, 105(2): 143–148.

Janku, F. et al. 2011. Autophagy as a target for anticancer therapy. *Nature Reviews Clinical Oncology*, 8: 528–539.

Jayamani, A. et al. 2014. Synthesis of mononuclear copper(II) complexes of acyclic Schiff's base ligands: Spectral, structural, electrochemical, antibacterial, DNA binding and cleavage activity. *Spectrochimica Acta - Part A: Molecular and Biomolecular Spectroscopy*, 122(2014): 365–374.

Jelovac, D. & Armstrong, D.K.D. 2011. Recent progress in the diagnosis and treatment of ovarian cancer. *CA: a cancer journal for clinicians*, 61(3): 183–203.

Jimenez, P., Pathak, A. & Phan, A.T. 2011. The role of taxanes in the management of gastroesphageal cancer. *Journal of gastrointestinal oncology*, 2(4): 240–9.

Johnstone, T.C., Park, G.Y. & Lippard, S.J. 2014. Understanding and Improving Platinum Anticancer Drugs – Phenanthriplatin. *Anticancer Research*, 34(1): 471–476.

Kaneko, S. et al. 2016. Incremental Expression of 14-3-3 Protein Beta / Alpha in Urine Correlates with Advanced Stage and Poor Survival in Patients with Clear Cell Renal Cell Carcinoma. *Asian Pacific journal of cancer prevention*, 17(3): 1399–1404.

Karsani, S.A. et al. 2014. Comparative proteomics analysis of oral cancer cell lines: identification of cancer associated proteins. *Proteome science*, 12(1): 3.

Katiyar, S.K., Roy, A.M. & Baliga, M.S. 2005. Silymarin induces apoptosis primarily through a p53-dependent pathway involving Bcl-2/Bax, cytochrome c release, and caspase activation. *Molecular cancer therapeutics*, 4(2): 207–216.

Kazemi, Z. et al. 2015. Synthesis, characterization, crystal structure, DNA- and HSA-binding studies of a dinuclear Schiff base Zn(II) complex derived from 2-hydroxynaphtaldehyde and 2-picolylamine. *Journal of Molecular Structure*, 1096: 110–120.

Keck, M. V & Lippard, S.J. 1992. Unwinding of supercoiled DNA by platinum-ethidium and related complexes. *Journal of the American Chemical Society*, 114(9): 3386–3390.

Kigawa, J. 2013. New strategy for overcoming resistance to chemotherapy of ovarian cancer. *Yonago Acta Medica*, 56(2): 43–50.

Kim, K.H. & Sederstrom, J.M. 2016. Assaying cell cycle status using flow cytometry Kang. *Current Protocols in Molecular Biology*, 8(5): 583–592.

Kitagawa, M. et al. 2013. Cell cycle regulation by long non-coding RNAs. *Cellular and Molecular Life Sciences*, 70(24): 4785–4794.

Kozikowski, B.A. 2003. The Effect of Room-Temperature Storage on the Stability of Compounds in DMSO. *Journal of Biomolecular Screening*, 8(2): 205–209.

Kurosaka, K. et al. 2003. Silent cleanup of very early apoptotic cells by macrophages. *Journal of immunology,* 171: 4672–4679.

Lavrik, I.N. & Krammer, P.H. 2012. Regulation of CD95/Fas signaling at the DISC. *Cell Death and Differentiation*, 19(1): 36–41.

Leal, F. et al. 2015. Neoadjuvant Endocrine Therapy for Estrogen Receptor-Positive Breast Cancer: A Systematic Review and Meta-analysis. *The Breast*, 24(4): 406–412.

Ledermann, J.A. et al. 2013. Newly diagnosed and relapsed epithelial ovarian carcinoma: ESMO clinical practice guidelines for diagnosis, treatment and follow-up. *Annals of Oncology*, 24(6): vi24-32.

Li, B. & Dou, Q.P. 2000. Bax degradation by the ubiquitin/proteasome-dependent pathway: Involvement in tumor survival and progression. *Proceedings of the National Academy of Sciences*, 97(8): 3850–3855.

Lim, S. & Kaldis, P. 2013. Cdks, cyclins and CKIs: roles beyond cell cycle regulation. *Development*, 140(15): 3079–93.

Lipinski, C.A. et al. 2012. Experimental and computational approaches to estimate solubility and permeability in drug discovery and development settings. *Advanced Drug Delivery Reviews*, 46(1-3): 3-26.

Liu, Y. et al. 2006. Identification of 14-3-3 as a Contributor to Drug Resistance in Human Breast Cancer Cells Using Functional Proteomic Analysis. *Cancer Research*, 66(6): 3248–3255.

Lovitt, C., Shelper, T. & Avery, V. 2014. Advanced Cell Culture Techniques for Cancer Drug Discovery. *Biology*, 3(2): 345–367.

Luís, D. V. et al. 2014. Insights into the mechanisms underlying the antiproliferative potential of a Co(II) coordination compound bearing 1,10-phenanthroline-5,6-dione: DNA and protein interaction studies. *Journal of Biological Inorganic Chemistry*, 19(6): 787–803.

Marchi, S. et al. 2012. Mitochondria-Ros Crosstalk in the Control of Cell Death and Aging. *Journal of Signal Transduction*, 2012: 1–17.

Marchina, E. et al. 2010. BRCA1 and BRCA2 genetic test in high risk patients and families: Counselling and management. *Oncology reports*, 24: 1661–1667.

Mehren, M.V. 2008. The role of adjuvant and neoadjuvant therapy in gastrointestinal stromal tumors. *Ratio*, 20(4): 428–432.

Mendelsohn, J. 2013. Personalizing oncology: perspectives and prospects. *Journal of clinical oncology : official journal of the American Society of Clinical Oncology*, 31(15): 1904–1911.

Mihlon, F., Ray, C.E. & Messersmith, W. 2010. Chemotherapy agents: A primer for the interventional radiologist. *Seminars in Interventional Radiology*, 27(4): 384–390.

Millimouno, F.M. et al. 2014. Targeting apoptosis pathways in cancer and perspectives with natural compounds from mother nature. *Cancer Prevention Research*, 7(11): 1081–1107.

Monteiro, Â., Gonçalves, L.M. & Santos, M.M.M. 2014. Synthesis of novel spiropyrazoline oxindoles and evaluation of cytotoxicity in cancer cell lines. *European Journal of Medicinal Chemistry*, 79: 266–272.

Neubig, R.R. et al. 2003. International Union of Pharmacology Committee on Receptor Nomenclature and Drug Classification. XXXVIII. Update on terms and symbols in quantitative pharmacology. *Pharmacological reviews*, 55(4): 597–606.

Nishida, N. et al. 2006. Angiogenesis in cancer. *Hämostaseologie*, 2(3): 213–219.

Nunes, R.C.C.S. 2016. *The therapeutic potential of small molecules p53-MDM protein-protein interaction inhibitors*. Faculdade de Farmácia, Universidade de Lisboa.

Oldenburg, K. et al. 2005. High throughput sonication: evaluation for compound solubilization. *Combinatorial chemistry & high throughput screening*, 8(860): 499–512.

Ouyang, L. et al. 2012. Programmed cell death pathways in cancer: A review of apoptosis, autophagy and programmed necrosis. *Cell Proliferation*, 45(6): 487–498.

Ozaki, T. & Nakagawara, A. 2011. Role of p53 in cell death and human cancers. *Cancers*, 3(1): 994–1013.

Paget, S. 1889. The distribution of secondary growths in cancer of the breast. *Cancer and Metastasis Reviews*, 8(2): 98-101.

Penninger, J.M. & Kroemer, G. 2003. Mitochondria, AIF and caspases — rivaling for cell death execution. *Nature Cell Biology*, 5(2): 97–99.

Perelman, A. et al. 2012. JC-1: alternative excitation wavelengths facilitate mitochondrial membrane potential cytometry. *Cell death & disease*, 3(11): e430.

Petit, P.X., et al. 1995. Alterations in mitochondrial structure and function are early events of dexamethasone-induced thymocyte apoptosis. *Journal of Cell Biology*, 130(1): 157–167.

Pierrard, M.A. et al. 2012. Proteomic analysis of blood cells in fish exposed to chemotherapeutics: Evidence for long term effects. *Journal of Proteomics*, 75(8): 2454–2467.

Pressinotti, N. et al. 2009. Differential expression of apoptotic genes PDIA3 and MAP3K5 distinguishes between low- and high-risk prostate cancer. *Molecular Cancer*, 8(1): 130.

Promega, 2012. Non-Radioactive Cell Proliferation Assay. Available at: https://www.promega.com/-/media/files/resources/protocols/technical-bulletins/0/celltiter-96-aqueous-non-radioactive-cell-proliferation-systems-protocol.pdf. [Accessed November 1, 2016]

Qiao, H. et al. 2015. Insight into DNA Minor Groove Unspecific Binding of Pyrrole Polyamide. *Bioconjugate Chemistry*, 26(10): 2054–2061.

Rahal, R. et al. 2014. Adjuvant and neoadjuvant treatment for rectal cancer , colon cancer , and non-small-cell lung cancer in older patients. *Current Oncology*, 21(4): 193–195.

Rahman, S.S.A., AbdulWahab, N. & Malek, S.N.A. 2013. In vitro morphological assessment of apoptosis induced by antiproliferative constituents from the rhizomes of curcuma zedoaria. *Evidence-based Complementary and Alternative Medicine*, 2013: 1–14.

Rajendiran, V. et al. 2007. Mixed-ligand copper (II)-phenolate complexes: effect of coligand on enhanced DNA and protein binding, DNA cleavage, and anticancer activity. *Inorganic chemistry*, 46(20): 8208–8221.

Ranjan, K., Surolia, A. & Pathak, C. 2012. Apoptotic potential of Fas-Associated death domain on regulation of cell death regulatory protein cFLIP and death receptor mediated apoptosis in HEK 293T cells. *Journal of Cell Communication and Signaling*, 6(3): 155–168.

Reymond, N., D'Água, B.B. & Ridley, A.J. 2013. Crossing the endothelial barrier during metastasis. *Nature reviews Cancer*, 13(12): 858-70

Ribeiro, C.J.A. et al. 2016. Chemical variations on the p53 reactivation theme. *Pharmaceuticals*, 9(2): 25.

Ribeiro, C.J.A. et al. 2016. Spirooxadiazoline oxindoles with promising in vitro antitumor activities. *Medicinal Chemical Communications*, 7(3): 420–425.

Riss, T.L. et al. 2013. Cell Viability Assays. 2013 May 1 [Upadated 2016 Jul 1] In: Sittampalam GS, Coussens NP, Brimacombe K, et al., editors. Assay Guidance Manual [Internet]. Bethesda (MD): Eli Lilly & Company and the National Center for Advancing Translational Sciences; 2004-. Available from: https://www.ncbi.nlm.nih.gov/books/NBK144065/.

Sahin, E. & Depinho, R. 2010. Linking functional decline of telomeres, mitochondria and stem cells during ageing. *Nature*, 464(7288): 520–528.

Santos, M.M.M. 2014. Recent advances in the synthesis of biologically active spirooxindoles. *Tetrahedron*, 70(52): 9735–9757.

Sarto, C. et al. 2000. Heat shock proteins in human cancer. *Electrophoresis*, 21: 1218–1226.

Saúde, D.G. 2014. Portugal: Doenças Oncológicas em números. Available at: https://www.dgs.pt/estatisticas-de-saude/estatisticas-de-saude/publicacoes/portugal-doencas-oncologicas-em-numeros-2014.aspx [Accessed September 1, 2016].

Schedin, P. & Elias, A. 2004. Multistep tumorigenesis and the microenvironment. *Breast cancer research*, 6(2): 93–101.

Seetharamappa, J. & Kamat, B.P. 2004. Spectroscopic studies on the mode of interaction of an anticancer drug with bovine serum albumin. *Chemical & pharmaceutical bulletin*, 52(9): 1053–1057.

Shaaban, M.R., Mayhoub, A.S. & Farag, A.M. 2012. Recent advances in the therapeutic applications of pyrazolines. *Expert Opinion on Therapeutic Patents*, 22(3): 253–291.

Shahabadi, N., Mohammadi, S. & Alizadeh, R. 2011. DNA interaction studies of a new platinum(II) complex containing different aromatic dinitrogen ligands. *Bioinorganic Chemistry and Applications*, 2011: 1-8.

Sharma, P. et al. 2012. Reactive Oxygen Species, Oxidative Damage, and Antioxidative Defense Mechanism in Plants under Stressful Conditions. *Journal of Botany*, 2012: 1–26.

Shewach, D.S. & Kuchta, R.D. 2009. Introduction to Cancer Chemotherapeutics. *Computer*, 109(7): 2859–2861.

Silva, J. et al. 2014. Characterization of the antiproliferative potential and biological targets of a trans ketoimine platinum complex. *Inorganica Chimica Acta*, 423:156–167.

Silva, T.F.S. et al. 2012. Cobalt complexes bearing scorpionate ligands: synthesis, characterization, cytotoxicity and DNA cleavage. *Dalton transactions*, 41(41): 12888–97

Sirajuddin, M., Ali, S. & Badshah, A. 2013. Journal of Photochemistry and Photobiology B : Biology Drug – DNA interactions and their study by UV – Visible , fluorescence spectroscopies and cyclic voltametry. *Journal of Photochemistry & Photobiology, B: Biology*, 124: 1–19.

Smiley, S.T. et al. 1991. Intracellular heterogeneity in mitochondrial membrane potentials revealed by a J-aggregate-forming lipophilic cation JC-1. *Proceedings of the National Academy of Sciences of the United States of America*, 88(9): 3671–3675.

Smith, L.H. et al. 2005. Ovarian cancer: Can we make the clinical diagnosis earlier? *Cancer*, 104(7): 1398–1407.

Smolle, E. et al. 2013. Targeting signaling pathways in epithelial ovarian cancer. *International Journal of Molecular Sciences*, 14(5): 9536–9555.

Soares, P.I.P. et al. 2012. Application of Hyperthermia for Cancer Treatment: Recent Patents Review. *Recent Patents on Anti-Cancer Drug Discovery*, 7(1): 64–73.

Society, A.C. 2016. Treating Ovarian Cancer. Available at: https://www.cancer.org/cancer/ovarian-cancer/treating.html [Accessed February 1, 2017].

Souhami, R. et al. 2002. Oxford Textbook of Oncology, Second Edition. In *British Journal of Cancer*. Oxford.

Sun, L. et al. 1998. Synthesis and biological evaluations of 3-substituted indolin-2-ones: A novel class of tyrosine kinase inhibitors that exhibit selectivity toward particular receptor tyrosine kinases. *Journal of Medicinal Chemistry*, 41(14): 2588–2603.

Tarushi, A. et al. 2014. Antioxidant activity and interaction with DNA and albumins of zinc-tolfenamato complexes. Crystal structure of [Zn(tolfenamato)$_2$(2,2'-dipyridylketoneoxime)$_2$]. *European Journal of Medicinal Chemistry*, 74: 187–196.

Thost, A.K. et al. 2015. Fluorescence-based imaging of autophagy progression by human WIPI protein detection. *Methods*, 75: 69–78.

Tsai, Y.C., Wang, Y.H. & Liu, Y.C. 2017. Overexpression of PCNA Attenuates Oxidative Stress-Caused Delay of Gap-Filling during Repair of UV-Induced DNA Damage. *Journal of Nucleic Acids*, 2017:1-12.

Tukenova, M. et al. 2010. Role of cancer treatment in long-term overall and cardiovascular mortality after childhood cancer. *Journal of Clinical Oncology*, 28(8): 1308–1315.

Vergote, I. 2014. Novel therapies, including enzastaurin, in the treatment of ovarian cancer. *Expert Opinion on Investigational Drugs*, 23(5): 579–598.

Vergote, I. et al. 2011. Primary surgery or neoadjuvant chemotherapy followed by interval debulking surgery in advanced ovarian cancer. *European Journal of Cancer*, 47(3): S88–S92.

Vermeulen, K., et al. 2003. The cell cycle:a review of regulation,deregulation and therapeutic targets in cancer. *Cell Proliferation*, 36(3): 131–149.

Voorhees, P.M. et al. 2003. The proteasome as a target for cancer therapy. *Clinical Cancer Research*, 9(17): 6316–25.

Wang, P., Henning, S.M. & Heber, D. 2010. Limitations of MTT and MTS-based assays for measurement of antiproliferative activity of green tea polyphenols. *PLoS ONE*, 5(4): e10202.

Wang, X., 2001. The expanding role of mitochondria in apoptosis. *Gene Dev*, 15(214), pp.2922–33.

WHO, 2015. Fact Sheets by Cancer. Available at: http://www.who.int/mediacentre/factsheets/fs297/en/ [Accessed September 1, 2016].

WHO, 2014. Portugal Mortality and Incidence Ratios. Available at: http://www.who.int/cancer/country-profiles/en/#P [Accessed September 1, 2016].

Xu, H. et al. 2013. Characterization of the interaction between eupatorin and bovine serum albumin by spectroscopic and molecular modeling methods. *International Journal of Molecular Sciences*, 14(7): 14185–14203.

Yao, X. et al. 2013. A novel role of ribonuclease inhibitor in regulation of epithelial-to-mesenchymal transition and ILK signaling pathway in bladder cancer cells. *Cell and Tissue Research*, 353(3): 409–423.

Yap, T.A., Carden, C.P. & Kaye, S.B. 2009. Beyond chemotherapy: targeted therapies in ovarian cancer. *Nature Reviews Cancer*, 9(3): 167–181.

Yu, B., Yu, D.Q. & Liu, H.M. 2015. Spirooxindoles: Promising scaffolds for anticancer agents. *European Journal of Medicinal Chemistry*, 97(1): 673–698.

Zeiss, C.J. 2003. The Apoptosis-Necrosis Continuum: Insights from Genetically Altered Mice. *Veterinary Pathology*, 40(5): 481–495.

Zhang, L. et al. 2012. Prohibitin induces apoptosis in BGC823 gastric cancer cells through the mitochondrial pathway. *Asian Pacific Journal of Cancer Prevention*, 13(8): 3803–3807.

Van Zijl, F., Krupitza, G. & Mikulits, W. 2011. Initial steps of metastasis: Cell invasion and endothelial transmigration. *Mutation Research - Reviews in Mutation Research*, 728(1–2): 23–34.

# 6 APPENDIX

## 6.1 Appendix A

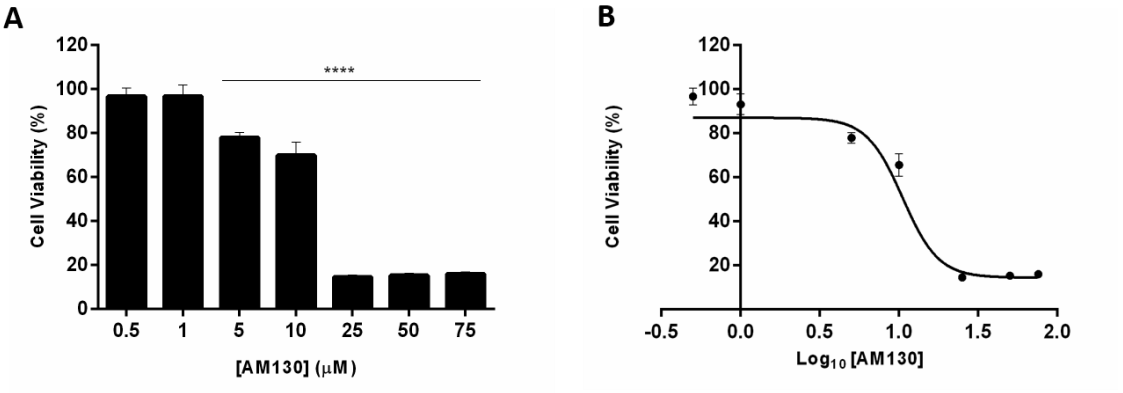


**Figure 6.1 -** Dose dependent cytotoxicity (A) and the correspondent dose-response curve (B) of AM130 in HCT116 cells followed by a 48 h incubation. Cell viability values were tested and function of the control (cells + 0.1 % (v/v) DMSO), which were set to 100 %. Data are the average of three independent assays and error bars correspondent to SEM (* $p \leq 0.05$, ** $p \leq 0.01$, *** $p \leq 0.001$, **** $p \leq 0.0001$).

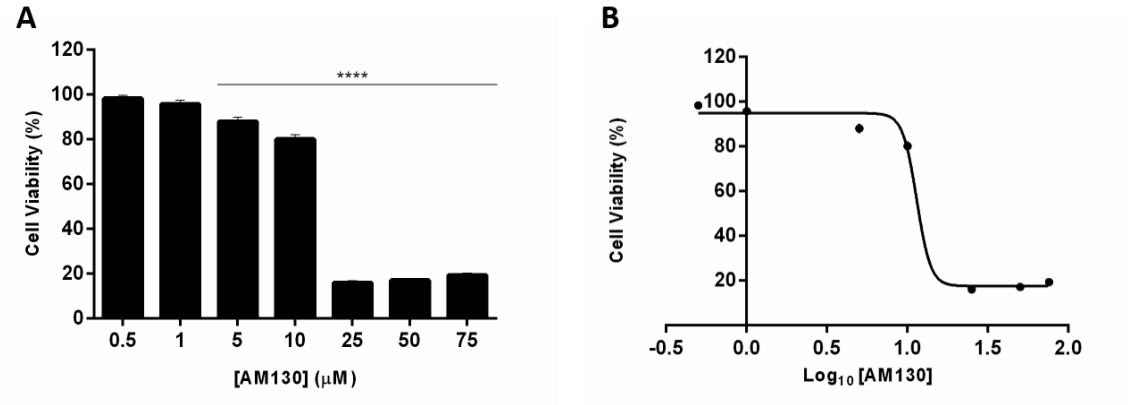


**Figure 6.2 -** Dose dependent cytotoxicity (A) and the correspondent dose-response curve (B) of AM130 in MDA-MB-453 cells followed by a 48 h incubation. Cell viability values were tested and function of the control (cells + 0.1 % (v/v) DMSO), which were set to 100 %. Data are the average of three independent assays and error bars correspondent to SEM (* $p \leq 0.05$, ** $p \leq 0.01$, *** $p \leq 0.001$, **** $p \leq 0.0001$).

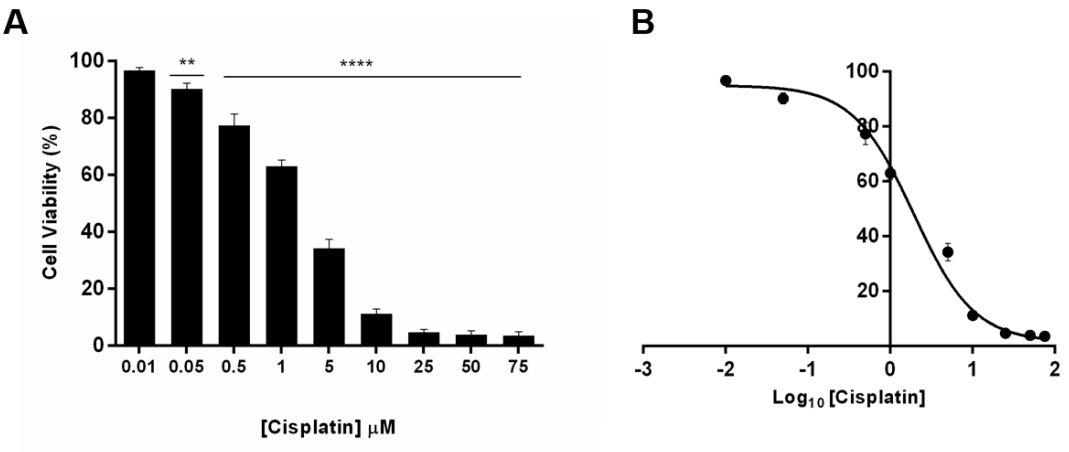


**Figure 6.3 -** Dose dependent cytotoxicity (A) and the correspondent dose-response curve (B) of cisplatin in A2780 cells followed by a 48 h incubation. Cell viability values were tested and function of the control (cells + 0.9 % (w/v) NaCl), which were set to 100 %. Data are the average of three independent assays and error bars correspondent to SEM (* $p \leq 0.05$, ** $p \leq 0.01$, *** $p \leq 0.001$, **** $p \leq 0.0001$).

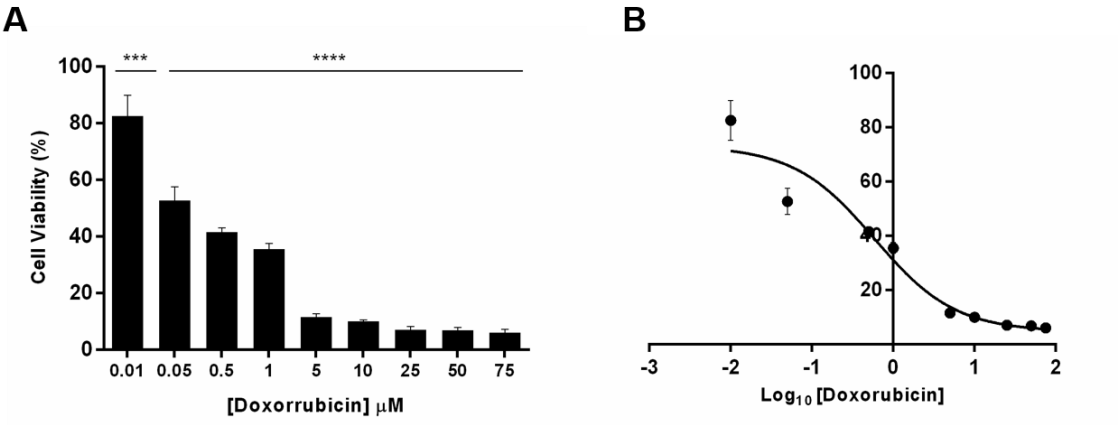


**Figure 6.4 -** Dose dependent cytotoxicity (A) and the correspondent dose-response curve (B) of doxorubicin in A2780 cells followed by a 48 h incubation. Cell viability values were tested and function of the control (cells + 0.2 % (v/v) DMSO), which were set to 100 %. Data are the average of three independent assays and error bars correspondent to SEM (* $p \leq 0.05$, ** $p \leq 0.01$, *** $p \leq 0.001$, **** $p \leq 0.0001$).

## 6.2 Appendix B

**Table 6.1 -** Percentage of A2780 cells in G1/G0, S and G2/M phases, when exposed to compound AM130 $IC_{50}$ concentration value or 0.1% (v/v) DMSO (vehicle control). Data were analyzed by flow cytometry after PI staining. Data values are represented as means ± SEM of two independent experiments.

| **Cell-cycle phases** | **4 h** | | **9 h** | | **12 h** | | **24 h** | |
|---|---|---|---|---|---|---|---|---|
| | DMSO | $IC_{50}$ AM130 | DMSO | $IC_{50}$ AM130 | DMSO | $IC_{50}$ AM130 | DMSO | $IC_{50}$ AM130 |
| **G0/G1** | 7.2 ± 0.1 | 8.1 ± 1.0 | 48.6 ± 5.4 | 41.2 ± 5.3 | 60.1 ± 1.9 | 61.1 ± 2.0 | 53.3 ± 2.6 | 47.1 ± 0.2 |
| **S** | 12.2 ± 3.9 | 10.9 ± 2.8 | 8.5 ± 2.7 | 7.6 ± 1.6 | 23.2 ± 1.9 | 17.6 ± 3.8 | 15.2 ± 7.9 | 18.8 ± 0.2 |
| **G2/M** | 80.6 ± 3.9 | 84.5 ± 7.3 | 42.9 ± 2.7 | 51.2 ± 3.8 | 16.7 ± 3.8 | 21.3 ± 1.8 | 31.5 ± 10.5 | 34.2 ± 0.0 |

## 6.3 Appendix C

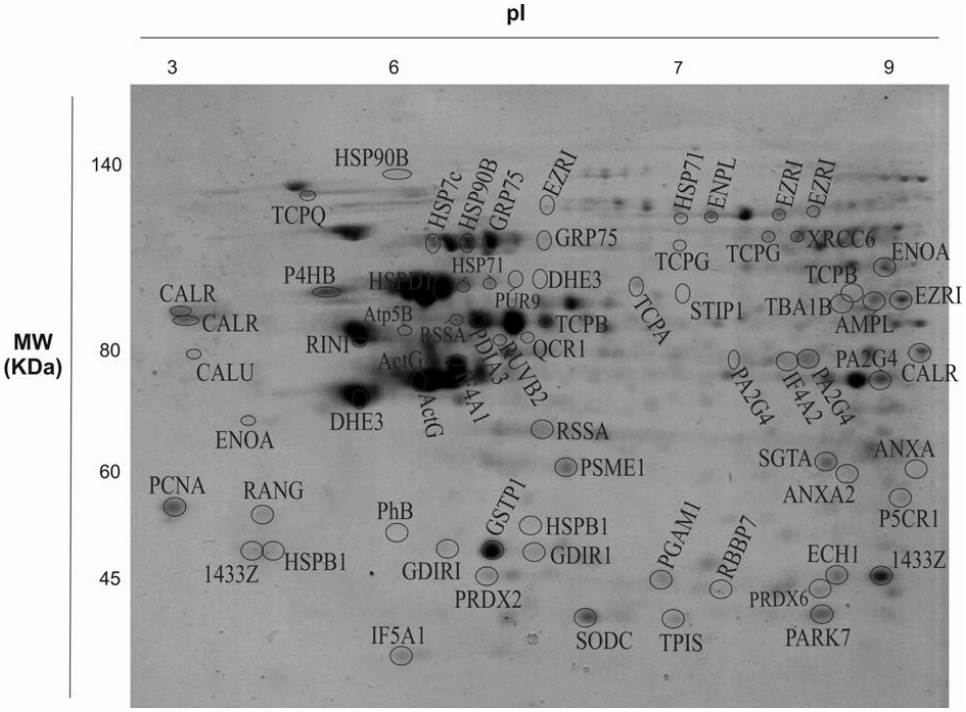


**Figure 6.5 -** Reference gel of HCT116 cell line.